2014-04-25

EspFU, an Enterohemorrhagic E. Coli Secreted Effector, Hijacks Mammalian Actin Assembly Proteins by Molecular Mimicry and Repetition: A Dissertation

YuShuan (Cindy) Lai
University of Massachusetts Medical School

$\mathbf{ESPF_U}$, AN ENTEROHEMORRHAGIC *E. COLI* SECRETED EFFECTOR, HIJACKS MAMMALIAN ACTIN ASSEMBLY PROTEINS BY MOLECULAR MIMICRY AND REPETITION

A Dissertation Presented

by

(CINDY) YUSHUAN LAI

Submitted to the Faculty of the
University of Massachusetts Graduate School of Biomedical Sciences, Worcester
in partial fulfillment of the requirements for the degree of

DOCTOR OF PHILOSOPHY

April 25th 2014

Microbiology and Physiology Systems

$\mathbf{ESPF_U}$, AN ENTEROHEMORRHAGIC *E. COLI* SECRETED EFFECTOR, HIJACKS MAMMALIAN ACTIN ASSEMBLY PROTEINS BY MOLECULAR MIMICRY AND REPETITION

A Dissertation Presented

by

(CINDY) YUSHUAN LAI

The signatures of the Dissertation Defense Committee signify completion and approval as to style and content of the Dissertation

---

John M. Leong, MD/PhD, Thesis Advisor

Jon Goguen, PhD, Member of Committee

Chris Sassetti, PhD, Member of Committee

Peter Pryciak, PhD, Member of Committee

Bruce Goode, PhD, Member of Committee

Beth McCormick, PhD, Chair of Committee

Anthony Carruthers, PhD, Dean of the Graduate School of Biomedical Sciences

ACKNOWLEDGEMENTS

To my faux family, mentors, and friends - thanks for believing in me.

To the *E. coli* group - **Brian Skehan** for getting me started and cloning the first $EspF_U$ truncation mutants; **Didier Vingadassalom** for being a friend and enthusiastic mentor; **Mike Brady** for always being helpful by email; **Sowmya Balasubramanian** for many fruitful discussions and advice during the darkest hours; **Doug Robbins** for being the best minion ever; and **Stacie Clark** for your wonderful helping hands - I couldn't have accomplished all of this without you.

To the rest of my lab - many thanks for making each day fun.

To Kenan Murphy - thank you for helping me with my initial clones.

To the McCormick lab, my sincerest thanks for taking me in, having baked goods whenever I visited, and treating me like a real lab member. Many thanks especially to **Andrew Zukauskas** and **Rose Szabady** for productive conversations and support. To **Erik Boll**, aka STDG - thanks for being my partner in crime (in crazy lab work) and for motivating me into the midnight hours with Eurodance.

To Beth McCormick - a **BIG THANK YOU** for helping to steer the course in so many ways.

ABSTRACT

$\mathbf{ESPF_U}$, AN ENTEROHEMORRHAGIC *E. COLI* SECRETED EFFECTOR, HIJACKS MAMMALIAN ACTIN ASSEMBLY PROTEINS BY MOLECULAR MIMICRY AND REPETITION

APRIL 25TH 2014

(CINDY) YUSHUAN LAI

B.A., MOUNT HOLYOKE COLLEGE

Ph.D., UNIVERSITY OF MASSACHUSETTS MEDICAL SCHOOL

Directed by: Professor John M. Leong, MD/PhD

Enterohemorrhagic *E. coli* (EHEC) is a major cause of food borne diarrheal illness worldwide. While disease symptoms are usually self-resolving and limited to severe gastroenteritis with bloody diarrhea, EHEC infection can lead to a life threatening complication known as Hemolytic Uremic Syndrome (HUS), which strikes children disproportionately and is the leading cause of kidney failure in children. Upon infection of gut epithelia, EHEC produces characteristic lesions called actin pedestals. These striking formations involve dramatic rearrangement of host cytoskeletal proteins. EHEC hijacks mammalian signaling pathways to cause destruction of microvilli and rebuilds the actin cytoskeleton underneath sites of bacterial attachment. Here, we present a brief study on a host factor, Calpain, involved in microvilli efface-

ment, and an in depth investigation on a bacterial factor, $EspF_U$, required for actin pedestal formation in intestinal cell models. Calpain is activated by both EHEC and the related pathogen, enteropathogenic *E. coli* (EPEC), during infection and facilitates microvilli disassembly by cleavage of a key membrane-cytoskeleton anchoring substrate, Ezrin. Actin pedestal formation is facilitated by the injection of two bacterial effectors, Tir and $EspF_U$, into host cells, which work in concert to manipulate the host actin nucleators N-WASP and Arp2/3. $EspF_U$ hijacks key host signaling proteins N-WASP and IRTKS by mimetic displacement and has evolved to outcompete mammalian host ligands. Multiple repeats of key functional domains of $EspF_U$ are essential for actin pedestal activity through proper localization and competition against the an abundant host factor Eps8 for binding to IRTKS.

PREFACE

Parts of this thesis that have appeared in separate publications include:

Chapter 1:

Lai, Yushuan, Rosenshine, Ilan, Leong, John M., and Frankel, Gad. Intimate host attachment: enteropathogenic and enterohaemorrhagic *Escherichia coli*. *Cell Microbiol* 15, 11 (Nov 2013), 1796-808.

Sections 1.4.4 and 1.4.5 were penned by Gad Frankel. Figures 1.2 and 1.3 are professional redrawings by a Wiley hired artist (Laura Symul) based on original figures.

Chapter 2:

Lai, Yushuan, Riley, Kathleen, Cai, Andrew, Leong, John M., and Herman, Ira M. Calpain mediates epithelial cell microvillar effacement by enterohemorrhagic *Escherichia coli*. *Front Microbiol* 2 (2011), 222.

Chapter 3:

Lai, Yushuan, Rosenshine, Ilan, Leong, John M., and Frankel, Gad. Intimate host attachment: enteropathogenic and enterohaemorrhagic *Escherichia coli*. *Cell Microbiol* 15, 11 (Nov 2013), 1796-808.

TABLE OF CONTENTS

LIST OF TABLES

Table **Page**

LIST OF FIGURES

Figure **Page**

CHAPTER 1

INTRODUCTION

1.1 Acknowledgements

The main body of this introduction starting from section 1.4 is adapted from a review that I co-authored with Ilan Rosenshine, John Leong, and Gad Frankel [70]. Sections 1.4.4 and 1.4.5 were penned by Gad Frankel. Figures are professional redrawings by a Wiley hired artist (Laura Symul) based on original figures.

1.2 EHEC Clinical Disease

Enterohemorrhagic *E. coli* (EHEC) causes serious diarrheal illnesses worldwide. Normally found as inconsequential coinhabitants in the gastrointestinal tract of cows and a variety of ruminants, EHEC can be transmitted to humans by ingestion of contaminated foods. Disease occurs only in humans and usually begins a few days after ingestion [117]. Symptoms of EHEC infection, though extremely unpleasant, usually resolve in one or two weeks and include severe abdominal cramping, watery diarrhea, hemorrhagic colitis, and bloody diarrhea. However, in an estimated 5-7% of cases, patients can progress to hemolytic uremic syndrome (HUS), a triad of hemolysis, thrombocytopenia, and renal failure [46]. Children are disproportionately susceptible and HUS, which is caused by systemic absorption of Shiga toxin (Stx), (for review, see [117]). HUS is the leading cause of renal failure in children.

EHEC is relatively new pathogen. First described in 1983, EHEC disease was once almost exclusively associated with the ingestion of undercooked beef or raw

dairy [98]. In more recent years however, EHEC outbreaks can be traced to foods as varied as fresh produce, cookie dough, and prepackaged frozen foods[6, 86]. Most outbreaks associated with HUS are caused by EHEC serotype O157:H7, though serotypes causing diarrheal disease and HUS are expanding. The CDC reported two multistate outbreaks in 2013, together involving 20 states, 68 hospitalizations and 4 cases of HUS [24]. Numerous local outbreaks commonly originating from restaurants and petting zoos are now documented yearly.

Treatment for EHEC induced diarrhea is limited to supportive therapy as antibiotics can increase the risk of HUS. No specific therapies for HUS exist and management involves empiric, careful monitoring of fluid levels and kidney function [117].

1.3 Virulence Mechanisms of AE Pathogens

EHEC is a member of the attaching and effacing (AE) pathogen family, which also includes enteropathogenic *E. coli* (EPEC), an important cause of infantile diarrhea in developing countries, and the mouse pathogen *Citrobacter rodentium*, and the rabbit pathogen RDEC [33, 113]. EHEC and EPEC are unique among human *E. coli* pathovars and other gut pathogens pathogens in that they colonize the intestinal mucosa via AE lesions that are the defining hallmark of this family [33]. AE lesions are characterized by effacement of the intestinal brush border, intimate bacterial attachment to the plasma membrane of infected enterocytes, and accumulation of electron dense material, consisting of mostly actin filaments, under the extracellularly bound bacteria [28]. This distinct attachment strategy aids in EHEC and EPEC pathogenesis.

1.3.1 The locus of enterocyte effacement (LEE)

EHEC and EPEC have both acquired numerous pathogenecity islands (PAI). Their defining PAI, called the locus of enterocyte effacement (LEE) is essential for virulence and the AE phenotype. The LEE encodes a complex bacterial effector delivery machinery called the type 3 secretion system (T3SS) as well as and key compenents needed for AE lesions [113, 132].

The T3SS is expressed and upregulated in response to specific, complex extracellular signals inside the gut [46]. Upon contact with host cells, the T3SS injects bacterial effectors directly into infected cells in a coordinated manner, thereby providing EHEC and EPEC intracellular access and exquisite control of infected enterocytes [132]. In addition to seven effectors encoded on the LEE, EHEC and EPEC strains possess a wide reperatoir of non-LEE encoded effectors [33, 132]. EHEC injects about twice as many effectors as EPEC, potentially up to 60 [33, 118]. While many effectors are as yet uncharacterized, several have been well documented to disrupt a number of cellular processes often through hijacking of highly regulated cell signaling cascades.

1.3.2 AE lesions in disease

The ability to form AE lesions is essential in establishing infection and disease. Numerous studies have now demonstrated that AE pathogens incapable of generating AE lesions display severe colonization defects and reduced disease phenotypes in variety of animal models [42, 77, 100, 116, 122, 75]. In addition, EHEC mutants defective in stimulating actin pedestal formation fail to expand their initial infectious niche [30, 99, 74].

1.4 Actin Pedestal Formation Pathways by AE Pathogens

The striking actin rich structures formed on infected cells by EPEC and EHEC have come to be known as actin pedestals. First visualized in microscopy studies in cultured cells [98], actin pedestals have been the subject of considerable study for the last two and a half decades. As seen in figure 1.1, actin rich structures protrude from the surface of cells infected by AE pathogens, such that the adherent bacteria appear to be lifted on a pedestal and sometimes cupped by the surrounding actin when viewed from above. Although these two related pathogens utilize highly homologous key effectors to promote actin pedestals that are morphologically indistinguishable, EPEC and EHEC utilize distinct signaling pathways to generate their pedestals. Studies comparing the two strategies have provided fascinating examples of how microbial pathogens can hijack related mammalian actin assembly signaling cascades in multiple ways.

1.4.1 Tir, a unique paradigm for host cell attachment and signaling by a microbial pathogen

Actin pedestal formation for both EPEC and EHEC requires the delivery of the LEE encoded effector called the translocated intimin receptor or Tir. Upon translocation into host cells, Tir inserts into the apical membrane such that the N- and C-terminal portions of Tir are cytosolic, with helical transmembrane domains traversing the host apical membrane. The central (100-residue) portion, known as the Intimin Binding Domain (IBD), forms two helices separated by a hairpin loop on the external surface of the host cell [65, 73]. This loop binds the C-terminus of intimin, which is expressed on the surface of EPEC and EHEC, with high affinity (K_d of 10 nM for EPEC and less than 1 nM for EHEC) thus facilitating extremely tight attachment of these pathogenic *E. coli* to the host cell [38, 101]. Also encoded by the LEE, intimins can interchangeably bind Tir from EHEC or EPEC strains.

In addition to its function as a bacterial receptor, Tir serves as a signaling effector that elegantly initiates the recruitment of host adaptors and actin nucleators from inside the host cytosol, a strategy commonly used by intracellular pathogens to exert pathophysiologic effects. Although EPEC and EHEC Tirs are homologous in structure and share 60% identity [65] they use divergent mechanisms of signaling that then converge on the activation of common actin nucleators to produce pedestals that are indistinguishable when examined by electron microscopy or fluorescence imaging of actin (Figure 1.1).

Both intimin and Tir appear to be adapted for multimerization. The beta barrel region of intimin, which anchors intimin to the bacterial outer membrane, and the IBD of Tir each encode dimerization domains, giving rise to a model in which the two proteins might efficiently form higher order lattices essential for downstream signaling [73, 120].

Within an infected host cell, Tir interacts with a number of host proteins through its N- and C-terminal cytosolic domains. The N-terminal tail is functionally interchangeable between EHEC and EPEC Tirs and binds various focal adhesion proteins, thereby potentially linking Tir to the cytoskeleton [56, 66]. However, such activity is insufficient for actin pedestal formation [66]. Both EPEC and EHEC require the C-terminal tail, the portion of Tir that is most divergent between these two highly related pathogens [38]. Notably, intimin binding enhances post-translocation modification of the C-terminus of Tir inside the host cell. These modifications, when fully characterized, were pivotal in revealing the mechanism of actin pedestal formation [67, 21, 19].

Figure 1.1: Actin Pedestals

Actin pedestals as visualized by transmission electron microscopy appear as electron dense protrusions beneath intimately attached bacteria (A). By immunofluorescence microscopy, actin pedestals can visualized with phalloidin conjugated fluorophores. EHEC (blue; DAPI stained) induces actin pedestals on infected HeLa cells (B) and HCT8 intestinal cells (C) stained with Alexa-488 conjugated phalloidin (green). White arrowheads point to typical actin pedestals for these cells types. Tir stained with Alexa-568 (red) colocalizes with actin at the tips of actin pedestals, forming yellow foci beneath intimately adhered bacteria.

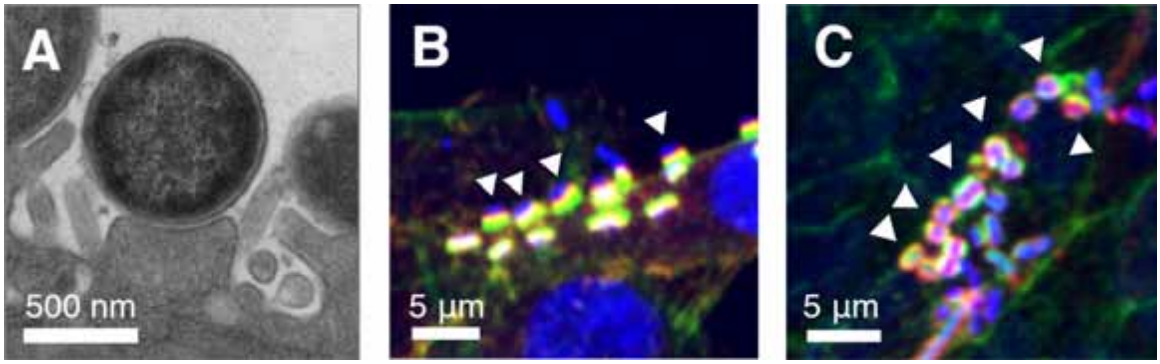

Figure 1.1: Actin Pedestals

1.4.2 EPEC pedestal formation pathways

Host modification of the C-terminus of EPEC Tir is critical for its activity. This domain contains multiple tyrosine, threonine, and serine residues that are available for potential host phosphorylation. Serine/threonine phosphorylation, which changes the apparent molecular weight of Tir by SDS-PAGE from less than 80 kDa to about 90 kDa, has been suggested to play a role in Tir insertion into the apical membrane, but otherwise does not contribute to actin pedestal formation. Tyrosine phosphorylation of EPEC Tir, on the other had, is absolutely required for efficient actin polymerization [67]. Multiple protein kinases, including members of the Abl and Src kinase families, have been localized to EPEC pedestal tips and thus implicated in pedestal formation; broad inhibition of both these classes of kinases by non-specific pharmacologic inhibitors can inhibit EPEC pedestals [115, 62]. However, EPEC can still induce pedestal formation on a variety of cultured cells lacking individual kinases from the Abl or Src families, suggesting that EPEC Tir is capable of utilizing multiple, redundant tyrosine kinases for Tir phosphorylation in vitro [115].

Of the Tir C-terminal tyrosine residues, phosphorylation of residue Y_{474} (in EPEC1 strain E2348/69) is the most critical for focal actin assembly and triggers the major pathway by which EPEC1 strains initiate pedestal formation in vitro (Figure 1.2, pathway 1) [67, 37]. In clinical isolates, this critical residue may be in other close positions due to small insertions or deletions. This pedestal formation pathway utilizes the host adaptor Nck, which contains an SH2 domain capable of binding a 12-residue region of EPEC Tir that includes the critical phosphorylated Y_{474} [58, 18]. Nck, found at the tips of EPEC-induced actin pedestals, also contains three SH3 domains that may directly or indirectly recruit the host actin nucleation promoting factor, N-WASP [58, 14]. N-WASP, in turn, subsequently recruits and activates the actin nucleating Arp2/3 complex [111, 79].

Due to similarities in the use of Nck and N-WASP by vaccinia virus for actin comet tail formation, a similar mechanism of actin assembly has been proposed for EPEC [19]. Vaccinia produces A36R, a Nck-binding protein, that, like EPEC Tir, is tyrosine phosphorylated by the host. An eight-residue sequence in the A36R Nck-binding region is nearly homologous to the Y_{474} region of EPEC Tir [19]. Recruitment of Nck by A36R leads to indirect activation of N-WASP through the intermediary adaptor, WASP Interacting Protein (WIP) [82]. WIP contains N-terminal proline rich domains that are capable of binding Ncks SH3 domains; its C-terminal WASP binding domain (WBD) activates N-WASP by binding to the N-WASP N-terminal WH1 domain [82]. Ectopic overexpression of the WBD decreases vaccinia actin comet tail formation, presumably by a dominant negative effect, and various mutations in the WH1 domain of N-WASP can abrogate its recruitment and actin comet tail formation by vaccinia [82].

Interestingly, a role for WIP in pathogen-mediated actin assembly appears to depend on the experimental system. Garber and colleagues showed that both EPEC and vaccinia are still able to induce actin assembly in a cell line lacking WIP [51]. N-WASP also contains a proline-rich domain that is capable of binding Nck directly, and thereby leading to its activation [3]. As is the case for the kinases(s) responsible for EPEC Tir phosphorylation, seemingly disparate observations concerning the mechanism of N-WASP activation by Nck and the role of WIP may indicate a degree of redundancy in the N-WASP activation pathway.

Although the major pathway for EPEC pedestal formation requires Nck, Nck-independent mechanisms of actin pedestal formation have also been uncovered, reflecting redundant pedestal formation pathways (Figure 1.2, pathways a and b). EPEC infection of Nck-deficient murine embryonic fibroblasts still generate roughly one-fifth the number of the actin pedestals generated upon infection of wild type

fibroblasts. Most of this activity, also requires Y_{474}, reaffirming its role as a key residue for triggering actin assembly by EPEC Tir. However, even in the absence of Y_{474}, about 2-5% of bound EPEC can generate actin pedestals, a rate more than ten-fold higher than for a Tir-deficient EPEC strain. An additional tyrosine residue at position 454 of EPEC Tir is critical for this minor Nck-independent actin assembly activity [19]. Initially considered of marginal importance, this pathway was later shown to be highly related to the major pathway of actin pedestal formation by EHEC.

Figure 1.2: EPEC and EHEC Actin Pedestal Pathways

EPEC and EHEC use different mechanisms of Tir activated signaling cascades that converge on common host actin nucleation factors, N-WASP and Arp2/3 to form actin pedestals. The major EPEC actin pedestal pathway requires phosphorylation of the critical Tir residue Y_{474}, which recruits Nck (pathway 1). Nck can activate N-WASP directly or through WIP. The major EHEC actin pedestal pathway requires Tir residues NPY_{458} and the EHEC effector $EspF_U$/TccP (pathway 2). $EspF_U$/TccP is linked to Tir via host adaptors IRTKS and IRSp53 and activates N-WASP. Minor EPEC actin assembly pathways utilize Tir residues Y_{474} or Y_{454} to initiate Nck independent activation of N-WASP (pathways a and b). A minor actin assembly pathway for EHEC utilizes $EspF_U$, but does not require N-WASP for Arp2/3 activation (pathway c).

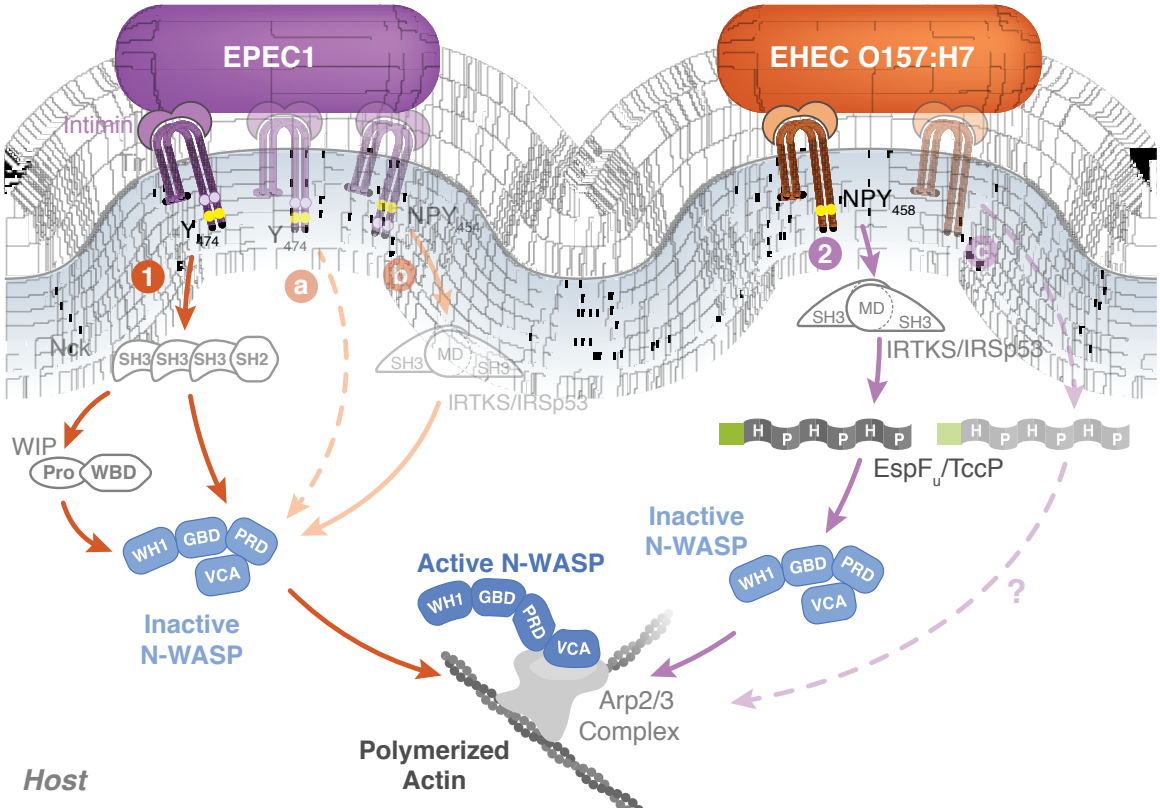

Figure 1.2: EPEC and EHEC Actin Pedestal Pathways

1.4.3 EHEC pedestal formation pathways

A critical first indication that EHEC and EPEC utilized distinct pedestal formation pathways came from studies showing that tyrosine phosphorylated proteins were absent from EHEC actin pedestals [37]. In fact, EHEC Tir lacks the equivalent of EPEC Tir Y_{474}, and EHEC does not require Nck for actin pedestal formation [65, 37]. Consistent with distinct pathways of actin assembly, EHEC tir cannot complement EPEC tir mutants for actin pedestal formation unless modified to encode the critical Y_{474}-containing region of EPEC Tir [66, 18]. Importantly, co-infection of cultured Tir and intimin deletion mutants of EPEC and EHEC revealed that EHEC requires an additional EHEC-specific effector for pedestal formation [66, 37]. These observations pointed to very different mechanisms of actin pedestal formation for EPEC and EHEC (Figure 1.2).

Experiments using chimeric Tir proteins suggested that the key to differences in EPEC and EHEC Tir lie in the C-terminus. While the N-terminus and IBD of EHEC and EPEC Tir are highly similar and functionally interchangeable, their cytosolic C-terminal domains are only 41% identical [38]. Further studies of this region revealed that an NPY sequence at residues 456 to 458 of EHEC Tir is critical for actin pedestal formation [9]. Interestingly, EHEC Tir residue Y_{458} corresponds to EPEC Tir Y_{454}, the residue previously shown to be essential for triggering one of the minor Nck-independent actin assembly pathways in EPEC pedestal formation, described above.

Instead of utilizing tyrosine phosphorylation and Nck recruitment, the EHEC Tir NPY-mediated pathway acts through a different category of host adaptors (Figure 1.2, pathway 2). The NPY_{458} sequence of EHEC Tir, and likely the equivalent sequence of EPEC Tir as well, binds to IRTKS and IRSp53, members of the I-Bar subfamily of membrane deforming and remodeling proteins. These proteins link to

Tir via their N-terminal IMD domains, which also form zeppelin-shaped homodimers associated with convex membrane protrusions [125, 128, 34, 137]. The C-terminal regions of IRTKS and IRSp53 contain additional motifs, such as an SH3 domain, that link their membrane deforming activity to signaling proteins and actin regulators [128, 125].

A paradox in this Tir NPY-mediated pedestal pathway is that it promotes pedestal formation with very low efficiency for EPEC, yet with very high efficiency for EHEC [19, 16]. This riddle was solved by the identification of an additional non LEE-encoded bacterial effector, termed $EspF_U$ (a homolog of the effector EspF encoded on prophage U) or TccP (Tir cytoskeleton coupling protein) [20, 53]. Found in exclusively EHEC, $EspF_U$ also greatly enhances NPY_{458} mediated pedestal formation if expressed in EPEC1 [16] and is essential for actin pedestal activity by EHEC.

$EspF_U$ connects the seemingly disparate Tir NPY_{458} actin assembly pathway back to N-WASP and Arp2/3; it simultaneously binds IRTKS or IRSp53 and activates N-WASP. Functional activity is conferred by repeating elements containing a helical domain that binds activates N-WASP and a proline rich domain that binds IRTKS [21, 53, 26, 125, 1]. Natural isolates of $EspF_U$ contain anywhere from three to eight repeats [54, 52].

Finally, just as EPEC encodes multiple actin assembly pathways, EHEC triggers yet another alternative pathway for pedestal formation in a cell culture model (Figure 1.2). Low levels of actin assembly can be observed when embryonic fibroblasts from N-WASP knockout mice are infected with an intimin-expressing *E. coli* strain that delivers EHEC Tir and $EspF_U$/TccP. This N-WASP-independent pathway depends on multiple repeats of $EspF_U$/TccP, again suggesting a functional role for multiple repeats [124], but the critical elements of this pathway are yet unidentified.

1.4.4 $TccP_2/EspF_M$-induced actin polymerization in non-O157 EHEC and EPEC

Typical EHEC O157:H7 also possesses a pseudogene of $EspF_U$/TccP encoded on prophage CP-933 M/Sp4, and thus called $TccP_2/EspF_M$, which lacks an intact type III secretion signal [89]. Beta-glucuronidase-positive and sorbitol-fermenting EHEC O157 strains harbor an intact $TccP_2/EspF_M$ gene as well as an *$espF_U$/tccP* gene [89]. Although they carry divergent N-terminal secretion signals, $EspF_U$/TccP and $TccP_2/EspF_M$ share the same repeat structure, and $EspF_U$/TccP and $TccP_2/EspF_M$ are functionally interchangeable in EHEC O157 strains [90].

Unexpectedly, $EspF_U$/TccP was also found in EPEC strains of the serotype O119:H6, which express Tir that contains both NPY_{458} and Y_{474} equivalents [90]. Infections of cultured cells have shown that EPEC O119:H6 can simultaneously utilize the Tir:Nck and Tir:IRTKS/IRSp53:$EspF_U$/TccP pathways (Figure 1.3) [130]. Later, this infection strategy was found to be common among EPEC strains belonging to the EPEC2 evolutionally lineage and non-O157:H7 strains, as they encode both a functional $TccP_2/EspF_M$ and a Tir protein that can be tyrosine phosphorylated [129, 89]. These results show the existence of yet another level of redundancy and suggest that Tir-induced actin polymerization is under strong selective pressure.

Figure 1.3: Atypical EPEC and non-O157 EHEC can use the major pathways of both typical EPEC and O157 EHEC to generate actin pedestals

Tir in these strains contain both an Y_{474} equivalent, which initiates actin assembly through Nck (pathway 1), and an NPY_{458} equivalent, which initiates actin assembly through IRTKS/IRSp53 and an $EspF_U$/TccP homologue, $TccP_2$/$EspF_M$ (pathway 2).

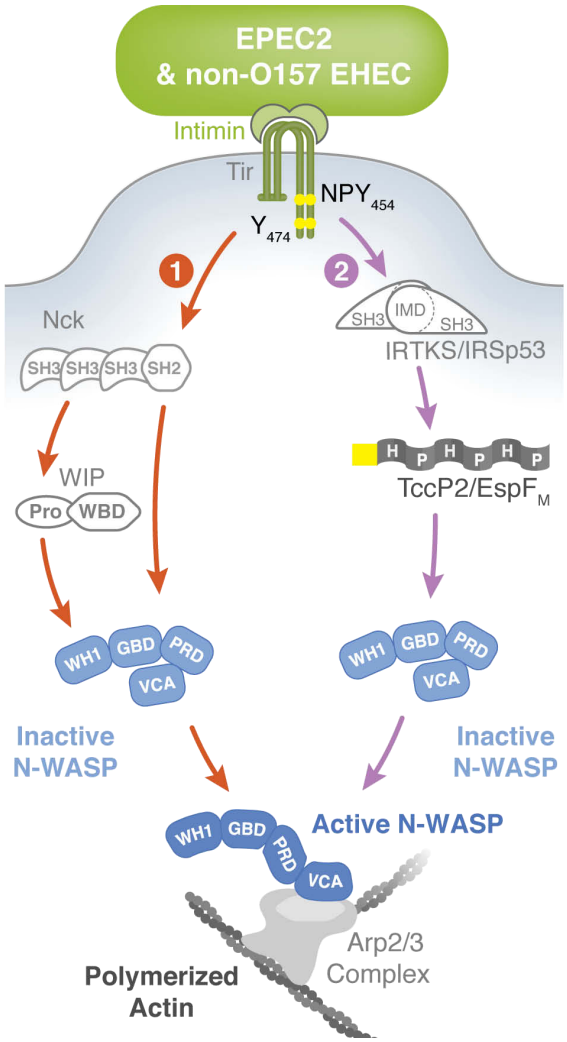

Figure 1.3: Atypical EPEC and non-O157 EHEC can use the major pathways of both typical EPEC and O157 EHEC to generate actin pedestals

1.4.5 Map and EspH impact on Tir-induced actin polymerization

Map and EspH have both been implicated in filopodia formation and modulation of Tir-induced actin polymerization in undifferentiated epithelial cells. While Map is a Cdc42 guanine nucleotide exchange factor (GEF) [15], EspH is a RhoGEF inhibitor that acts by competitively binding to the tandem Dbl-homology and pleckstrin-homology (DH-PH) domains of Dbl-family mammalian RhoGEFs [41]. Ectopic expression of EspH leads to cell detachment, while infections with strains either missing or over-expressing EspH result in short or elongated pedestals, respectively. Importantly, EPEC infection leads to accumulation of WASP-interacting protein (WIP) at the tip of the Tir-induced actin pedestals [51, 133] in a process involving EspH, which itself taggers actin polymerization in a Tir-dependent mechanism [131].

Activation of Cdc42 by Map leads to transient filopodia formation during early stages of infection; interaction of Map with NHERF1 via its PDZ-biding motif is needed for filopodia stabilization [5]. Recovery from the filopodial signals requires phosphorylation of Tir tyrosine Y_{474} and activation of the actin polymerization pathway as either infection of Nck-proficient cells with EPEC expressing Tir Y_{474} or infection of Nck-deficient cells with wild-type EPEC results in persistence of filopodia [5]. The relevance of these pathways in EPEC-induced mivrovilli effacement was recently reported following infection of polarized Caco-2 cells [36]. Taken together, these data show the existence of an elaborated cross talk between Tir and other effectors that subvert actin dynamics.

CHAPTER 2

MICROVILLI EFFACEMENT BY EHEC IS CALPAIN MEDIATED

2.1 Acknowledgements

This chapter is the result of collaborative efforts with the lab of Ira Herman and published in 2011 [69], with significant contributions by Kathleen Riley and Andrew Cai. SEM images were collected by Lara Strittmater in the electron microscopy core at UMMS.

2.2 Introduction

AE pathogens presumably must first dismantle highly organized cell surface structures, namely microvilli, on the apical surface of gut epithelia prior to pedestal formation. Highly specialized to enhance function of the intestines, microvilli not only increase the apical surface area of intestinal epithelial by about 30-fold, but serve as sites of robust transport of water and nutrients [12, 71, 121]. Loss of microvilli would therefore severely impair absorptive capacity and facilitate diarrheal disease. And while pedestal formation by AE pathogens has been well characterized, much less is known about the mechanisms promoting microvillar effacement.

Microvilli are highly organized and uniform. Each microvillus consists of a core bundle of F-actin that is stabilized internally by villin and fimbrin and tethered laterally to adjacent plasma membrane by myosin1A:calmodulin cross-bridges. The bundle is anchored at the base to the terminal web via conventional acto-myosin

interactions that ultimately associate with the basolateral membrane domain terminating in adherens and tight junctions where adjacent epithelial cells are tethered to one another [12, 121]. In addition, ezrin, an ERM family protein required for microvillar development, is found at this apical cytoskeletal-membrane interface of polarized intestinal epithelia, and is thought to bridge the apical plasma membrane to microvillar F-actin core [11, 44]. Core microvillar components are also in constant turnover, making microvilli highly dynamic structures [12, 121]. Because of this, there are several potential host proteins that could be targeted by EHEC to alter the cytoskeleton and yield AE lesions. Given the complexity and inherent dynamic nature of microvilli, AE pathogen-induced microvilli effacement likely involves participation of key host adaptor proteins, just as pedestal formation does.

An important class of eukaryotic cytoskeletal regulators are the calpains, Ca^{+2} dependent proteases that cleave a variety of enzymes and regulatory proteins to modulate cellular function. Calpains are ubiquitously expressed in vertebrates and have been implicated in many important cellular processes, such as regulation of signal transduction, cell spreading and motility, membrane repair, cell death, embryogenesis, and tumor suppression [31, 95, 112]. Many reported calpain substrates are involved in regulating the actin dynamics, especially during cellular adhesion and migration [25, 48, 68, 72, 95, 107]. Several microbial pathogens, promote disease through the inappropriate activation of calpain [35, 45, 55, 93, 114, 127, 136]. EPEC infection results in an increase intracellular Ca^{+2} levels in mammalian cells[4], and induces calpain activity in a manner dependent on type III secretion system [35, 61]. Calpain was previously shown to control EPEC-induced enterocyte effacement in vitro [94].

While calpains roles in effacement and intestinal barrier disruption have been documented for EPEC, its involvement in EHEC infection has not been character-

ized. Since comparative analysis of pedestal formation by EPEC and EHEC have revealed that these related pathogens generate actin pedestals by fundamentally different means [22, 63], we sought to determine if calpain plays an important role in EHEC effacement, as it does in EPEC [94].

2.3 Materials and Methods

2.3.1 Cell culture

CaCo-2a enterocytes, stably transfected with the calpastatin high over-expression plasmid pRC/CMV-3ΔCSN (HOX) or the pRC/CMV empty vector (CON), have been previously described [94]. Cells were grown in Dulbecco's Modified Eagle's Medium supplemented with 10% fetal bovine serum, 1% each penicillin-streptomycin-fungizone (PSF) and L-glutamine. Sub-confluent cultures were maintained in T175 flasks. For experiments, cultures were washed twice with HBSS, released with trypsin-EDTA, and seeded at confluence (approximately 1.5 x 10^5 cells/cm^2) in tissue cultures vessels precoated with collagen (BD #354236). CaCo-2a cells were then allowed to differentiate for 7 to 14 days, and fed every 2 or 3 days. For electron microscopy, cells were seeded onto standard plastic 6-well, tissue culture plates. For immunofluorescence staining, cells were seeded into 24-well glass bottom tissue culture plates (Mattek #P24G-1.5-13F). For calpain activity, cells were seeded into plastic 96-well black walled tissue culture plates with optically clear bottoms (Ibidi #89626).

2.3.2 Bacterial culture and infection

Table C.1 lists all bacterial strains used in this study. The wild type, Stx deficient EHEC strain of serotype O157:H7, strain TUV-93 has been previously described [18]. In preparation for infection, individual colonies from freshly streaked plates were grown in 1 mL of LB with appropriate antibiotics for up to 8 hours. 10 mL of this day culture was transferred to DMEM/100mM HEPES/antibiotics and incubated overnight at 37°C with 5% CO_2 to induce T3SS expression. For infection, bacteria were resuspended in DMEM/2% FBS/20 mM HEPES/2mM glutamine to the following MOIs: EHEC at 500:1, EPEC at 100:1. Higher MOIs were used for

EHEC infections because pilot studies indicated that strain TUV-93 does not adhere to cells as well as EPEC strain JPN15 (data not shown).

2.3.3 Quantification of calpain activity

Calpain activity was assayed using a fluorogenic calpain substrate kit (Anaspec #72150) specific for calpains 1 and 2. CaCo-2a cell monolayers are seeded in 96-well TC treated plates with clear bottoms and black walls (Ibidi #89626) 10 to 14 days prior to use. Cells were infected as described above. Infected monolayers were washed twice with HBSS. 50 mL of assay buffer was added to each well and incubated at room temperature for 5 to 10 minutes. Cells were scraped with a pipette tip and 50 mL of fluorogenic substrate in assay buffer was added to each well. Plates were spun at 1000 rpm (200 x g) on a tabletop centrifuge for 5 minutes to reduce bubbles and incubated at room temperature in the dark for up to 60 minutes. Fluorescence was measured using a Molecular Devices SpecraMax Gemini XS at 354 nm excitation and 442 nm emission and corrected for background fluorescence (i.e. that of wells with substrate only).

2.3.4 Calpastat treatment

Calpastat, a cell-penetrating calpastatin peptide [32] was synthesized at the Tufts Peptide Core Facility using solid phase F-moc chemistry. Peptides were purified by high performance liquid chromatography; molecular mass and purity were confirmed by mass spectrometry. A 25 mM peptide stock was prepared in 100mM HEPES, pH 7.4 and stored at -20°C. For treatments, cell monolayers were washed once with HBSS and cell culture media containing Calpastat at the specified concentrations was added. Cells were incubated at 37°C in 5% CO_2 for 1 hour.

2.3.5 Scanning electron microscopy (SEM)

Cell monolayers were washed twice with HBSS, then fixed by immersion in 2.5% glutaraldehyde in 100 mM sodium phosphate buffer (pH 7.2) for a minimum of 2 hours at room temperature. The fixed samples were then washed three times in the same buffer. Following the third wash, monolayers were dehydrated through a graded series of ethanol to 100% and then critical point dried in liquid CO_2. The bottoms of the dishes were cut off and using silver conductive paste, the plastic disks with the cells attached on the surface were affixed to aluminum SEM stubs and sputter coated with Au/Pd (80/20). The specimens were then examined using an FEI Quanta 200 FEG MK II scanning electron microscope at 10 Kv accelerating voltage. Each specimen was systematically observed at 1000x, 2500x, and 5000x at five separate areas spaced throughout the disk. Representative images at 10,000x were taken with disks tilted about 30°.

2.3.6 Immunofluorescence microscopy

For indirect immunofluorescence imaging studies, CaCo-2a cells were seeded at confluence and allowed to differentiate in 24-well glass bottom culture plates (Mattek #P24G-1.5-13F). At the indicated time points following infection, cells were washed with warm DMEM, then fixed in 4% formaldehyde/DMEM for 5 minutes at room temperature (RT). Cells were permeabilized with 0.1% Triton buffer for 90 seconds at RT, washed 3 times with PBS, and then incubated with the specified primary antibodies for 1 hour at RT. Primary antibodies used were mouse anti-ezrin (Zymed # 357300), rabbit anti-O157 (Gibco), and goat anti-O157 (Fitzgerald Industries #70-XG13). Alexa-flour conjugated secondary antibodies and/or Alexa-488- or 594-conjugated phalloidin (Invitrogen #A12379 or #A12381) were applied for 45 minutes at RT. Images were acquired on a Zeiss 200M inverted microscope with a Hamamatsu

cooled-CCD digital camera (ER) and MetaMorph 7.0 imaging software (Molecular Devices Corp, PA).

2.3.7 Subcellular fractionation and western blotting

Infected and uninfected cells were washed with warm TBS to remove media and unattached bacteria. Extraction buffer containing 40mM HEPES pH 7.2, 50mM PIPES, 75mM NaCl, 1mM $MgCl_2$, 0.5mM EGTA, Protease Inhibitor Cocktail (1:1000, Sigma), 1mM sodium orthovanadate, and 0.1% Triton detergent was applied to the cultures, 0.5ml per well of a 6-well plate, and plates were placed on an orbital shaker at 50 rpm for 10 minutes at room temperature. The extraction buffer was then removed to tubes held on ice. The remaining cellular residue was collected with 200 μL boiling hot Laemmli sample buffer. All extracts were dialyzed against 4L distilled water at 4°C for 4 hours with one water change at 2 hours, using SnakeSkin dialysis tubing, 10K MWCO (Pierce). Dialyzed samples were snap frozen in liquid nitrogen, lyophilized overnight, and brought up in 200 μL each Laemmli sample buffer. All samples were boiled for 3 minutes and loaded onto 10% acrylamide gels for SDS-PAGE, followed by transfer to nitrocellulose membranes. Membranes were stained for ponceau to confirm equal protein loading, then probed for ezrin using monoclonal mouse anti-ezrin (Zymed #357300).

2.4 Results

2.4.1 Calpain activity increases upon EHEC infection

To investigate whether calpain activity is affected by EHEC, we used a calpain-specific fluorogenic substrate (Suc-LLVY-AMC) to measure calpain activity in extracts of EHEC-infected, polarized colonic carcinoma CaCo-2a CON cells. Compared to uninfected cell monolayers, calpain activity increased after three hours of infection by EHEC (Figure 2.1). Pretreatment of polarized cell monolayers with a cell penetrating calpastatin inhibitor for one hour prior to EHEC infection reduced EHEC induced calpain activation to near uninfected levels (Figure 2.1).

Figure 2.1: EHEC increased calpain activity during infection.

Calpain activity was measured with a fluorogenic, calpain-specific substrate (Suc-LLVY-AMC) in lysates of uninfected CaCo-2a cells, or of cells infected with EHEC for three hours with or without pretreatment with 5 mM of Calpastat, a calpain inhibitor. Shown are the means (+/- SE) of 6 determinations.

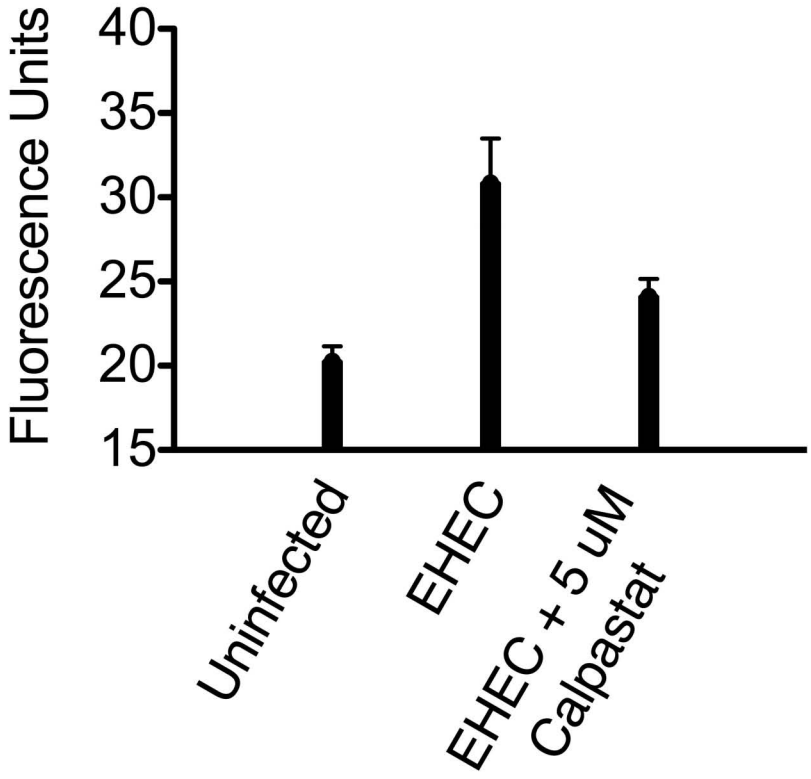

Figure 2.1: EHEC increased calpain activity during infection.

2.4.2 Calpastat, a cell-penetrating calpain inhibitor prevents EHEC-induced effacement

To assess the role of calpain in EHEC induced effacement, we infected polarized CaCo-2a CON cells with or without pretreatment with Calpastat, a cell-penetrating version of the endogenous calpain inhibitor, calpastatin [23, 32]. Scanning electron microscopy of uninfected control cells revealed distinct microvilli and cellular borders, although some variation in the density and arrangement of microvilli was observed (Figure 2.2A, and data not shown).

When CON cells were infected with EHEC and assessed by SEM at low (1000x) magnification (Figure 2.2) or TEM (data not shown), CON cells suffered severe blebbing and rounding, indicating cellular damage (Figure 2.2B). This apparent toxicity was not observed after infection with EPEC (Figure 2.2C), in which cell monolayers looked nearly identical to uninfected monolayers (Figure 2.2A). Pretreatment with 2.5 mM Calpastat for one hour prior to EHEC infection diminished these effects (Figure 2.2D), suggesting that calpain activity is required for this cellular damage and raising the possibility that calpain may be critical for EHEC-induced cellular pathogenesis.

Figure 2.2: EHEC infection produced additional gross monolayer damage that was diminished by inhibition of calpain.

Uninfected CaCo-2a CON monolayers (A), or monolayers infected for two hours with EPEC (C) or EHEC, with (D) or without (B) a one-hour pretreatment with Calpastat (2.5 μM) were visualized by SEM under 1000x magnification. Scale bars are 100 μm.

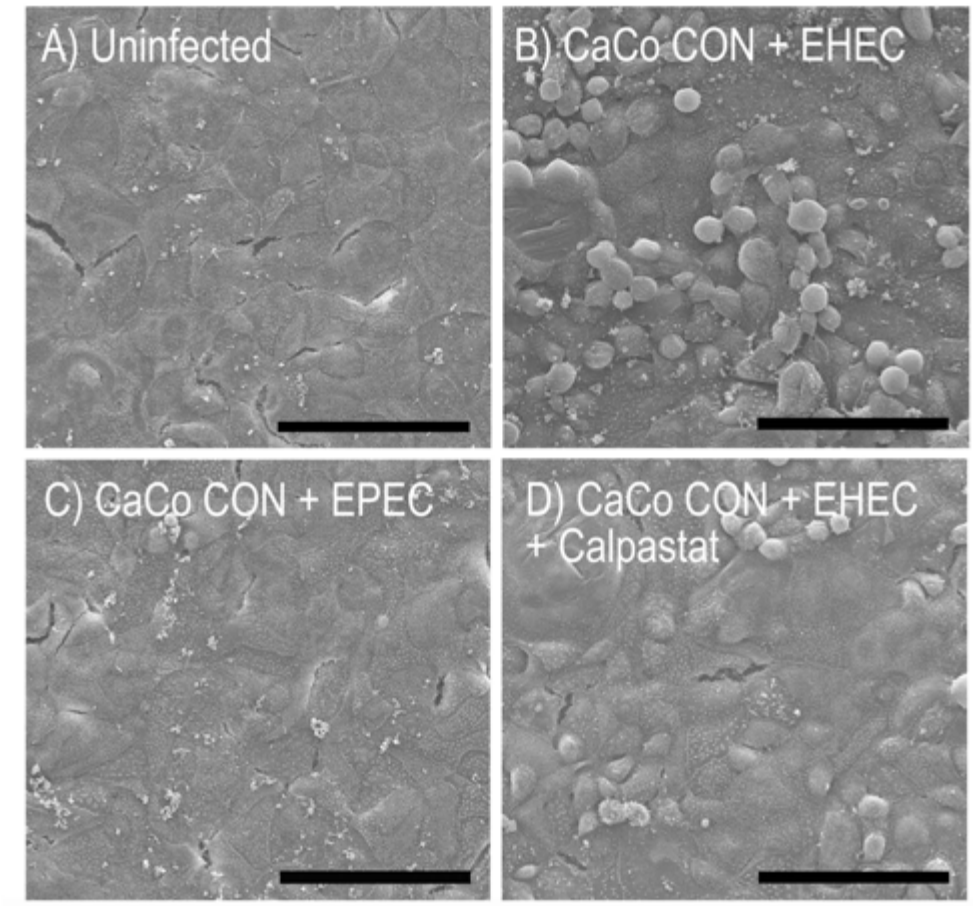

Figure 2.2: EHEC infection produced additional gross monolayer damage that was diminished by inhibition of calpain.

Higher magnification assessment of monolayers at 5000x to 10,000x revealed that a two-hour infection by EHEC resulted in the predicted microvillar effacement (Figure 2.3B) as compared to uninfected controls (Figure 2.3A). When CON cells were subjected to a one-hour pretreatment with 2.5 μM of Calpastat prior to EHEC infection and assessed by 10,000x magnification SEM, most EHEC-bound cells retained largely intact microvilli (Figure 2.3C), similar in quality to uninfected CaCo-2a CON monolayers (Figure 2.3A). As expected, the control infection by EPEC in the absence of Calpastat treatment also revealed effacement (Figure 2.3D).

Figure 2.3: A cell-penetrating calpain inhibitor prevents microvilli effacement by EHEC.

Uninfected CaCo-2a CON monolayers (A) and monolayers infected for 2 hours with EHEC without (B) or with (C) 1 hour pretreatment with 2.5 μM Calpastat, or infected with EPEC (D) were visualized by SEM at 10,000x magnification with a 30°tilt. Arrows point to bacteria infecting surface of Caco-2a CON monolayers. Scale bars are 10 μm.

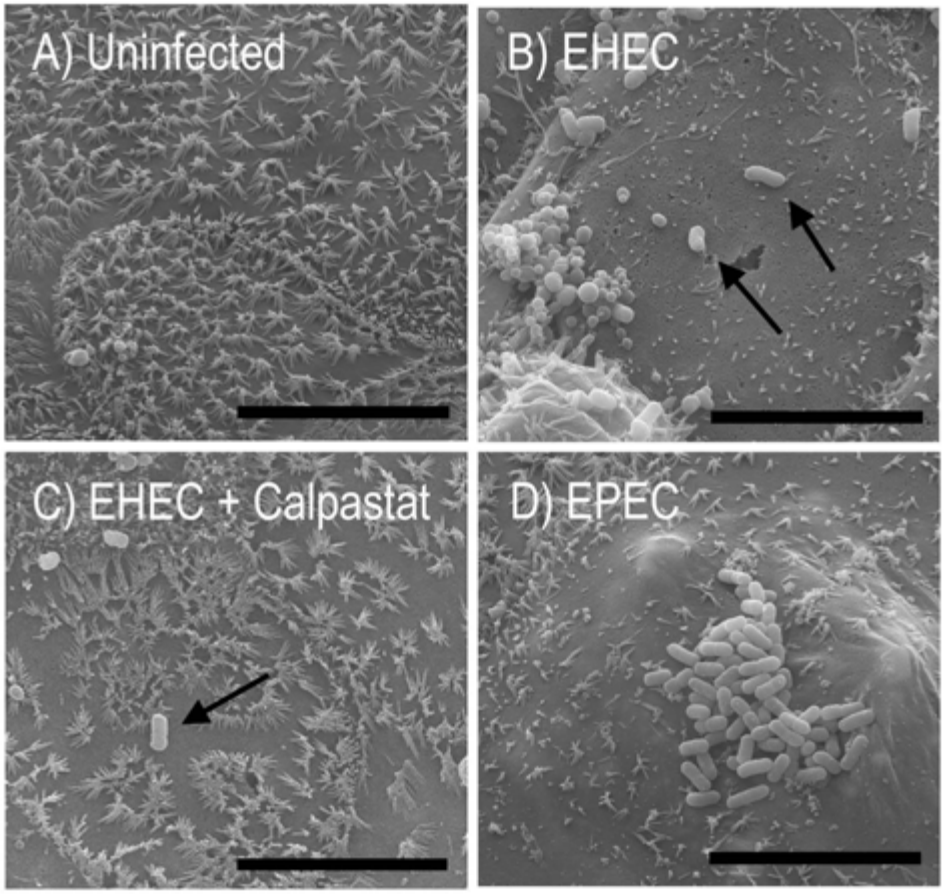

Figure 2.3: A cell-penetrating calpain inhibitor prevents microvilli effacement by EHEC.

2.4.3 Ectopic expression of calpastatin inhibits effacement by EHEC

We previously showed that the calpastatin-overexpressing CaCo-2a cell line, HOX, for which the pRC/CMV vector-transfected CaCo-2a CON line serves as an appropriate wildtype control, resists effacement by EPEC [94]. Like CON cultures, SEM assessment revealed some cell-to-cell variability with respect to microvillar length and density (data not shown); microvilli in HOX cells were, intact and in general, shorter than those observed in CON cells, as previously described [94] (Figure 2.4A).

When stained for F-actin using fluorescent phalloidin, the microvillar F-actin core bundles of polarized CON and HOX cells appeared as a punctate fluorescent pattern on the apical surface (Figure 2.4C and 2.4E) when viewed end-on, while the circumferential belt of F-actin encircling the apical cytoskeletal-membrane domain could also be readily distinguished. This apical F-actin staining pattern was consistent with the pattern of microvilli observed by SEM (Figure 2.3D and Figure 2.4A). In addition, infection of polarized CON cells by EHEC induced the loss of this punctate fluorescent staining (Figure 2.4D), consistent with the loss of microvilli observed during EHEC-induced effacement as revealed by high magnification SEM (Figure 2.3A).

In stark contrast to the effacement of CON cells by EHEC, infected HOX cells retained their microvillar-associated punctate F-actin fluorescence staining (Figure 2.4F). The retention of microvillar integrity by HOX cells after two hours (Figure 2.4F) or three hours (data not shown) was confirmed by SEM (Fig. 2.4B and data not shown). These results indicate that ectopic expression of calpastatin and the concomitant inhibition of calpain renders HOX cells resistant to effacement by EHEC infection.

Figure 2.4: The calpstatin overexpressing cell line, HOX, resisted microvillar effacement by AE pathogens.

Uninfected polarized CaCo-2a HOX monolayers (A) and polarized HOX monolayers infected for 2 hours with EHEC (B) were visualized by SEM at 10,000x magnification and with a 30 tilt. Scale bars for SEMs are 10μm. Polarized control CaCo-2a CON (C and D) and calpastatin-overexpressing CaCo-2a HOX cells (E and F) were stained for F-actin (red) and EHEC (green) without (C and E) or with infection (D and F) by EHEC. F-ctin was stained using Alexa-568-conjugated phalloidin; EHEC were stained with anti-O157 antibody.

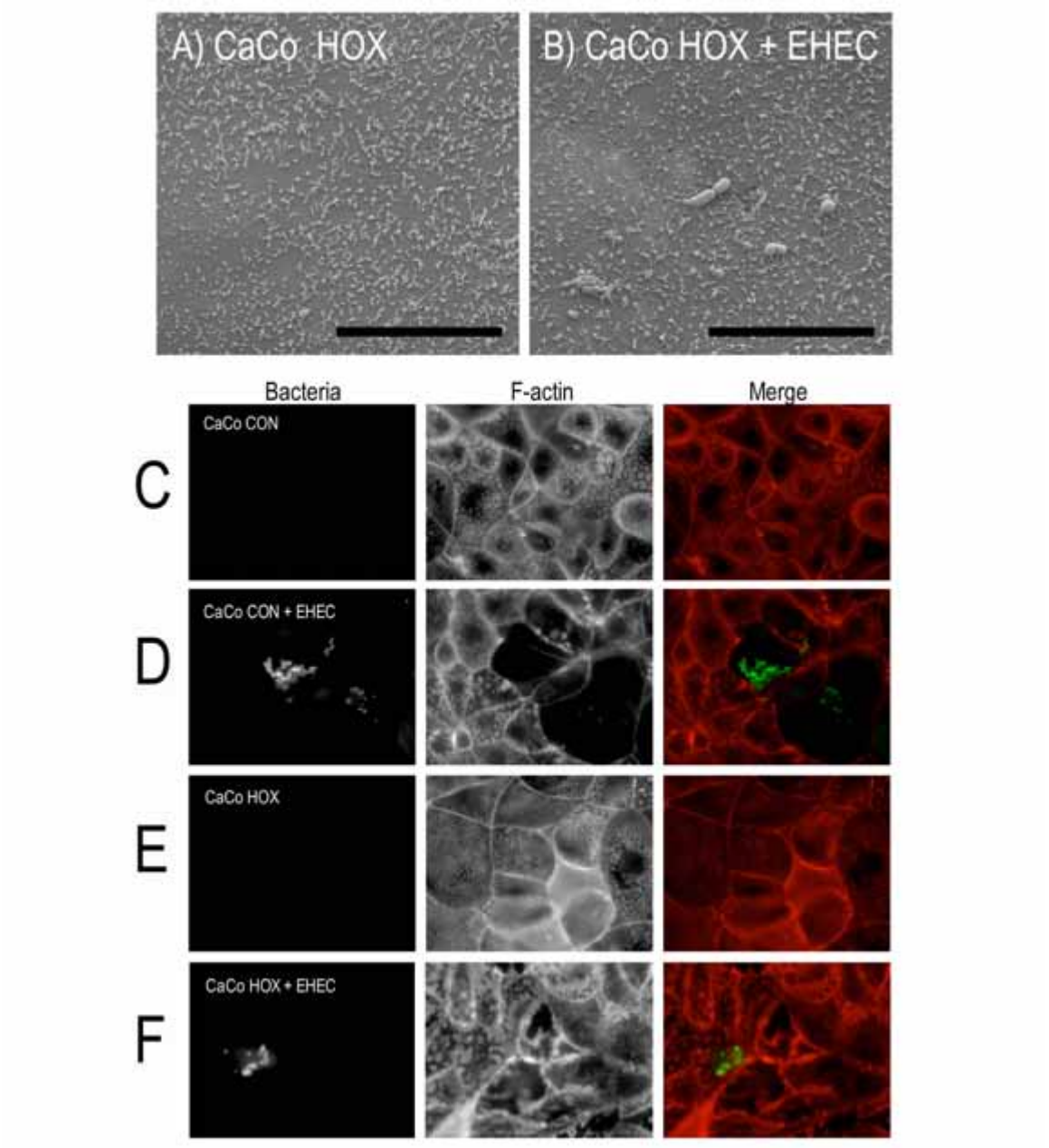

Figure 2.4: The calpstatin overexpressing cell line, HOX, resisted microvillar effacement by AE pathogens.

2.4.4 The calpain substrate ezrin is cleaved in response to EHEC infection and lost from microvilli

We have previously shown that calpain-mediated cleavage of ezrin occurs during cell spreading and migration, a process that, like effacement, involves extensive actin remodeling [95, 94, 107]. Given that EHEC induces calpain activity upon infection of mammalian cells, we tested for ezrin cleavage upon infection by EHEC. Immunoblotting of subcellular fractions of EHEC infected CaCo-2a CON cells revealed ezrin cleavage (Figure 2.5A). The full-length 80 kDa species was detected in both soluble and insoluble fractions. The cleaved 55 kDa ezrin fragment, which is not associated with the plasma membrane, was detected at very slight levels in the soluble fraction of uninfected CON cells. Infection with EHEC increased this pool of cleaved ezrin. This cleavage product was not observed in uninfected or EHEC-infected HOX cells, indicating that calpain is required for its generation (Figure 2.5A).

Immunofluorescence staining of ezrin in polarized CaCo-2a CON cells revealed a punctate pattern at the apical surface almost identical to that of microvilli staining by phalloidin (Figure 2.5B). This staining pattern is consistent with its role in linking the plasma membrane to core microvillar actin bundles [44]. To determine if EHEC-mediated cleavage of ezrin correlated with a change in the cellular distribution of ezrin, we stained CON cells for ezrin after EHEC infection. Interestingly, the punctate ezrin pattern disappeared throughout the entire infected cell (Figure 2.5C). This change in localization was dependent on calpain activity, because calpastatin-overexpressing HOX cells retained their punctate ezrin staining pattern during infection (Figure 2.5D).

Figure 2.5: EHEC infection caused calpain dependent loss of mirovillar ezrin and ezrin cleavage.

Lysates from subcellular fractions of polarized control CaCo-2a CON and HOX monolayers with and without 6 hour EHEC infection by were probed for ezrin by western blot. Asterisk (or arrow) indicates the 55 kDa ezrin cleavage product (A). Polarized CaCo-2a CON cells without (B) and with 6 hour infection by EHEC (C) and EHEC infected polarized HOX monolayers (D) were stained for ezrin (green) and EHEC (red). EHEC was detected by anti-O157 antibody.

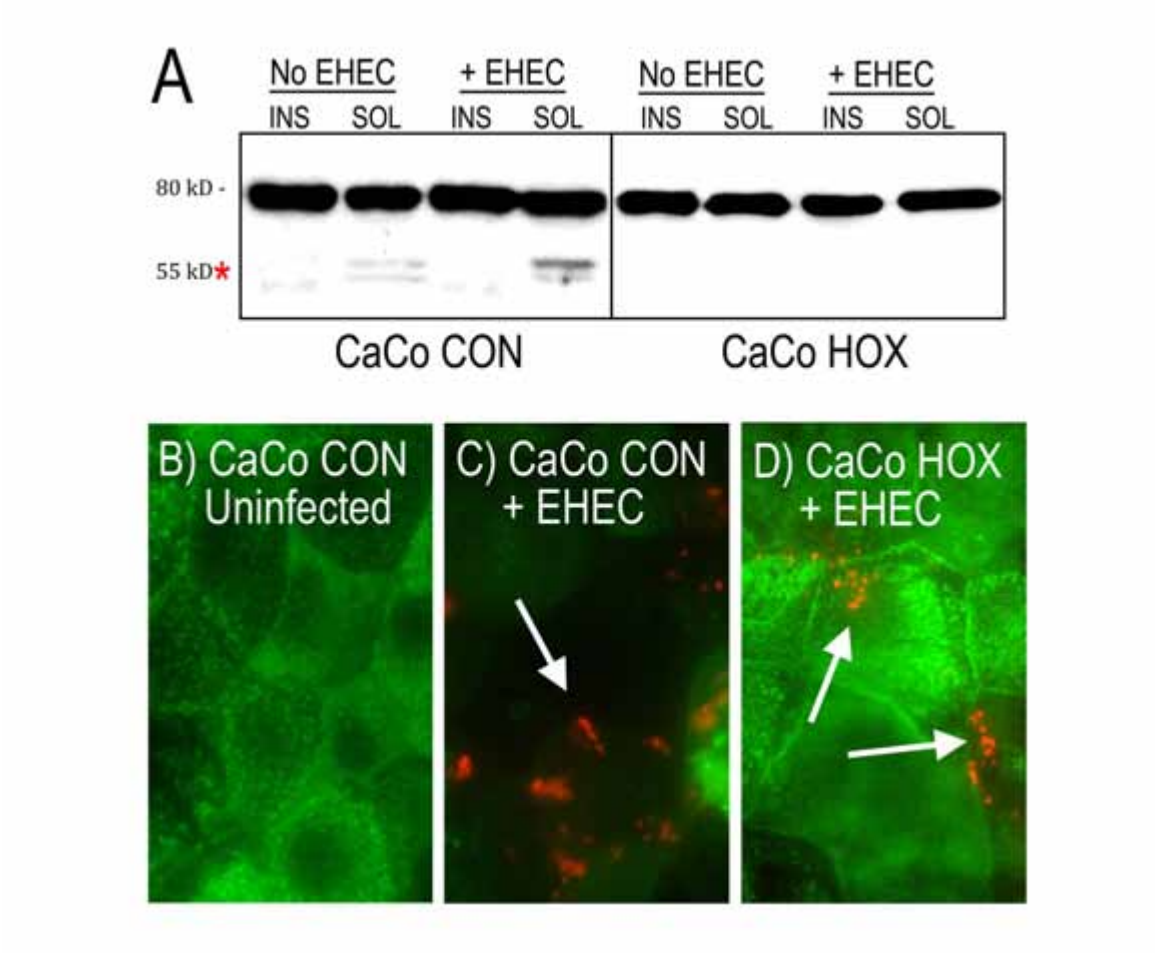

Figure 2.5: EHEC infection caused calpain dependent loss of mirovillar ezrin and ezrin cleavage.

2.5 Conclusions

In response to challenge by AE pathogens, intestinal epithelial cells undergo a coordinated and robust remodeling of the apical membrane-cytoskeletal domain [22, 56, 61]. Highly organized core bundles of actin in the microvilli are disassembled while the apical membrane conforms to newly synthesized actin pedestals. These structural alterations likely disrupt overall epithelial cell function and integrity and contribute to EHEC- and EPEC-induced gasteroenteritis and diarrhea. While the process of pedestal formation is well characterized, the mechanisms of microvillar effacement are poorly understood. Previous work indicated that EPEC infection triggers a rise intracellular Ca^{+2} in mammalian cells [4], and EPEC-mediated effacement requires the Ca^{+2}-regulated host protease, calpain [94]. In this study, we showed that EHEC infection of CaCo-2a cells induces an increase in calpain activity that is required for EHEC-mediated effacement. By analogy to EPEC, we postulate that type III secreted effectors play a role in both calpain activation and microvillar effacement [35, 61].

Effacement likely involves disruption of protein-protein and protein-plasma membrane interactions that contribute to microvillar integrity. Calpain is known to target a number of cytoskeletal elements, including the ERM family member ezrin [47, 48, 72, 95, 107], which contributes to microvillar integrity by indirectly linking the plasma membrane to the axial actin microfilamentous bundles [11, 105, 108]. Another gut pathogen, H. pylori, triggers calpain-dependent cleavage of ezrin in gastric parietal cells, resulting in redistribution of the protein, distortion of microvillar structure and disruption of apical secretory function [127]. We showed here that EHEC-mediated effacement of microvilli is accompanied by calpain-dependent cleavage of ezrin and loss of its apical localization.

The targeting of ezrin by AE pathogens is likely to induce widespread changes in the structure and function of intestinal epithelial cells. EPEC triggers the transient formation of filopodia that are significantly destabilized by the expression of a dominant negative ezrin mutant [6]. Ezrin has also has been implicated in the assembly of junctional complexes [96], and we found that EHEC infection results in a calpain-dependent redistribution away from cell-cell junctions. This relocalization may well have functional consequences on epithelial barrier function, given the observations that the addition of calpain-inhibitory peptides [35] and or the expression of a dominant negative ezrin mutant [109] diminish EPEC-induced disruption of tight junctions and trans-epithelial resistance.

More generally, apical and junctional cytoskeletal domains are functionally integrated: F-actin rich microvillar rootlet structures penetrate the terminal web, making intimate contact with the circumferentially-disposed array of filamentous actin, conventional myosins and intermediate filaments, which all join together in the terminal web at adherens and tight, occluding junctions [10, 43, 87]. Thus, the ability of AE pathogens to dramatically alter the apical cytoskeleton is likely to induce changes in the basolateral and terminal web-associated cytoskeleton including the membrane-cytoskeletal interface. Consistent with this notion, EPEC infection is known to cause the redistribution of many junctional and basolateral domain proteins [59, 60, 84, 85], some of which are recruited to actin pedestals [64, 92]. It will be of interest to determine whether the requirement for calpain in the redistribution of ezrin is reflected in a similar requirement for the redistribution of some or all of these molecules. Finally, we observed EHEC infection of confluent epithelial cell monolayers resulted in striking cell blebbing and rounding, consistent with a general disruption of cell adhesion. Although this damage was calpain-dependent, similar cellular damage was not induced by EPEC, indicating that this manifestation is sep-

arable from effacement and that features specific to EHEC likely contribute to this toxicity. And, while EHEC-mediated cell rounding could be specifically linked to ezrin cleavage, other actin-associated calpain substrates, such as the focal adhesion protein talin and actin assembly factor cortactin may also be involved in the host cytoskeletal adaptive responses [47, 48, 72].

In summary, AE pathogens such as EHEC induce a broad range of cytoskeletal disruption, among them pedestal formation, tight junction disruption and microvillar effacement. These alterations are predicted to diminish both the absorptive capacity and the barrier function of intestinal epithelium, thereby contributing to diarrhea, a major and potentially life-threatening manifestation of disease. The manifold cellular consequences of infection are undoubtedly in part due to diversity of effectors translocated to the cell [118]. In addition, an emerging picture is that a central modulator such as calpain, which has the potential to alter many cytoskeletal structures, may be a conduit through which AE family members, as well as other infectious agents, exert pleomorphic pathogenic effects.

CHAPTER 3

MULTIPLE REPEATS OF ESPF$_U$ ARE REQUIRED FOR PEDESTAL FORMATION BY EHEC

3.1 Acknowledgements

The introduction for this chapter is adapted from the review that I co-authored with Ilan Rosenshine, John Leong, and Gad Frankel [70]. HCT8 cells were a generous gift from the lab of Beth McCormick (UMMS). Douglas Robbins, formerly in the Leong Lab (UMMS), assisted with various infection and immunofluorescence experimets.

3.2 Introduction

Discovered before IRTKS/IRSp53 or the critical NPY$_{548}$ residues of EHEC Tir, EspF$_U$/TccP provided structural insights that helped elucidate both the identity of its linker to EHEC Tir and the mechanism of N-WASP activation. EspF$_U$/TccP consists of an N-terminal secretion signal, followed by (in nearly all isolates) between three and eight repeating elements [54, 52]. Each functional repeating unit contains two structurally and functionally distinct domains, an N-terminal helical section (H) that binds and activates N-WASP, and a C-terminal proline-rich domain (P) with two tandem canonical SH3 binding PxxP motifs that are recognized by the SH3 domain in the C-terminus of IRTKS or IRSp53 [52, 26, 1] (figure 3.1).

Figure 3.1: Diagram of $EspF_U$ structure

$EspF_U$ consists of an N-terminal T3SS signal sequence followed by multiple functional repeating units of helical, N-WASP activation domains (H) and proline rich, IRTKS binding domains (P). Amino acid sequences for the laboratory "full length" $EspF_U$ and the constructed three repeat $EspF_U$ are shown, including the 5 myc tag. Bolded amino acids at L12 and W33 in each repeat of the three repeat $EspF_U$ indicate positions used for single alanine point mutations.

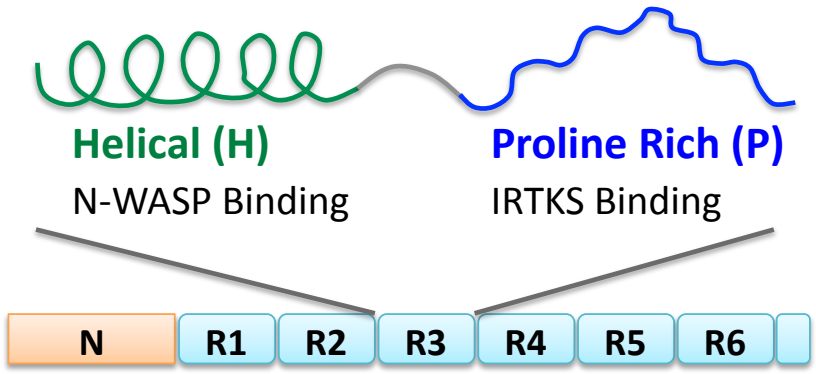

Full Length $EspF_U$:

N-term	MINNVSSLFPTVNRNITAVYKKSSFSVSPQKITLNPVKISSPFSPSS
	SSISATTLFRAPNAHSASFHRQSTAESSLHQQ
R1	LPNVRQRLIQHLAEHGIKPARSMAEHIPPAPNWPAPPPPVQNEQSRP
R2	LPDVAQRLVQHLAEHGIQPARNMAEHIPPAPNWPAPPLPVQNEQSRP
R3	LPDVAQRLVQHLAEHGIQPARSMAEHIPPAPNWPAPPPPVQNEQSRP
R4	LPDVAQRLVQHLAEHGIQPARSMAEHIPPAPNWPAPPPPVQNEQSRP
R5	LPDVAQRLMQHLAEHGIQPARNMAEHIPPAPNWPAPTPPVQNEQSRP
R6	LPDVAQRLMQHLAEHGIQPARNMAEHIPPAPNWPAPTPPVQNEQSRP
	LPDVAQRLMQHLAEHGINTSKRSGSHRFKA
Myc-Tag	MEQKLISEEDLNEMEQKLISEEDLNEMEQKLISEEDLNEMEQKLISE
	EDLNEMEQKLISEEDLNEMESLGDLT

Three repeat $EspF_U$ (HPHPHP):

N-term	MINNVSSLFPTVNRNITAVYKKSSFSVSPQKITLNPVKISSPFSPSS
	SSISATTLFRAPNAHSASFHRQSTAESSLHQQGT
R1	LPDVAQRLMQH**L**AEHGIQPARNMAEHIPPAPN**W**PAPTPPVQNEQSRP
R2	LPDVAQRLMQH**L**AEHGIQPARNMAEHIPPAPN**W**PAPTPPVQNEQSRP
R3	LPDVAQRLMQH**L**AEHGIQPARNMAEHIPPAPN**W**PAPTPPVQNEQSRP
	GSHRFKAMEQKLISEEDLNEMEQKLISEEDLNEMEQKLISEEDLNEM
Myc-Tag	EQKLISEEDLNEMEQKLISEEDLNEMESLGDLT

Figure 3.1: Diagram of $EspF_U$ structure

$EspF_U$/TccP acts through structural mimicry and, remarkably, has evolved to outcompete some endogenous host ligands, making it a most efficient hijacker of mammalian signaling pathways. The H domain of $EspF_U$ is structurally similar to an amphipathic helix in N-WASP's VCA domain. The VCA domain, which functions to activate Arp2/3, is normally maintained in an autoinhibited state by binding of the amphipathic helix to a hydrophobic groove in another domain of N-WASP, the GBD [111, 79, 26]. Endogenous N-WASP activators such as Cdc42 bind the GBD to disrupt this autoinhibition indirectly by altering the GBD structure [111, 79]. In contrast, $EspF_U$'s H domain can bind the GBD in the exact same hydrophobic groove and directly displace the VCA from the GBD, thereby activating N-WASP [26].

Likewise, the P domains of $EspF_U$ act by mimicking natural host proteins. SH3 domains are an abundant and common motif for facilitating cellular interactions and scaffolding proteins. The P domains of $EspF_U$ carry two PxxP motifs, commonly found in mammalian ligands of SH3 domains and recognize the SH3 domain of IRTKS with a higher affinity than some of its natural ligands [1]. This enhanced binding affinity may allow $EspF_U$ to better recruit IRTKS, stealing it away from its natural locales and binding partners within the host cell.

In vitro structural studies show that one single $EspF_U$ repeat is capable of accommodating both the GBD of N-WASP and the SH3 domain of IRTKS without spatial hinderance [54]. However, it is worth noting that more than 99% of $EspF_U$ alleles possess at least three repeats of the functional (i.e. H and P) domains, suggesting that multiple repeats confer a selective advantage to EHEC [54]. Two repeats of $EspF_U$ have been shown to synergistically enhance activation of Arp2/3 *in vitro* [17, 104] through enhanced recruitment of Arp2/3. Arp2/3 is a large multimeric complex that can accommodate two N-WASP proteins [91]. The enhanced actin assembly activity *in vitro* by two $EspF_U$ repeats (HPHP) is due to the scaffolding of

two N-WASP proteins into close proximity by the H domains, which is better able to bind Arp2/3. A single repeat (HP), able to recruit only one N-WASP protein, was less able to recruit and activate Arp2/3. This *in vitro* study makes a compelling case for the advantages of multiple $EspF_U$ repeats. However, the upstream components of pedestal formation, namely IRTKS and Tir have not been studied in regards to this aspect of $EspF_U$'s repeat structure. The ability to recruit actin assembly machinery by avidity is potentially enhanced by the fact that IRTKS and Tir both form homodimers. In addition, dimerization of intimin on the surface of EHEC adds another layer of multimer formation. EHEC may be using a strategy of multimeric complexing through both bacterial and mammalian components not only to hijack essential actin assembly components, but also to concentrate these normally tightly regulated components to sites of bacterial contact in order to enhance attachment to the colonic epithelium.

3.3 Materials and Methods

3.3.1 Cell Culture

HeLa cells were cultured in DMEM supplemented with 10% fetal bovine serum (FBS), penicillin-streptomycin, and 2mM L-Glutamine. Cells were passed when confluent. For immunofluorescence experiments, HeLa cells were washed with PBS, lifted with trypsin-EDTA, and seeded onto #1.5, 12 mm coverslips in 24-well tissue culture plates 12-18 hours before infection.

HCT8, a human intestinal adenocarcinoma cell line, generously provided by the lab of Beth McCormick, were cultured in RPMI 1640 (Invitrogen) supplemented with 10% FBS, 25 mM HEPES, penicillin-streptomycin, and 2mM L-Glutamine. Subconfluent cultures were maintained at below 80% confluence. For experiments, HCT8 cells were washed twice with HBSS, once with trypsin-EDTA, incubated with trypsin-EDTA for 5 to 10 minutes at 37°C, and seeded onto collagen coated tissue culture vessels. For non-polarized cell conditions, cells were seeded onto collagen (BD #354236) coated #1.5, 12 mm coverslips in at approximately 100,000 cells/cm^2 for 50% confluence or 2.5 x 10^5 cells/cm^2 for 100% confluence. For polarized cell conditions, cells were seeded at confluence (approximately 2.5 x 10^5 cells per cm^2) onto collagen coated polyester transwells with 3.0 μm pores (Coring # 3462) and allowed to differentiate for 5 to 6 days.

3.3.2 Bacterial strains

Table C.1 lists all bacterial strains used in this work. TUV-93.0, a clinical EHEC isolate with both STX toxin phages removed was used at the background EHEC strain [18]. TUV-93.0 Δdam strains were generated by λ red recombineering as described in [83] to increase infectivity of TUV93.0 on polarized HCT8 cells. Mutants were screened by PCR. Primers and plasmids used for recombineering are listed in tables C.2 and C.3.

3.3.3 Mutation of $EspF_U$

The $EspF_U$ truncation mutants HP, HPH, PHP, HPHP, and HPHPH were generated by restriction digestion of previously constructed mammalian expression plasmids and ligation into pDV48, a bacterial expression plasmid containing the N-terminal T3SS signal sequence of $EspF_U$, followed a short MCS containing KpnI and BamHI restriction sites, and a 5-myc tag. The sequence for 3 repeats (HPHPHP) (figure 3.1) was ordered as a mini-gene from IDT with flanking Kpn I and BamHI sites. All inserts were cloned into the pDV48 in between KpnI and BamHI.

PHPHP, PH*PHP, PHPH*P, and the series of mutants based on HPHPHP were generated by SLIM PCR mutagenesis according to [27] using Platinum Pfx (Invitrogen #11708013) or Phusion (NEB #M0530S) high fidelity polymerases. Tables C.2 and C.3 list all primers used for SLIM and product plasmids generated respectively.

All plasmid constructs were confirmed by sequencing.

3.3.4 Infection

In preparation for infection, 1 mL of LB with appropriate antibiotics were inoculated with strains from single colonies from plates that were less than two weeks old and incubated at 37°C on a rotating wheel for up to 8 hours. 10 μL of this "day culture" was transferred to DMEM/100mM HEPES/antibiotics and incubated overnight, standing at 37°C with 5% CO_2 to induce T3SS expression. Overnight cultures were then diluted 1/5 to 1/6 in fresh DMEM/100 mM HEPES and grown to mid-log on a wheel at 37°C. Cultures were collected for use between an OD_{600} of 0.5 to 0.6. For infection, bacteria were then resuspended in DMEM/2% FBS/20 mM HEPES/2mM glutamine ("FAS media") to the following MOIs: EHEC at 1:10 to 1:50 for cells on coverslips and 1:100 to 1:200 for cells in transwells. Cells seeded in coverslips were infected with 500 μL of bacteria resuspended in FAS media. Cells seeded in 12-well transwells were infected with 200 μL of resuspended bacteria api-

cally (top/inner transwell) with 1 mL of FAS media in the bottom/outer well. Infected cells were then spun at low speed (200 x g) for 10 minutes at room temperature to facilitate settling of bacteria onto cell monolayers. Infected cells were incubated at 37°C with 5% CO_2 for 5 to 6 hours.

3.3.5 Congo red induction of T3SS effectors

Bacteria were grown in the same manner as in preparation for infections. 5 mL of mid-log cultures in DMEM/100 mM HEPES were spun down and resuspended in 1 mL of PBS with 20 μm congo red. Bacteria were incubated on a wheel at 37°C for and additional hour. Bacteria were spun down at 5000x g. Bacterial pellets and congo red solution with secreted T3SS effectors were collected separately. Effector proteins were precipitated from congo red solutions by addition of 20% TCA per volume and incubation at 4°C overnight. TCA precitipated proteins were spun down at 14,000 rpm at 4°C for 30 minutes and washed once with 500 μL acetone. After a 10 minute spin at 14,000 rpm at 4°C, removal of acetone and air drying at room temperature, samples were boiled in equal volumes of 1x SDS laemmli dye, run on SDS-PAGE, and probed for myc to confirm secretion of myc-tagged $EspF_U$ mutants.

3.3.6 Immunoflourescence and imaging

During the last half hour of infection, bacterial cells were "pre-stained" with DAPI. Briefly, cells were washed twice apically with warm FAS media. A 1:200 DAPI solution in FAS media was gently pipetted onto the apical surface (inner chamber of transwell) of infected cells. Cells were incubated for and additional 30 minutes at 37°C with 5% CO_2.

Infected cells were then processed for routine immunofluorescent staining. Cells were washed twice with warm HBSS (HCT8 cells) or PBS (all other cells), fixed in 4% paraformaldehyde in PBS for 25 to 30 minutes standing at room temperature,

washed twice with PBS, permeabilized with 0.1% triton X-100 in PBS for 5 minutes with gentle rocking at room temperature and washed twice again with PBS. Each wash was performed with gentle rocking for 2 to 5 minutes at room temperature. Samples were incubated in primary antibody solutions, made in sterile 1% BSA in PBS, with gentle rocking for 1 hour at room temperature or overnight at 4°C. Samples were washed twice in PBS before incubation with secondary antibodies and Alexa-fluor conjugated phalloidin at 1:400 in 1% BSA in PBS for 1 hour at room temperature with gentle rocking. For some experiments, primary antibodies were directly conjugated to Alexa-Fluors using APEX Alexa-Fluor antibody labeling kits (Invitrogen #A10494, #A10475) according to manufacturer instructions. Table C.4 lists all antibodies used in this work and their concentrations . Adobe Photoshop, ImageJ, and Volocity were used for general image processing.

Images were acquired on a Leica SP5 scanning confocal microscope (200 Hz, frame averaged 4 times, at 0.21 μm steps), Ziess Axiovert 200M with Apotome attachment (0.22 μm steps), or Deltavision deconvolution microscope system (0.22 μm steps). Laser power, gain, offset, and exposure levels were adjusted to positive controls and fixed for acquisition of images for each experiment. Volocity (Perkin Elmer) and Photoshop (Abode) were used for general image processing.

3.4 Results

Expression and T3SS secretion of all myc tagged $EspF_U$ constructs from complemented EHEC strains were confirmed by Congo red T3SS induction assay (data not shown).

3.4.1 PHP is the minimum $EspF_U$ requirement for actin pedestal activity in non-polarized cells

To investigate whether multiple $EspF_U$ repeats enhanced actin pedestal activity in infected cells, truncations of $EspF_U$ were cloned and used to complement an EHEC $\Delta EspF_U$ strain.

While one repeat of $EspF_U$ is sufficient to bind both the SH3 domain of IRTKS and the GBD of N-WASP *in vitro* [26, 104], it was not able to generate pedestals when delivered into cultured cells by infection. Figure 3.2 shows HeLa cells infected with EHEC Δdam $\Delta espF_U$, complemented with various truncation mutants of $EspF_U$ up to 3 full repeats and a wildtype $EspF_U$ construct, consisting of six and a half repeats. (for sequences, see figure 3.1). Actin pedestals appear as distinct concentrations of actin next to or underneath intimately bound bacteria. When able to generate pedestals, Myc tagged $EspF_U$ constructs are localized as distinct foci at pedestal tips immediately beneath attached bacteria.

An $EspF_U$ construct with an additional H domain following one repeat (HPH) did not allow for pedestal formation. However, a construct with an additional P domain preceeding a repeat (PHP) did produce pedestals that were indistinguishable from pedestals formed by wildtype $EspF_U$. $EspF_U$ constructs containing two (HPHP) or three full repeats (HPHPHP) also made wildtype-like pedestals upon infection of HeLa cells.

Figure 3.2: The minimal $EspF_U$ repeat requirement for pedestal formation is PHP.

HeLa cells infected with EHEC Δdam $\Delta espF_U$ strains complemented with truncation mutants of $EspF_U$ or full length $EspF_U$ (last row) were stained for bacteria (blue), tagged $EspF_U$ construct (red), and actin (green).

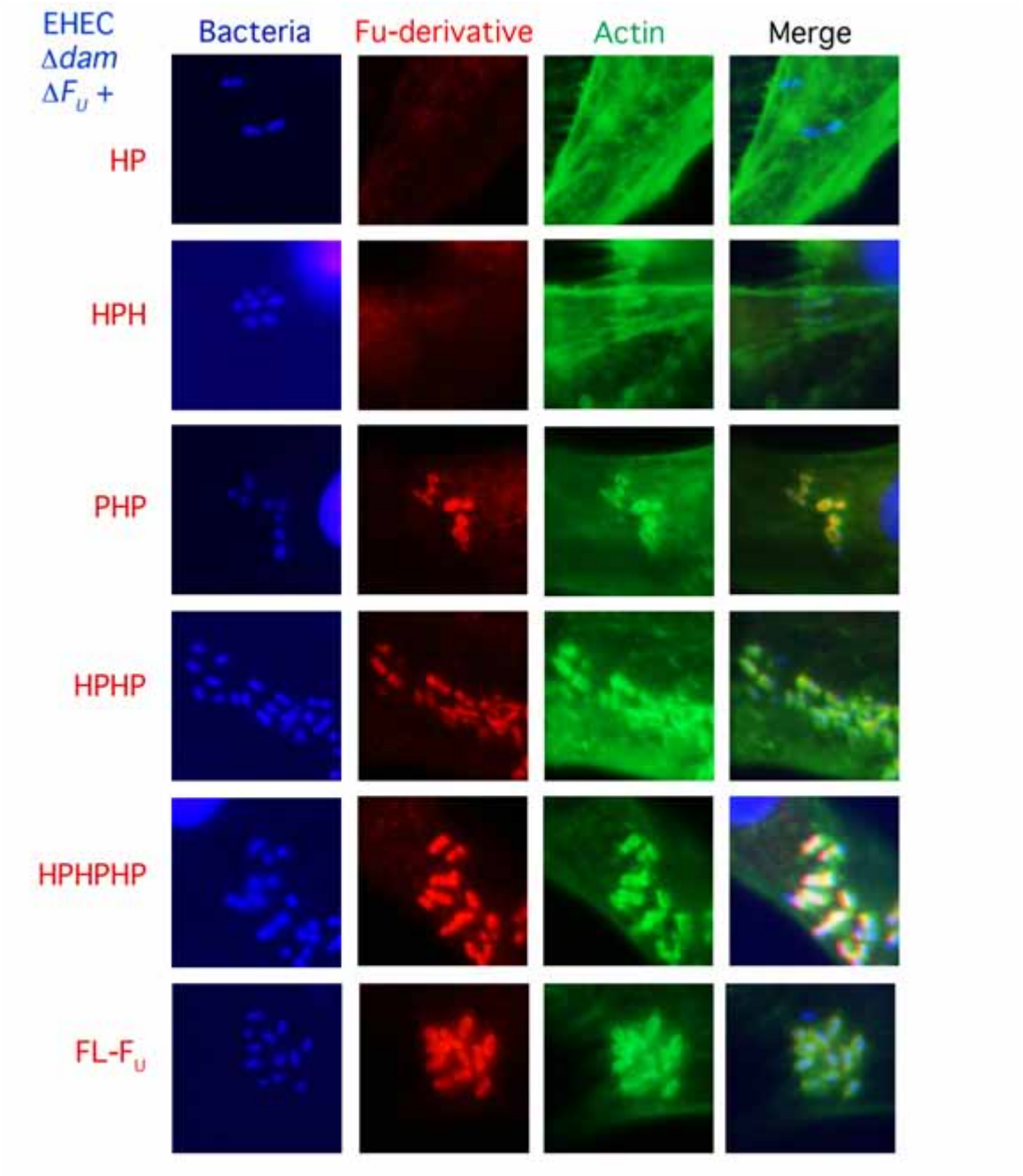

Figure 3.2: The minimal $EspF_U$ repeat requirement for pedestal formation is PHP.

3.4.2 At least 3 repeats of $EspF_U$ are needed to generate pedestals in polarized intestinal cells

While HeLa cells have been a mainstay of cultured cell models for decades, they may lack proteins, signaling pathways, or structures that are found in gut epithelia. Several existing intestinal cell lines can be induced to form more physiologically relevant monolayers which may be more appropriate for the study of gut pathogens such as EHEC. Cell lines such as T84, Caco-2, and HCT8 can be cultured in transwell supports, porous membranes that hang within wells of media, which induce differentiation of these cell lines to organize and produce structures that are more characteristic of intestinal epithelia. HCT8 cells were chosen as our model for studying pedestal formation for their ease of culture, minimal time for polarization, and lack of true mirovilli, which would eliminate the need for effacement. After polarization for 5 to 7 days in 3.0 μm polyester transwells, HCT8 monolayers adopt a honeycomb-like arrangement with apical and basolateral surfaces that can be clearly seen upon actin staining.

HCT8 cells were polarized as described in materials and methods and infected with EHEC Δdam $\Delta espF_U$ strains complemented with various truncation mutants of $EspF_U$. The minimal pedestal competent $EspF_U$ construct in HeLa cells, PHP, does not allow for pedestal formation in polarized HCT8 cells; three full repeats are now required to generate pedestals (figure 3.3). HPHPHP was able to generate pedestals that were similar to those produced by full-length $EspF_U$. Of the bacteria attached for these two pedestal competent strains, only a minority of bacteria generated pedestals.

Figure 3.3: A minimum of 3 $EspF_U$ repeats are required for actin pedestal formation in polarized HCT8 cells

Polarized HCT8 cells infected with EHEC Δdam $\Delta espF_U$ complemented with truncation mutants of $EspF_U$ or full length $EspF_U$ (last row) were stained for bacteria (blue), tagged $EspF_U$ construct (red), and actin (green).

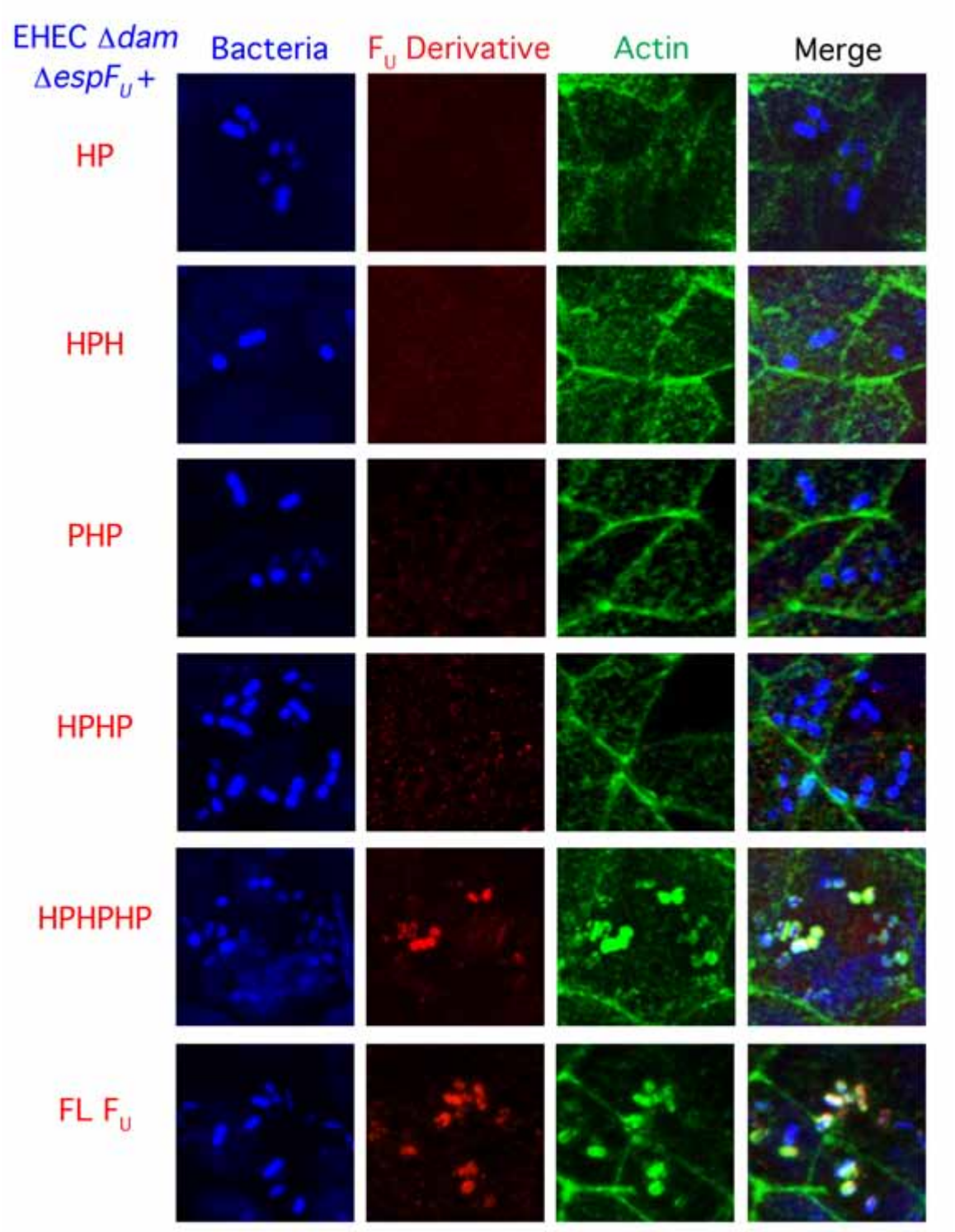

Figure 3.3: A minimum of 3 $EspF_U$ repeats are required for actin pedestal formation in polarized HCT8 cells

The difference in the $EspF_U$ repeat requirement could be a reflection of the change in cell type. To investigate this phenotype difference, HCT8 cells were seeded onto collagen coated coverslips at subconfluence (roughly 50% or 100,000 cells per cm^2) and confluence (roughly 100% or 250,000 cells per cm^2) and infected the next day. EHEC $\Delta dam\ \Delta espF_U$ complemented with PHP were able to generate actin pedestals in HCT8 cells at subconfluence, as were strains complemented with HPHP and HPHPH. Interestingly, when HCT8 cells were seeded at confluence, the cell monolayer adopted a honeycomb-like arrangement similar to that of HCT8 cells polarized on transwells. Confluent HCT8 cells in this state also required at least 3 repeats of $EspF_U$ for actin pedestal formation (figure 3.4). In areas where the confluent monolayer was discontinuous, PHP was able to generate pedestals only in cells at edges of the monolayer.

Figure 3.4: HCT8 cell confluence affects $EspF_U$ repeat requirements for pedestal formation

HCT8 cells seeded onto coverslips at subconfluence (50%) and confluence (100%) were infected with EHEC Δdam $\Delta espF_U$ complemented with PHP. Infected cells were stained for bacteria (blue), tagged $EspF_U$ construct (red), and actin (green). The bottom image shows an area at an edge of a confluent HCT8 monolayer. White arrows point to bacteria producing actin pedestals on cells at and edge of the monalayer. White arrowheads point to bacteria attached to areas of confluent HCT8 that are unable to generate actin pedestals.

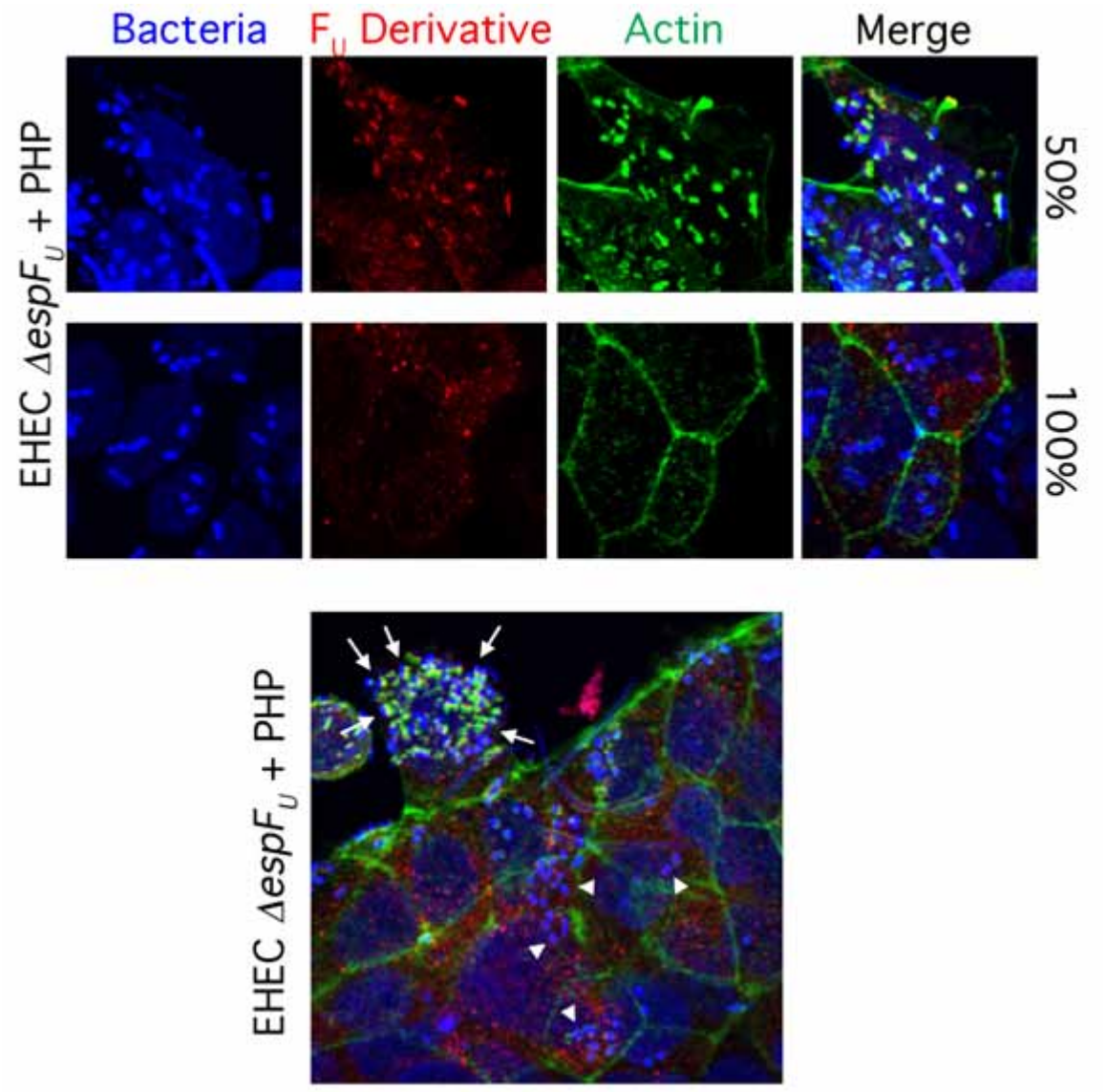

Figure 3.4: HCT8 cell confluence affects $EspF_U$ repeat requirements for pedestal formation

3.4.3 Both H and P domains are necessary for actin pedestal formation in infected cells

Previous work in our lab [110] and by Sallee et al [104] have identified key amino acid residues within the H and P domains of $EspF_U$ which are required for binding to the GBD of N-WASP and the SH3 domain of IRTKS respectively. Within the H domains, alanine mutations at positions V4, L8, or L12, residues which face into the VCA binding pocket of N-WASP's GBD, can individually abrogate binding to N-WASP.

Within each P domain, mutation of the prolines in either of the two tandem PxxP motifs, can disrupt binding to the IRTKS SH3. Mutation of a critical W residue at position 33 in between the two tandem PxxP's can also significantly disrupt binding [2, 110].

To further investigate the nature of the requirement for $EspF_U$ repeats in actin pedestal formation, a series of mutants based on the three repeat construct HPHPHP was generated using the L12A mutation to disrupt binding and activation of N-WASP and the W33A mutation to disrupt binding and recruitment by IRTKS. Domains carrying these point mutations are indicated by *.

Figure 3.5: Both H and P domains are required for actin pedestal activity in polarized HCT8 cells

Polarized HCT8 cells infected with EHEC Δdam $\Delta espF_U$ strains complemented with HPHPHP, H*PH*PH*P or HP*HP*HP* were stained for bacteria (blue), tagged $EspF_U$ construct (red), and actin (green).

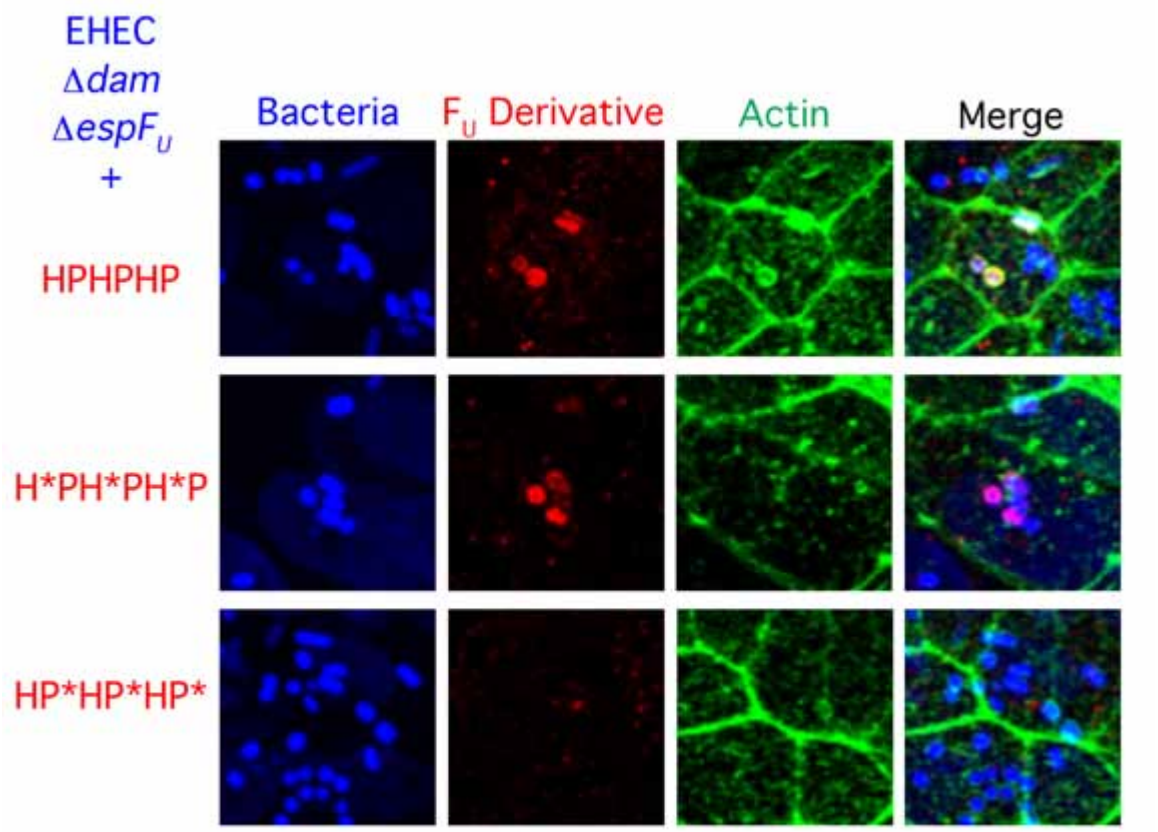

Figure 3.5: Both H and P domains are required for actin pedestal activity in polarized HCT8 cells

Sufficient binding activity of both the H and P domains to N-WASP and IRTKS respectively are required for pedestal formation. When all three H domains of HPHPHP are mutated, the construct (H*PH*PH*P) was unable to generate actin pedestals in infected polarized HCT8 cells. The construct itself can be recruited to sites of bacterial attachment, appearing as distinct foci closely associated with bound bacteria. However, actin is not organized around these foci, indicating that the three point mutations in the H domains have not activated N-WASP (Figure 3.5). The presence of the W33A mutation in all three repeats (HP*HP*HP*) prevents recruitment of the construct, thus preventing actin organization at sites of bacterial attachment. No foci are seen associated with attached bacteria in polarized HCT8 monolayers infected with EHEC Δdam $\Delta espF_U$ complemented with HP*HP*HP*.

3.4.4 Only one active H domain is needed for pedestal formation

The H and P domains of each $EpsF_U$ repeat serve distinct and separate functions. Are multiple units of each domain also required to form actin pedestals in polarized HCT8 monolayers?

To investigate the requirement for the H domains, polarized HCT8 cells were infected with EHEC Δdam $\Delta espF_U$ strains complemented with various 3 repeat constructs with the L12A mutation in one or two H domains. All constructs were able to generate pedestals in polarized HCT8 cells, regardless of the position of the H* mutation or mutations within the three repeats (Figure 3.6).

In non-polarized cells (HeLa, or subconfluent HCT8), all mutants also generated pedestals as robustly as the fully fuctional 3 repeat construct, HPHPHP (Table 3.1).

Figure 3.6: One H domain is sufficient to generate actin pedestals in polarized HCT8 cells

Polarized HCT8 cells infected with EHEC Δdam $\Delta espF_U$ strains complemented with mutants of HPHPHP containing one or two L12A mutations in H domains were stained for bacteria (blue), tagged $EspF_U$ construct (red), and actin (green).

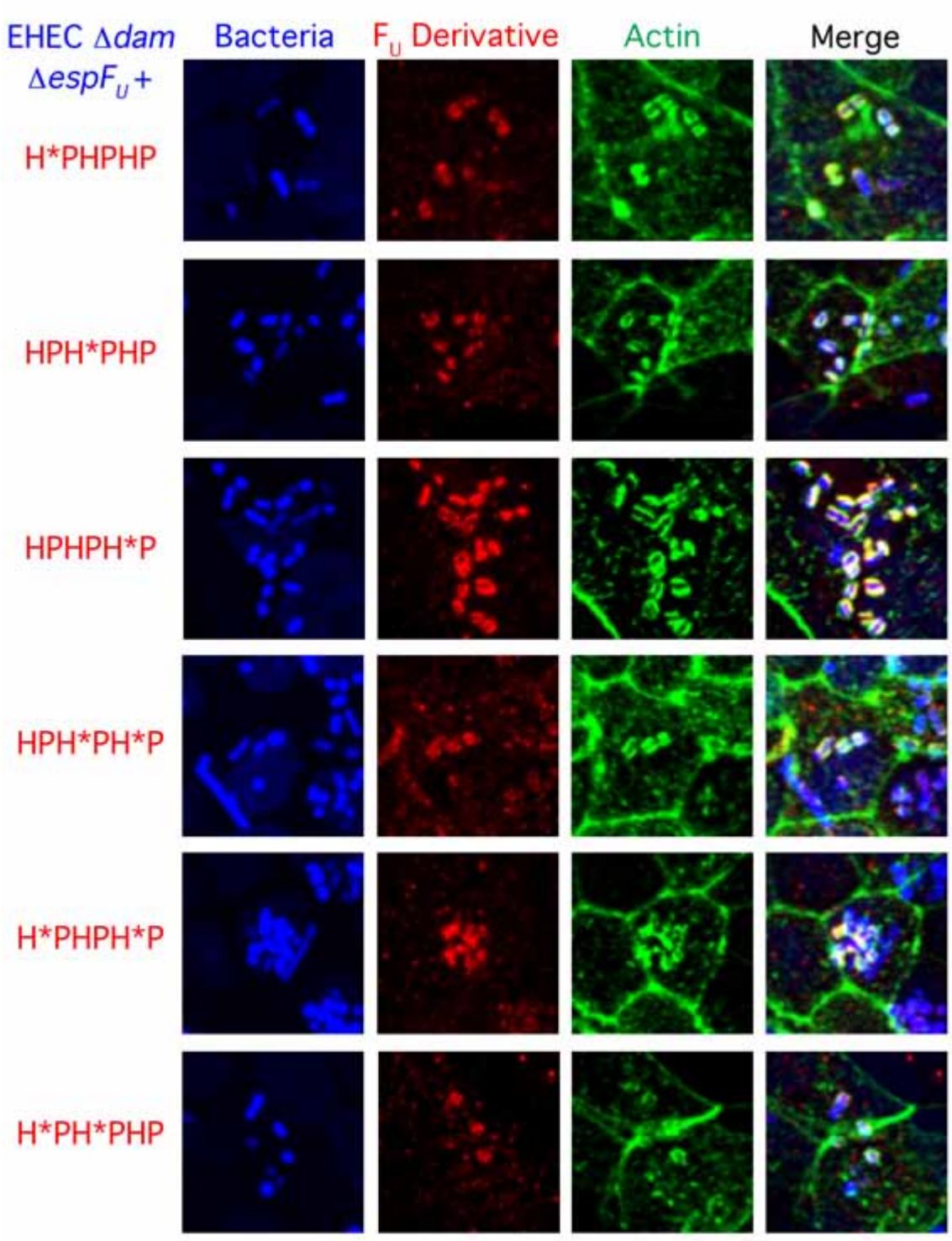

Figure 3.6: One H domain is sufficient to generate actin pedestals in polarized HCT8 cells

3.4.5 Multiple P domains are required for pedestal formation

To investigate the requirement for the P domains, polarized HCT8 cells were infected with EHEC Δdam $\Delta espF_U$ strains complemented with various 3 repeat constructs with the W33A mutation in one or two P domains. A mutation in any one of the P domains prevents pedestal formation in polarized HCT8 cells.

In non-polarized cells (HeLa, or subconfluent HCT8), all mutants with 2 functional P domains in any position were able to generate pedestals as robustly as the fully fuctional 3 repeat construct, HPHPHP. Mutants with only one functional P domain in any position were able to generate pedestals with much less efficiency.

An $EspF_U$ construct of less than 3 full repeats was able to generate actin pedestals in polarized HCT8 cells if it contained three functional P domains and at least one H domain. Pedestals were apparent in cells were infected with EHEC Δdam $\Delta espF_U$ strains complemented with a PHPHP (Figure 3.8). Variants of this construct bearing one L12A mutation in either H domain were also able to form actin pedestals. In contrast, the mutant HPHPH was not able to generate actin pedestals.

Figure 3.7: 3 Functional P domains are required to generate actin pedestals in polarized HCT8 cells

Polarized HCT8 cells infected with EHEC Δdam $\Delta espF_U$ strains complemented with mutants of HPHPHP containing one or two W33A mutations in P domains were stained for bacteria (blue), tagged $EspF_U$ construct (red), and actin (green).

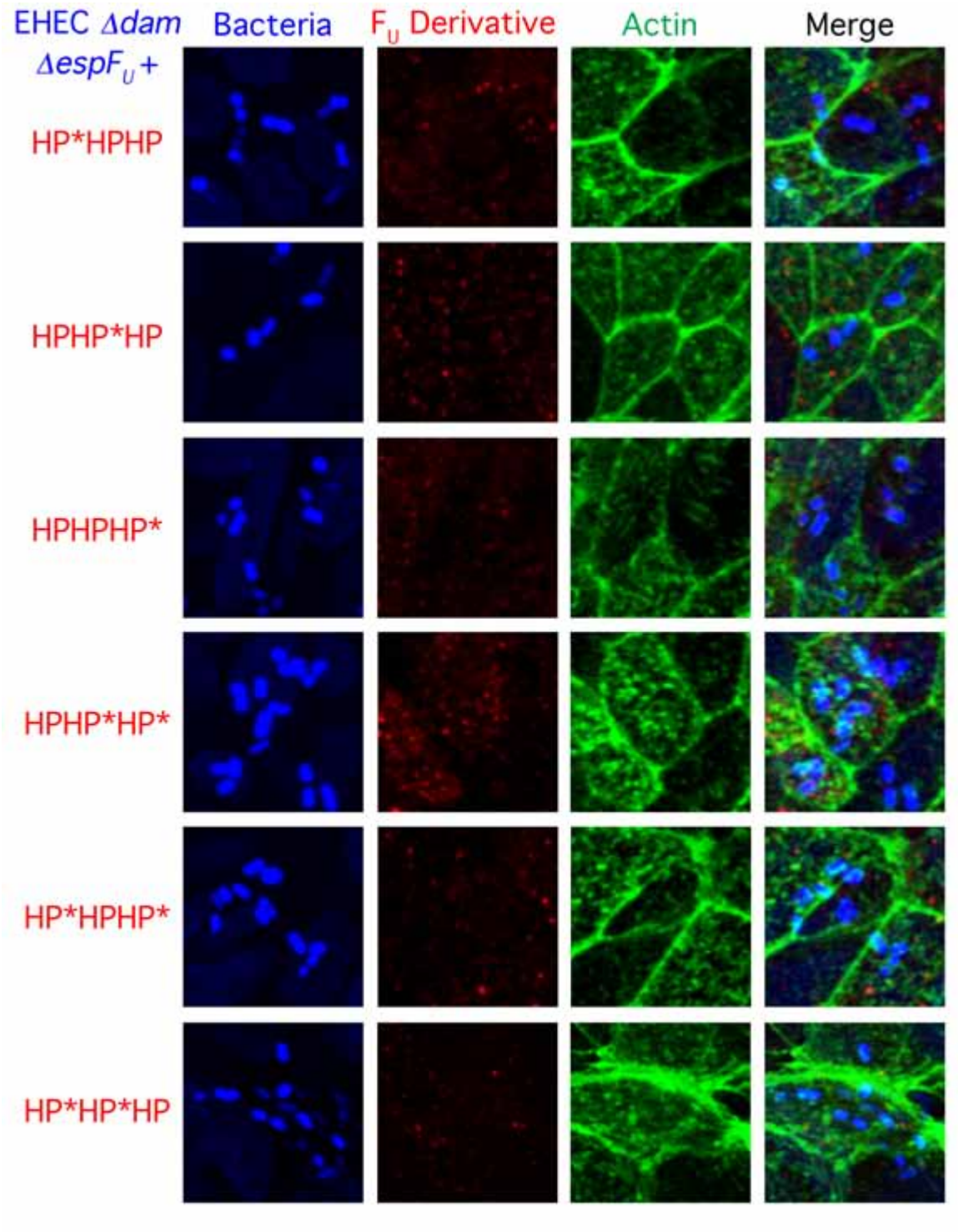

Figure 3.7: 3 Functional P domains are required to generate actin pedestals in polarized HCT8 cells

Figure 3.8: PHPHP but not HPHPH is able to generate actin pedestals in polarized HCT8 cells

Polarized HCT8 cells infected with EHEC Δdam $\Delta espF_U$ strains complemented with HPHPHP (top row) or two and a half repeat versions of $EspF_U$ were stained for bacteria (blue), tagged $EspF_U$ construct (red), and actin (green).

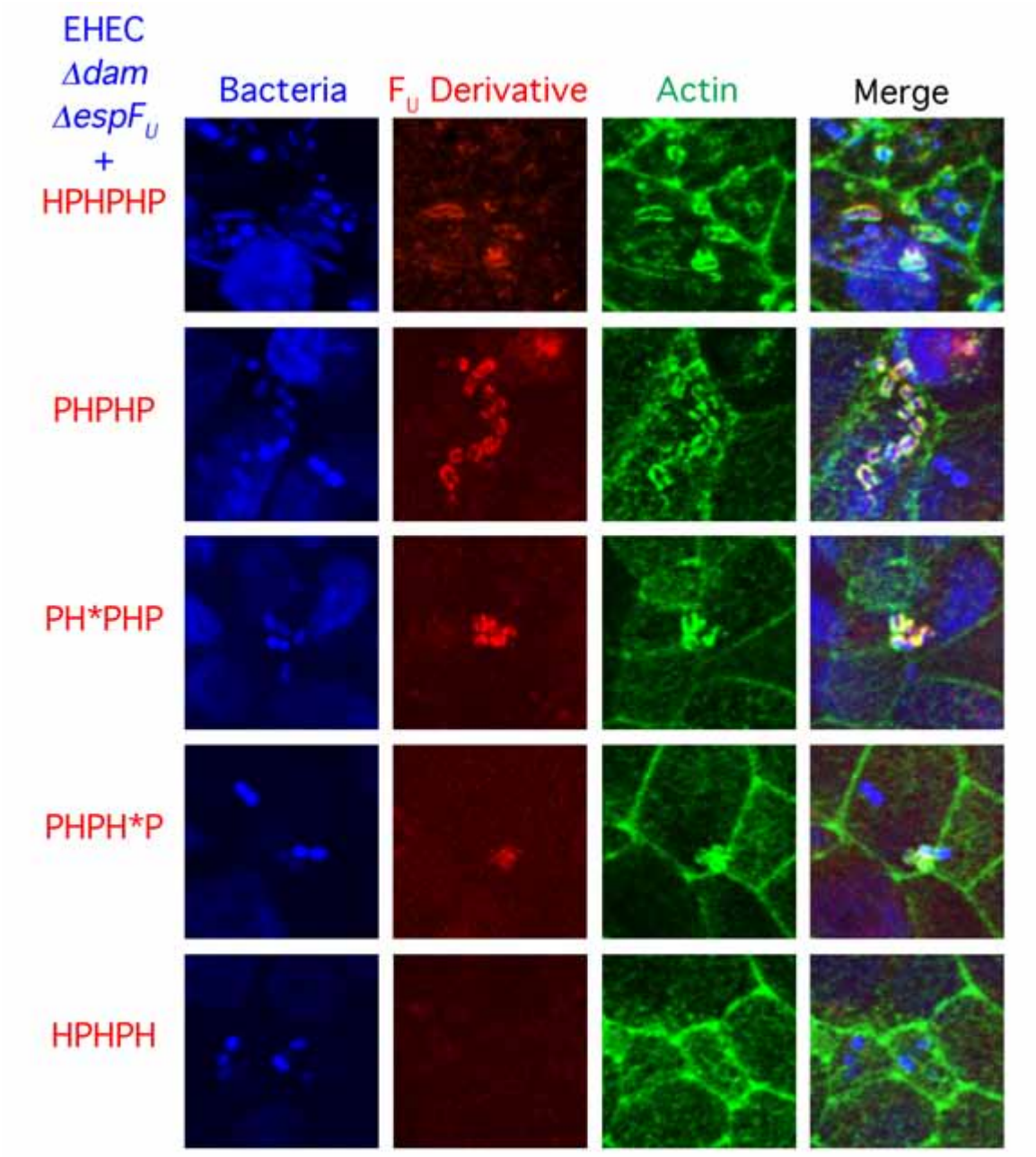

Figure 3.8: PHPHP but not HPHPH is able to generate actin pedestals in polarized HCT8 cells

3.4.6 P domain mutants show partial pedestal activity in non-polarized cells

Actin pedestals can be observed in HeLa cells infected with EHEC $\Delta dam\ \Delta espF_U$ strains complemented with HPHPHP constructs with two W33A mutations, leaving one functional P domain (Table 3.1). Infection with these strains result in an attenuated pedestal phenotype. About half of the attached bacteria have EspF_U foci underneath sites of bacterial attachment, indicating recruitment of the EspF_U mutant; about half of these bacteria with EspF_U foci form pedestals. This implies that P domains with W33A mutations may have residual activity.

Table 3.1: Actin Pedestal Assembly in HeLa Cells

Strain	**EspF_U Foci**	**Pedestals**
EHEC$\Delta dam\ \Delta espF_U$	No	No
EHEC$\Delta dam\ \Delta espF_U$ + HP	No	No
EHEC$\Delta dam\ \Delta espF_U$ + HPH	No	No
EHEC$\Delta dam\ \Delta espF_U$ + PHP	Yes	Yes
EHEC$\Delta dam\ \Delta espF_U$ + HPHP	Yes	Yes
EHEC$\Delta dam\ \Delta espF_U$ + HPHPH	Yes	Yes
EHEC$\Delta dam\ \Delta espF_U$ + HPHPHP	Yes	Yes
EHEC$\Delta dam\ \Delta espF_U$ + EspF_U	Yes	Yes
EHEC$\Delta dam\ \Delta espF_U$ + H*PHPHP	Yes	Yes
EHEC$\Delta dam\ \Delta espF_U$ + HPH*PHP	Yes	Yes
EHEC$\Delta dam\ \Delta espF_U$ + HPHPH*P	Yes	Yes
EHEC$\Delta dam\ \Delta espF_U$ + HPH*PH*P	Yes	Yes
EHEC$\Delta dam\ \Delta espF_U$ + H*PHPH*P	Yes	Yes
Continued on the next page		

Strain	**EspF$_U$ Foci**	**Pedestals**
EHECΔdam $\Delta espF_U$ + H*PH*PHP	Yes	Yes
EHECΔdam $\Delta espF_U$ + HP*HPHP	Yes	Yes
EHECΔdam $\Delta espF_U$ + HPHP*HP	Yes	Yes
EHECΔdam $\Delta espF_U$ + HPHPHP*	Yes	Yes
EHECΔdam $\Delta espF_U$ + HPHP*HP*	Yes	Atten.
EHECΔdam $\Delta espF_U$ + HP*HPHP*	Yes	Atten.
EHECΔdam $\Delta espF_U$ + HP*HP*HP	Yes	Atten.
EHECΔdam $\Delta espF_U$ + HP*H*P*H*P	Yes	Atten.
EHECΔdam $\Delta espF_U$ + HP*HP*HP*	No	No
EHECΔdam $\Delta espF_U$ + H*PH*PH*P	Yes	No

3.4.7 IRTKS is recruited to sites of bacteria attachment independently of EspF$_U$

With the exception of H*PH*PH*P, pedestal incompetent constructs of EspF$_U$ appear to not be recruited to sites of bacterial attachment during infection. For EHEC strains complemented with a number of pedestal incompetent mutants (not all were tested), staining for Tir and IRTKS showed that these two upstream pedestal components are clearly localized to nearly every attached bacteria (figure 3.9). IRTKS is able to localize to Tir independently of EspF$_U$. These results indicate that pedestal incompetent mutants with W33A mutations in the P region do not prevent recruitment of IRTKS or Tir to sites of bacterial .

Figure 3.9: IRTKS recruitment to sites of bacterial attachment does not depend on $EspF_U$.

Polaized HCT8 cells infected for 3 hours with EHEC Δdam $\Delta espF_U$ complemented with pedestal incompetent PHP were stained for attached bacteria (blue), Tir (red) IRTKS (yellow), and actin (green).

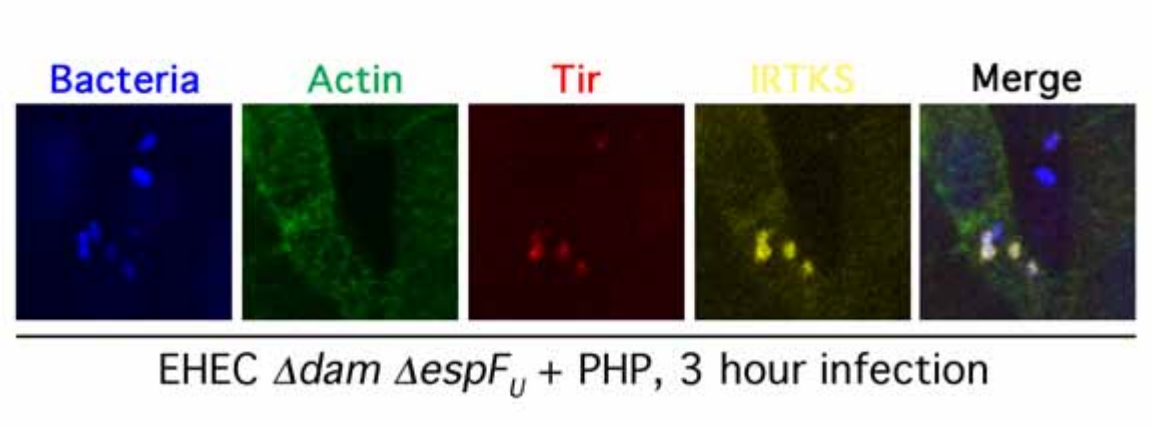

Figure 3.9: IRTKS recruitment to sites of bacterial attachment does not depend on $\mathrm{EspF_U}$.

3.5 Conclusion

While one repeat of $EspF_U$ can spatially accommodate both the GBD of N-WASP and the SH3 domain of IRTKS *in vitro* and theoretically trigger the Arp2/3 actin assembly cascade [2], it appears unable to generate actin pedestals when delivered into mammalian cells by infection. Based on studies by Campellone et al. [17], an additional H domain might facilitate recruitment of actin assembly machinery by pulling two N-WASP proteins into close proximity, thus enhancing recruitment of Arp2/3 [91]. Surprisingly, this construct, HPH, was also unable to generate actin pedestals in infected cells and appears not to be recruited to sites of EHEC attachment. However, an equivalent length construct with one H and two P domains (PHP) was able to form actin pedestals in non-polarized cells and is cleared localized to the tips of pedestals underneath bound bacteria. While the previously mentioned *in vitro* studies have provided important biophysical insights, our observations indicate a more complex picture in infected cell culture models.

Polarized epithelia display obvious structural differences from non-polarized cells that facilitate the specialized physiological functions needed from this type of cell layer. Polarization of HCT8 intestinal cells results in a different phenotype for the minimum domains of $EspF_U$ required for actin pedestal formation. Whereas non-polarized cells required a minimum of two P domains, at least three were needed in polarized HCT8 cells. Though HCT8 cells do not develop robust or well organized microvilli, organization of actin and other cytoskeletal proteins at the apical surface may nonetheless hinder the ability of shorter $EspF_U$ constructs from functioning.

Actin pedestal activity is dependent on the recruitment of $EspF_U$ to sites of bacterial attachment. Except for H*PH*PH*P, all pedestal incompetent $EspF_U$ constructs were not localized underneath intimately bound bacteria. Immunofluorescent staining of IRTKS and Tir show that these upstream components of the EHEC actin

pedestal pathway are able to localize the sites of bacterial attachment in the absence of $EspF_U$ (data not shown) or with pedestal incompetent $EspF_U$ mutants. This indicates that the lack of $EspF_U$ recruitment is not due to a defect in IRTKS localization and that IRTKS recruitment to Tir does not depend on binding to $EspF_U$.

The H domains do not appear to play a role in recruitment of $EspF_U$ to IRTKS in our infection model. H domains alone have been shown to polymerize actin *in vitro* in the presence of N-WASP and Arp2/3 [104]. Despite having up to three fully functional H domains, the construct HP*HP*HP*, and other pedestal incompetent truncation constructs with wildtype H domains (HP and HPH in non-polarized cells; HP, HPH, PHP, HPHP, HPHPH in polarized cells), were unable to produce actin pedestals in infected cells. On immunofluorescent staining, these pedestal incompetent constructs also were not localized to any particular location, and aberrant actin assembly activity was not readily observed within infected cells. Though *in vitro* studies have shown an enhancement of actin assembly with two H domains over one H domain [17], it is unclear wether this enhancement affects recruitment of $EspF_U$ to sites of bacterial attachment. Unfortunately, our infection model is not well suited to address the exact degree of benefit gained by additional H domains in $EspF_U$ recruitment to the IRTKS/Tir complex underneath intimately attached EHEC.

The P domains target $EspF_U$ to IRTKS [125] and this activity does not depend on the function of the H domains. Even without N-WASP activating activity, the construct H*PH*PH*P can localize to sites of bacterial attachment in both non-polarized and polarized cells. It is interesting to note that three repeat constructs with one wildtype P domain have partial actin pedestal activity in non-polarized cells. Furthermore, the construct HP*H*P*H*P displays partial actin pedestal activity comparable to those constructs with no mutations in the H domains but W33A mutations in two P domains (HPHP*HP*, HP*HPHP*, and HP*HP*HP). Given

that we see no discernible differences in actin pedestal activities in polarized cells between three repeat constructs with L12A mutations in one or two H domains, HP*H*P*H*P might be thought of as being comparable to HP in that both of these constructs have one wildtype H and one wildtype P domains. However, the partial recruitment and actin pedestal activity of HP*H*P*H*P on non-polarized cells would suggest that the W33A mutations in $EspF_U$'s P domains may not abrogate binding to binding to IRTKS's SH3 domain completely. And in a cellular environment that is more permissible to $EspF_U$ recruitment to sites of bacterial attachment at the membrane, these partially active P domains may still contribute to binding to IRTKS.

Thus, recruitment and concentration of $EspF_U$ via P domains to the IRTKS/Tir complex is essential for hijacking the host cell actin assembly machinery for actin pedestal formation. If an $EspF_U$ construct has enough fully functional P domains to be recruited to IRTKS/Tir, one functional H domain is enough to generate actin pedestals. While this result seems contradictory to the *in vitro* observations made by Campellone and co-workers [17], the concentration of multiple single active H domains to IRTKS may produce the same structural effect of pulling pairs of N-WASP proteins within close enough proximity to enhance Arp2/3 activation.

Our results match well with the observation that $EspF_U$'s in nature nearly always have at least three functional repeats [54]. Multiple repeating H and P domains may have evolved to overcome the challenges of inducing dramatic rearrangements of cytoskeletal proteins in a subcellular location that is already highly organized and regulated. Additional repeats may also confer further selective advantage for EHEC strains in colonizing gut epithelia. Although EHEC expresses type IV pili, it does not express bundle forming pili, a potent bacterial adhesin found on the surface of EPEC [33], and our laboratory experience has shown that 10 to 100 fold higher MOI's are needed for EHEC infection over EPEC infection in cultured cells. EHEC may have

needed to evolve a more enhanced system of intimate attachment to compensate for lower overall binding efficiency of its other surface adhesins. Through utilizing additional host and bacterial factors that can dimerize and bind multiple partners, EHEC's mechanism of actin pedestal may facilitate enhanced attachment through multimeric complexing of proteins that link Tir to the cytoskeleton.

CHAPTER 4

ESPF$_U$ COMPETES WITH THE HOST PROTEIN EPS8 FOR IRTKS BINDING

4.1 Acknowledgements

Experiments and figures in sections 4.4.1 and 4.4.2 where executed by Stacie Clark in the Leong Lab under supervision. Lentiviral transduction was performed with the assistance of Abe Brass (UMMS) and Chris Louissaint of the McCormick lab (UMMS). HCT8 cells and Eps8-/- cells were generous gifts from the labs of Beth McCormick (UMMS) and Giorgio Scita (FIRC Institute of Molecular Oncology Foundation and the Department of Experimental Oncology of the European Institute of Oncology, Milan, Italy) respectively.

4.2 Introduction

Like the H domain, EspF$_U$'s P domains may have evolved to outcompete endogenous host ligands and function by mimetic displacement of native intracellular protein-protein interactions. The P domains of EspF$_U$ appear to direct localization of the protein to sites of bacterial attachment, where they bind the SH3 domain of IRTKS molecules clustered by Tir [125, 2]. IRTKS belongs to the I-BAR family of membrane bending proteins; its zeppelin shaped homodimers aid in producing membrane protrusions and may thereby contribute to architecture of EHEC pedestals [80, 102, 29].

SH3 domains are an abundant and common motif for affecting cellular interactions. Several cellular ligands have been shown to bind the SH3 domain of IRTKS

and the high binding affinity of $EspF_U$'s P domain ranks well among them [1]. The IRTKS SH3 domain is unusual in that in it can accommodate two PxxP motifs (such as that found in the P domain if $EspF_U$) in its specificity binding pocket rather than just one [103]. Some cellular ligands or potential ligands that also possess tandem PxxP motifs include Esp8, Shank and BRAG [1].

The tandem PxxP binding regions of Eps8 and $EspF_U$ are nearly identical, suggesting that $EspF_U$ may be mimicking Eps8 [2]. In support of a model where $EspF_U$ must outcompete Eps8, the P domain of $EspF_U$ binds to the IRTKS SH3 domain with much higher affinity due to the presence of a tryptophan between its two PxxP motifs, rather than an alanine residue, which is found in the equivalent position in between Eps8's tandem PxxP motifs. Furthermore, swapping these two amino acids between $EspF_U$ and Eps8 switches their relative binding affinities for the IRTKS SH3 [2]. Thus, this $EspF_U$ "tryptophan switch" may allow EHEC to usurp control of IRTKS from Eps8.

Eps8 is a multifunction regulator of actin dynamics that integrates various signaling pathways in the cell. It can act to induce disparate actin remodeling events such as membrane ruffling and endocytosis by associating with different signaling regulators and scaffolding proteins [39, 88, 123]. Its importance in regulating cellular structure and actin associated signaling is highlighted by studies linking Eps8 to the motility and invasive potential of cancer cells as well as to the development of microvilli and apical intestinal cells structure in animal models [49, 57, 119, 76]

Among its many partners, Eps8 that has been well documented to be the major binding partner of IRSp53, an I-BAR protein closely related to IRTKS [49]. With IRSp53, Eps8 participates in actin remodeling at membrane ruffles [40, 106]. IRTKS-Eps8 interactions in vivo have been less well studied. However, its role in the proper development and maintenance of apical structures [119] in intestinal cells makes

Eps8 a potential target for bacterial effectors that are tasked with remodeling apical cytoskeletal structures.

4.3 Materials and Methods

4.3.1 Cell culture

Wildtype and Eps8-/- mouse embryonic fibroblasts (MEF), were cultured in DMEM supplemented with 10% fetal bovine serum (FBS), penicillin-streptomycin, and 2mM L-Glutamine. Cells were passed when confluent. For immunofluorescence experiments, cells were washed with PBS, lifted with trypsin-EDTA, and seeded onto #1.5, 12 mm coverslips in 24-well tissue culture plates at approxiately 50% confluence 12-18 hours before infection. For western blotting, cells were seeded into 6-well tissue culture treated plates. HCT8 cells were cultured as described in section 3.3.1.

4.3.2 Transfection

MEFS were seeded at roughly 50% confluence onto #1.5 12mm coverslips 12 - 15 hours prior to transfection with 1-2 μg of mammalian expression plasmids using Lipofectamine 2000 (Invitrogen #11668027) or FuGene (Promega #E2691) transfection reagents according to manufacturer's instructions. Cell media was replaced with Opti-MEM during transfection and replaced again with normal cell media 6 hours after transfection.

4.3.3 Bacterial strains and plasmids

KC12, an EPEC strain that expresses EHEC Tir [21].was as the background strain for infection studies in MEFS as EHEC strains induced too much cellular damage to MEF cells before actin pedestal formation could be clearly observed. $EspF_U$ mutant constructs in pDV48 were transformed into KC12 strains by electroporation. Refer to tables C.1 and C.3 for strains plasmids.

4.3.4 Infection

KC12 strains were cultured for transfection in the same manner as described in section 3.3.4. For infection, bacteria were then resuspended in DMEM/2% FBS/20 mM HEPES/2mM glutamine to the following MOIs roughly 1:10. Infection was carried out for 3 to 3.5 hours at 37°C with 5% CO_2.

4.3.5 Immunoflourescence and imaging

Processing of infected samples for immunofluorenscence imaging was carried out as described in section 3.3.6. Infected mouse embryonic fibroblasts were imaged on an Olympus X70 or Ziess Axiovert 200M with the Ziess Apotome attachment. Exposure times were set to capture 75% maximum intensity for postive samples for each experiment. Z-sections were taken at 0.22 μm steps. HCT8 cells on transwells were imaged on a Leica SP5 scanning confocal as described in section 3.3.6.

4.3.6 Co-immunoprecipitation (CO-IP)

For CO-IP experiments, HCT8 cells were seeded in 75 mm Transwell dishes (Corning #3420) at about 1.25 x 10^7 cells per dish and allowed to polarize for 5 days. After 3 days, half of the spent media was replaced with fresh media. Cells were infected as described in section 3.3.4. with the following exceptions: Bacteria were resuspended in FAS media at an MOI of about 1:500. Cells were infected with 3 mL of resuspended bacteria with 6 mL of FAS media in the outer well. Infection was carried out for 6.5 to 7 hours. 2 mL of warm FAS media was added to the both the inner transwells and the outer wells 3 hours after initiation of infection. After infection, CO-IP of infected whole cell lysates was performed using Thermo Scientific's Pierce Co-immunoprecipitation kit (# 26149) according to manufacturer's instructions. 10 μg of anti-IRTKS or anti-IRSp53 antibody and 5 μg of anti-Eps8 antibody was crosslinked per reaction. Protease inhibitors (Roche cOmplete mini EDTA-free

protease inhibitor pill (Roche #04693159001) and 1 mM sodium orthovanodate) were added the the IP/Lysis buffer prior to cell lysis. IP was conducted at 4°C for at least 15 hours.

4.3.7 Mithramycin treatment

HCT8 cells were polarized for 5 days as described in section 3.3.1. Mithramycin (Santa Cruz #sc-200909) was stored as a 1 M stock in PBS at -20°C. Stock mithramycin was diluted to working concentrations in cell culture media before use and handled in the dark as much as possible. Media was removed from cells and replaced with media with mithramycin for drug treatment. Treated cells were washed with HBSS twice before experiments.

4.3.8 shRNA knockdown of Eps8 via lentivirus

Five shRNA sequences directed against Eps8 in the pLKO.1 lentiviral packing vector were ordered from the UMass RNAi core (Gene ID #2059, Oligo ID #TRCN 00000 61543, TRCN 00000 61544, TRCN 00000 61545, TRCN 00000 61546, TRCN 00000 61547). shRNA plasmids and scramble control were transfected into 293T cells along with psPAX2, expressing gag-pol, and pMD.2G, expressing VSV-G envelope protein) using Mirus TransIT-293 Transfection reagent (Mirus #MIR 2704) in Opti-MEM (Invitrogen #31985070). Viral supertants were collected from 293T cells at 24 hours and 48 hours after transfection, filtered through 45 μm mesh, and added with 8 μg per mL polybrene to subconfluent HCT8 cultures in two batches. Transduced HCT8 cells were selected for stable knock down 48 hours after the last transduction with 10 μg/mL puromycin through two passages.

4.3.9 Western blots

Whole cell lysates were collected using Cytobuster (EMD Millipore #71009-3) lysis buffer with Roche cOmplete mini-EDTA free protease inhibitor pill (Roche #04693159001) according to manufacturer's instructions. Subcellular fractions were collected using "Henrik's protocol". Briefly, cells were lysed in a triton extraction buffer (1 % triton X-100, 100 mM sodium chloride, 10 mM HEPES, 2 mM EDTA, 4 mM sodium orthovanadate, 40 mM sodium fluoride) with gentle rocking at 4°C for 10 minutes. Cells were scraped from transwells or tissue culture vessels and lysates were passed through a 25G needle three times and incubated on ice for 20 minutes with occasional vortexing. After spinning at 14,000 rpm at 4°C for 30 minutes, the supernatant was collected as the "soluble fraction." The pellet was then resuspended in 1/5 volume SDS extraction buffer (triton extraction buffer with 1% SDS and 2 mM PMSF) and sonicated on ice for three rounds (5 seconds each round) at level 5 using a probe sonicator. After spinning at 14,000 rpm for 10 minutes at 4°C, this supernatant was collected as the "insoluble fraction." Biorad's DC or BCA protein concentration assay kits were used to determine protein concentrations for lysate samples against BSA standards. Samples were boiled in with laemmli buffer for 5 to 10 minutes before loading into precast SDS Tris-glycine polyacrylamide gels and run at 120 to 180 V until desired separation of protein bands. Proteins were transferred onto PVDF membranes by overnight wet transfer or onto nitrocellulose membranes by semi-dry transfer. Membranes were blocked in 5% milk in PBST or TBST for one hour at room temperature before incubation with primary antibody solutions in 5% milk in PBST or TBST overnight at 4°C with gentle rocking. After 3 washes in PBST or TBST of at least 10 minutes each, membranes were incubated with HRP conjugated secondary antibodies in 5% milk in PBST or TBST and incubated for 1 to 3 hours at room temperature with gentle rocking. Membranes were washed

3 times prior to development with SuperSignal Pico West reagent (ThermoFisher). Blots were imaged using the G:Box (Syngene) multi-purpose imager under automatic exposure settings for each protein being probed.

4.4 Results

4.4.1 Pedestal incompetent $EspF_U$ constructs with mutations in the P domain can form pedestals in the absence of Eps8

Eps8 knock out mouse embryonic fibroblast (MEF) cells, were initially used to study the possible role of Eps8 as a competitor of $EspF_U$ for binding to IRTKS. Eps8 -/- cells grew more slowly than wildtype embryonic fibroblasts and appeared more stretched and spiny, possibly reflecting important role of Eps8 in proliferation and actin remodeling.

In order to study EHEC pedestal formation in MEF lines, KC12 was used as the background strain instead of wildtype EHEC, which caused significant damage to infected cells such that pedestal formation could not be easily assessed. KC12 is an EPEC strain that has been engineered to make pedestals via EHEC pedestal pathways [21] by replacement of its *tir* allele with EHEC *tir*. Thus, KC12 alone cannot generate pedestals unless complemented with pedestal competent $EspF_U$ constructs.

Upon infection, the absence of Eps8 permitted pedestal formation by constructs of $EspF_U$ that are normally pedestal incompetent. HP*HP*HP* and HP*H*P*H*P were both able to make robust pedestals in Eps8-/- cells that were indistinguishable from pedestals made by wildtype $EspF_U$. Neither construct was able to make pedestals in wildtype fibroblasts (figure 4.1).

Infection of Eps8 -/- cells by KC12 strains complemented with shorter pedestal incompetent constructs of $EspF_U$ also resulted in some enhanced pedestal activity. While recruitment of HP and HPH to sites of bacterial attachment was not very strong in infected Eps8-/- cells, weak actin pedestals were associated at these sites. No recruitment or recognizable actin pedestals were seen in wildtype cells infected with KC12 complemented with HP or HPH (figure 4.2).

Figure 4.1: Pedestal incompetent mutants can form pedestals in the absence of Eps8.

Wildtype or Eps8 -/- cells MEFS infected with KC12 complemented with HP*HP*HP* or HP*H*P*H*P were stained for bacteria (blue), the myc-tagged $EspF_U$ construct (red), and actin (green).

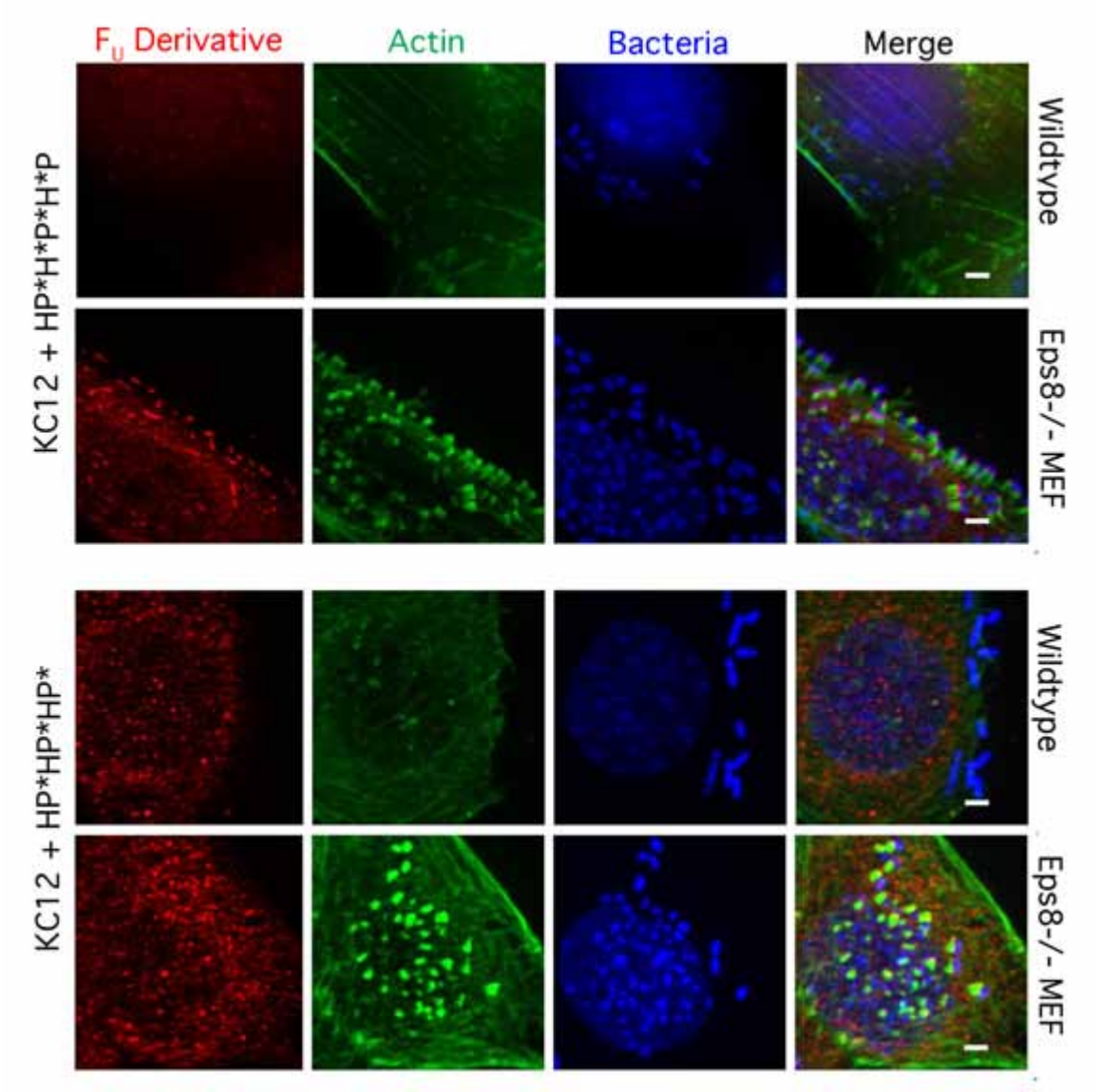

Figure 4.1: Pedestal incompetent mutants can form pedestals in the absence of Eps8.

Figure 4.2: One P domain can generate weak actin pedestals in the absence of Eps8.

Wildtype or Eps8 -/- cells MEFS infected with KC12 complemented with HP or HPH were stained for bacteria (blue), the myc-tagged $EspF_U$ construct (red), IRTKS (yellow) and actin (green).

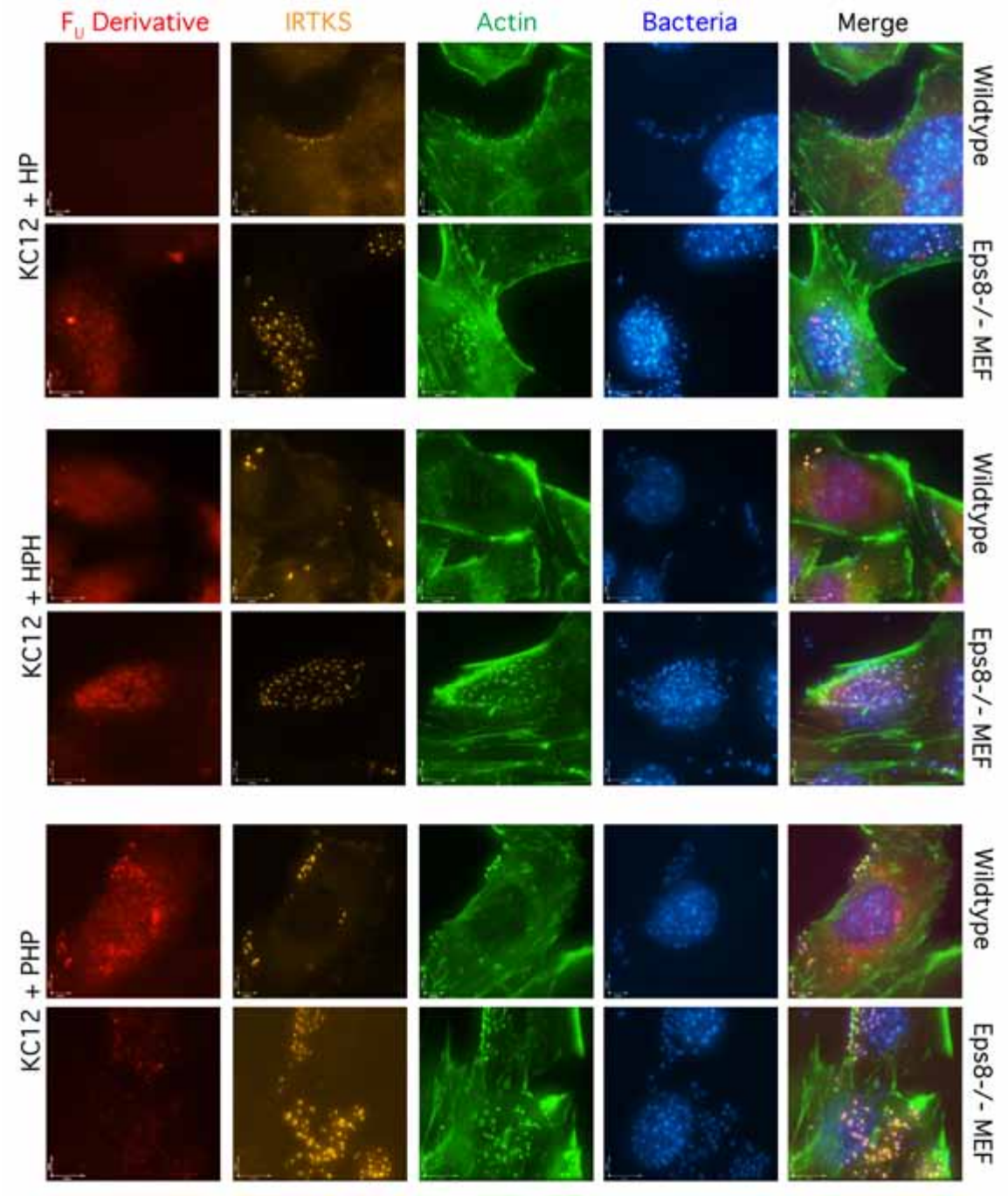

Figure 4.2: One P domain can generate weak actin pedestals in the absence of Eps8.

4.4.2 Ectopic expression of Eps8 decreases pedestal formation activity by pedestal competent $EspF_U$ mutants in MEF cells

Transfection of a plasmid expressing wildtype mouse GFP-Eps8 into Eps8-/- MEF cells prevented pedestal formation by HP*HP*HP*, thus restoring the wildtype MEF $EspF_U$ requirement phenotype. When ectopic GFP-Eps8 was expressed in wildtype MEF cells, HPHPHP was able to make pedestals less efficiently, suggesting that Eps8 overexpression can compete against pedestal competent $EspF_U$ constructs. Ectopically expressed GFP-Eps8 could be localized to sites of bacteria attachment by immunofluorescence with anti-GFP antibody (figure 4.3).

Figure 4.3: Ectopic expression of Eps8 decreases pedestal activity.

Wildtype and MEFS overexpressing Eps8-GFP or GFP alone and infected with KC12 complemented with HPHPHP were stained for bacteria (blue), the myc-tagged $EspF_U$ construct (red), IRTKS or GFP-tagged Eps8 (yellow) and actin (green).

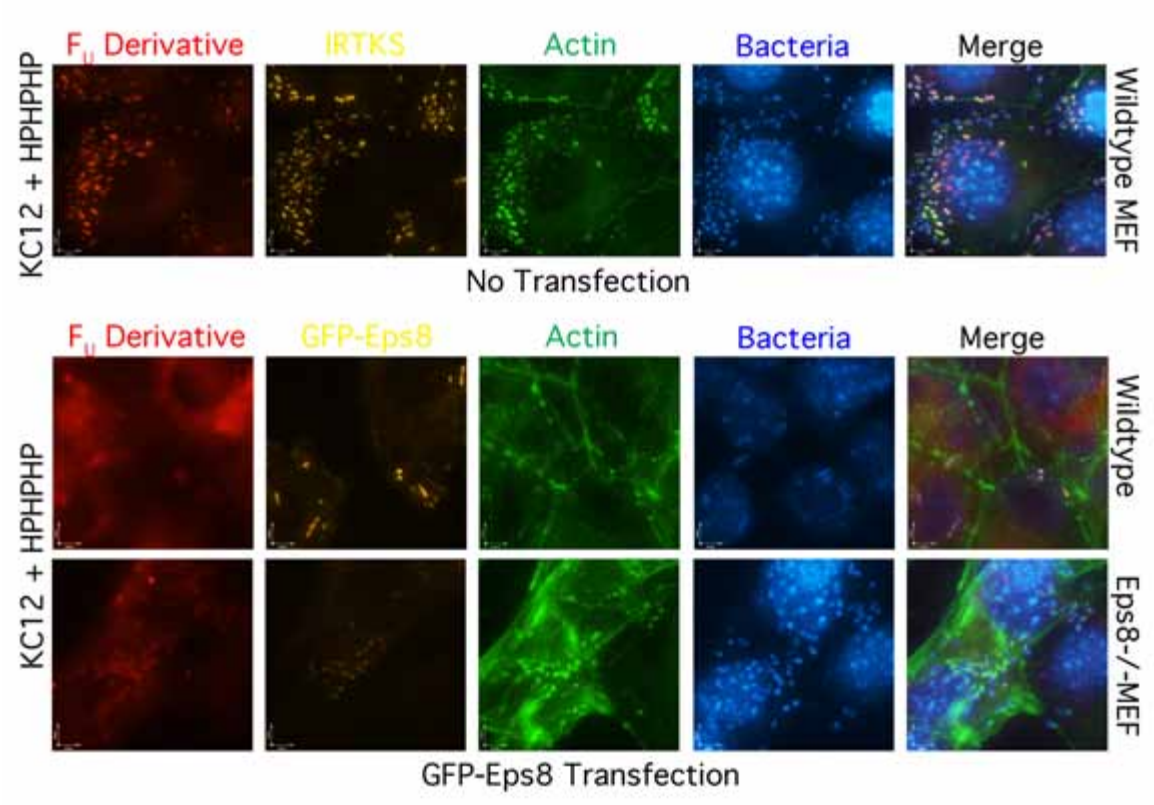

Figure 4.3: Ectopic expression of Eps8 decreases pedestal activity.

4.4.3 Eps8 is localized to apical membrane surfaces in polarized HCT8 cells

Eps8 appears highly abundant in polarized HCT8 cells. Total Eps8 levels were not significantly different between subconfluent, confluent and polarized HCT8 cells when lysates were adjusted for total protein concentration, while total IRTKS levels increased in confluent and polarized HCT8 cells (figure 4.4). Interestingly, GADPH levels appear to decrease when HCT8 cells were confluent or polarized. Eps8 was found to be mostly membrane associated (in insoluble fraction) while IRTKS was distributed in both the soluble and insoluble fractions in roughly equal amounts (figure 4.6). Exact concentrations of Eps8 in cell lysates could not be determined because a recombinant protein was not available.

On immunofluorescence, Eps8 appeared to be concentrated at the apical surface of polarized HCT8 monolayers. Figure 4.5 shows single apical Z-slices of uninfected and infected cell monolayers and corresponding X-Z and Y-Z projections. In infected polarized cells, the apical localization of Eps8 did not appear to change. No Eps8 foci were apparent when polarized HCT8 cells were infected with EHEC Δdam $\Delta espF_U$ strains complemented with pedestal incompetent $\mathrm{EspF_U}$ constructs. Cell monolayers infected with pedestal competent mutants also did not show enhanced Eps8 localization around attached bacteria that were not making pedestals. Membrane associated Eps8 in subcellular fractions appeared to increase slightly after infection with pedestal competent strains (figure 4.6) on western blot. However, figure 4.6 represents a preliminary pilot experiment and requires repetition and pedestal incompetent infection controls.

Figure 4.4: Eps8 is abundant in HCT8 cells; protein levels do not change in with polarization.

Whole cell HCT8 lysates of two subconfluent, one confluent, and one polarized culture were probed for Eps8, IRTKS, Tubulin and GAPDH. Protein loading was normalized to 20 μg in each lane.

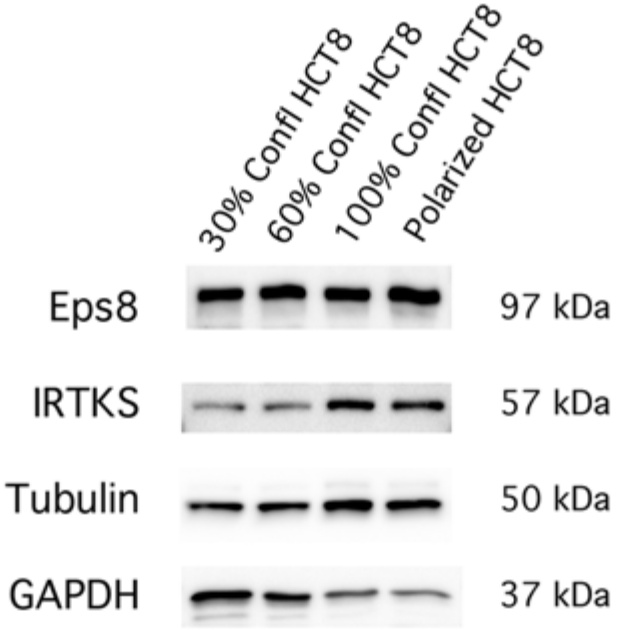

Figure 4.4: Eps8 is abundant in HCT8 cells; protein levels do not change in with polarization.

Figure 4.5: Eps8 is concentrated at the apical surface in polarized HCT8 cells.

Polarized HCT8 cells infected with various EHEC Δdam $\Delta espF_U$ strains were stained for bacteria (blue), Eps8 (magenta) and actin (green). Images of X-Y planes (largest square panel in each image) are single Z slices taken at apical planes. X-Z and Y-Z projections above and to the left of X-Y planes represent projections at crosshairs in the X-Y planes. Arrowheads point to apical surface of cells in X-Z and Y-Z projections.

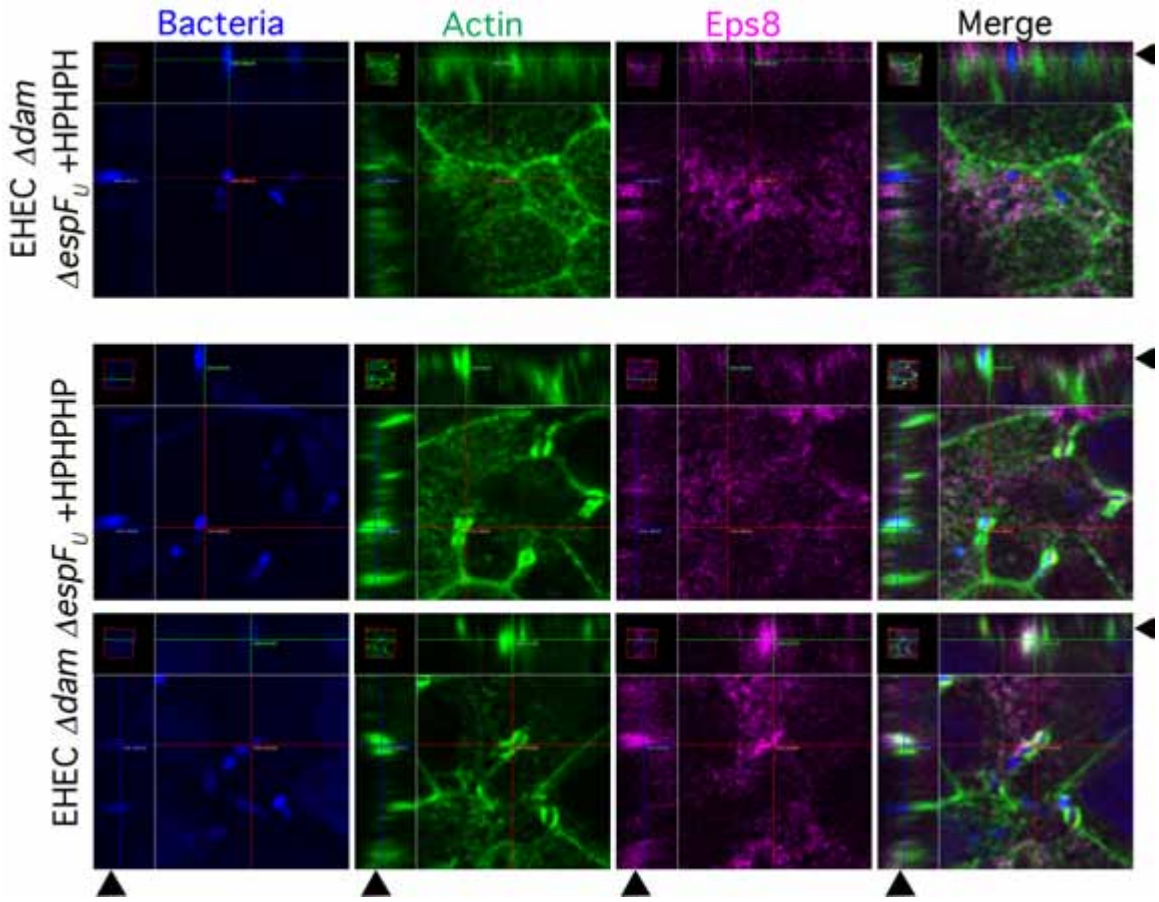

Figure 4.5: Eps8 is concentrated at the apical surface in polarized HCT8 cells.

Figure 4.6: Infection with pedestal competent strains of $EspF_U$ may affect the relative subcellular localization of Eps8.

Fractionated lysates of uninfected polarized HCT8 or polarized HCT8 infected with pedestal competent EHEC strains were probed for membrane associated and cytosolic Eps8 and IRTKS.

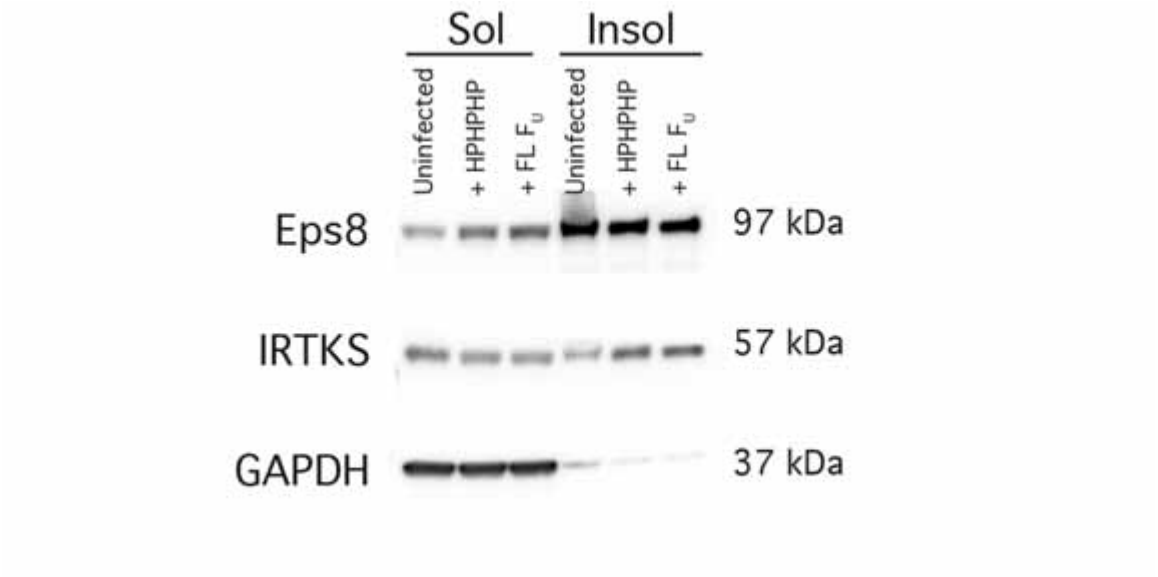

Figure 4.6: Infection with pedestal competent strains of $EspF_U$ may affect the relative subcellular localization of Eps8.

4.4.4 Co-immunoprecipitation (CO-IP) of IRTKS with Eps8 cells suggests competition between $EspF_U$ and Eps8 in polarized HCT8 cells

If the requirement for multiple P domains of $EspF_U$ for actin pedestal formation in polarized HCT8 cells is also due to competition against Eps8 for the same binding site of IRTKS, then recruitment of IRTKS by $EspF_U$ might displace any Eps8 that is already bound to IRTKS. Co-immunoprecipitation of infected cell lysates for either IRTKS or Eps8 should thus show a change in levels of IRTKS bound to Eps8 upon infection of HCT8 cells with pedestal competent $EspF_U$ constructs.

Crosslinking of anti-IRTKS antibody to CO-IP beads was able to capture nearly all IRTKS from uninfected and infected whole cell lysates of polarized HCT8 cells. However, Eps8 was not detected in the CO-IP eluate (figure 4.7). Likewise, crosslinking of anti-IRSp53 antibody to did not capture Eps8 even though IRSp53 is reported to be the major binding partner of Eps8 (data not shown).

Figure 4.7: Eps8 is not captured by CO-IP with IRTKS.

Uninfected and infected polarized HCT8 whole cell lysates were immunoprecipitated (IP) with anti-IRTKS antibody. Pre-IP lysates, IP, and flow through from IP were probed for Eps8 and IRTKS. Pre-IP lysates were also probed for GAPDH as loading control. Lanes are 1. Uninfected, 2. Infected with EHEC Δdam $\Delta espF_U$, 3. Infected with EHEC Δdam $\Delta espF_U$ complemented with full length $EspF_U$, 4. Infected with EHEC Δdam $\Delta espF_U$ complemented with HPHPHP, and 5. Infected with EHEC Δdam $\Delta espF_U$ complemented with HP*HP*HP*.

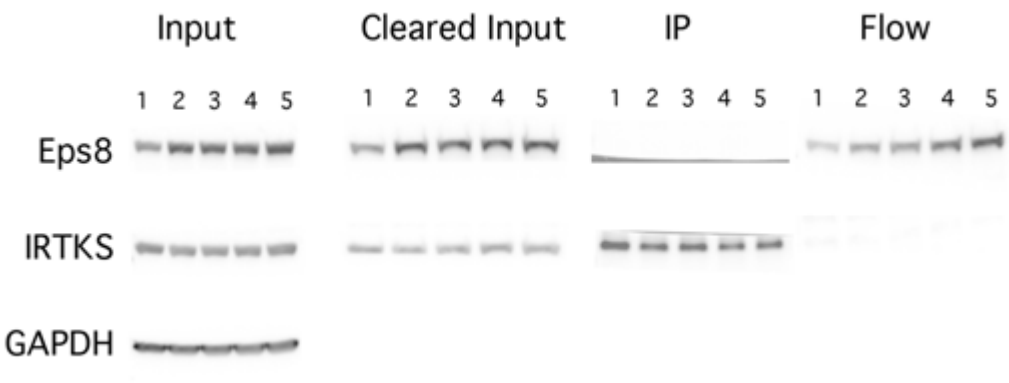

Figure 4.7: Eps8 is not captured by CO-IP with IRTKS.

Crosslinking of anti-Eps8 antibody to CO-IP beads on the other hand was able to capture both IRTKS and IRSp53 by CO-IP. Only a fraction of total cellular IRTKS is bound to Eps8. IRSp53, normally undetectable in HCT8 whole cell lysates, becomes enriched and easily detected by CO-IP with Eps8 (figure 4.8). The level of IRSp53 enrichment and detection after IP is curious given that volume-wise, the IP eluate is only 3.33 times as concentrated as the input lysate. Both IRTKS and IRSp53 show an apparent 5 to 6 kDa reduction in size when captured by CO-IP with Eps8, suggesting a possible modification after Eps8 binding.

No Eps8 or IRTKS bands were detected in control CO-IP's using non-specific mouse IgG's crosslinked to protein G beads (figure 4.9), indicting that the above bands seen on CO-IP are specific. The IRTKS antibody used detects recombinant IRTKS specifically over recombinant IRSp53 and gives a clean band on western blot of cellular lysates at the predicted molecular size (data not shown).

Figure 4.8: IRTKS and IRSp53 are captured by CO-IP with Eps8

Uninfected polarized HCT8 whole cell lysates were immunoprecipitated (IP) with anti-Eps8 antibody. Pre-IP lysates (Ly), pre-IP lysates cleared through agarose beads (CL), IP, and flow through from IP (FT) were probed for Eps8 and IRTKS. L stands for molecular weight ladder.

Figure 4.8: IRTKS and IRSp53 are captured by CO-IP with Eps8

Polarized HCT8 cells infected with pedestal competent strains delivering HPH-PHP or full-length $EspF_U$, showed decreased levels of IRTKS bound to Eps8 compared to cells infected with EHEC Δdam $\Delta espF_U$ or EHEC Δdam $\Delta espF_U$ complemented with the pedestal incompetent PHP construct. More IRTKS was bound to Eps8 in cells infected with EHEC Δdam $\Delta espF_U$ complemented with the pedestal incompetent HP*HP*HP* construct compared to its pedestal competent counterpart, HPHPHP, indicating that HP*HP*HP* was less able to compete against Eps8 for IRTKS binding (figure 4.9). Figure 4.9 represents a preliminary experiment that needs to be repeated for final conclusions.

Figure 4.9: Pedestal competent $EspF_U$ constructs decrease IRTKS bound to Eps8.

Whole cell lysates from uninfected polarized HCT8 (1) and polarized HCT8 infected with EHEC Δdam $\Delta espF_U$(2) and EHEC Δdam $\Delta espF_U$ complemented with PHP (3), HPHPHP (4), HP*HP*HP*(5), and full length $EspF_U$(5) were immunoprecipitated (IP) with anti-Eps8 antibody (A) and probed for Eps8 and IRTKS. Control western blots (B) of input lysates, flow through from IP with anti-Eps8 antibody, and control IP with non-specific IgG were probed for Eps8, IRTKS, and GAPDH.

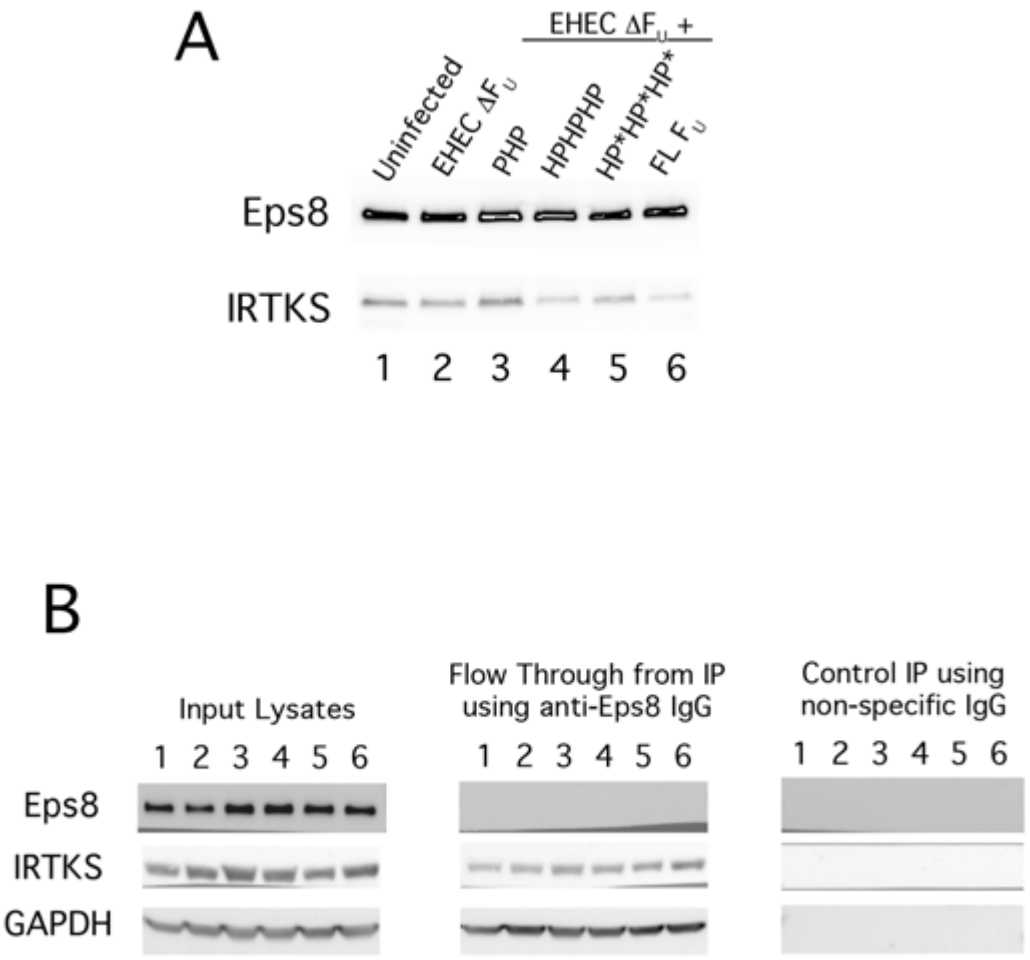

Figure 4.9: Pedestal competent $EspF_U$ constructs decrease IRTKS bound to Eps8.

4.4.5 Mithramycin treatment reduces Eps8 but does not permit pedestal formation by pedestal incompetent $EspF_U$ constructs

Mithramycin, a DNA and RNA polymerase inhibitor has been reported to decrease Eps8 mRNA and protein levels in a dose dependent manner [135] and has been used to study phenotypes of cancer cell lines that involve Eps8 [135, 57].

Mithramycin treatment of polarized HCT8 cells decreased Eps8 protein in a dose dependent manner, with no obvious gross changes in the polarized monolayer up to 5 μM. Treatment for 24 hours at 5 μM resulted in roughly the same level of Eps8 decrease as treatment for 42 hours (figure 4.10).

Treatment of polarized HCT8 cells for 24 hours with doses up to 50 μM Mithramycin was not sufficient, however, to allow for pedestal formation of any $EspF_U$ mutant with a W33A mutation in any P domain (figure 4.11).

Figure 4.10: Mithramycin decreased Eps8 in polarized HCT8 cells.

Fractionated subcellular lysates of untreated polarized HCT8 cells or polarized HCT8 cells treated for 24 or 42 hours with 3 concentrations of Mithramycin were probed for Eps8.

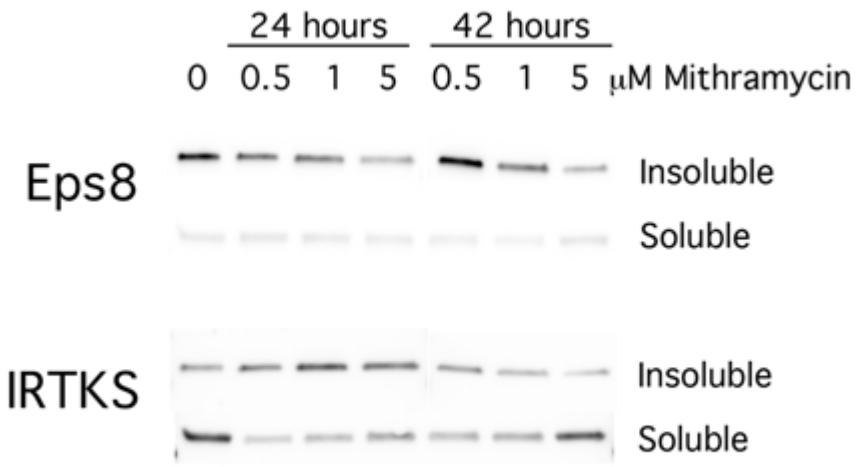

Figure 4.10: Mithramycin decreased Eps8 in polarized HCT8 cells.

Figure 4.11: Mithramycin treatment of polarized HCT8 cells did not permit pedestal formation by pedestal incompetent $EspF_U$ mutants with W33A mutation.

Polarized HCT8 cells treated with various doses of mithramycin and infected with pedestal incompetent $EspF_U$ mutants were stained for bacteria (blue), myc-tagged $EspF_U$ construct (red) and actin (green).

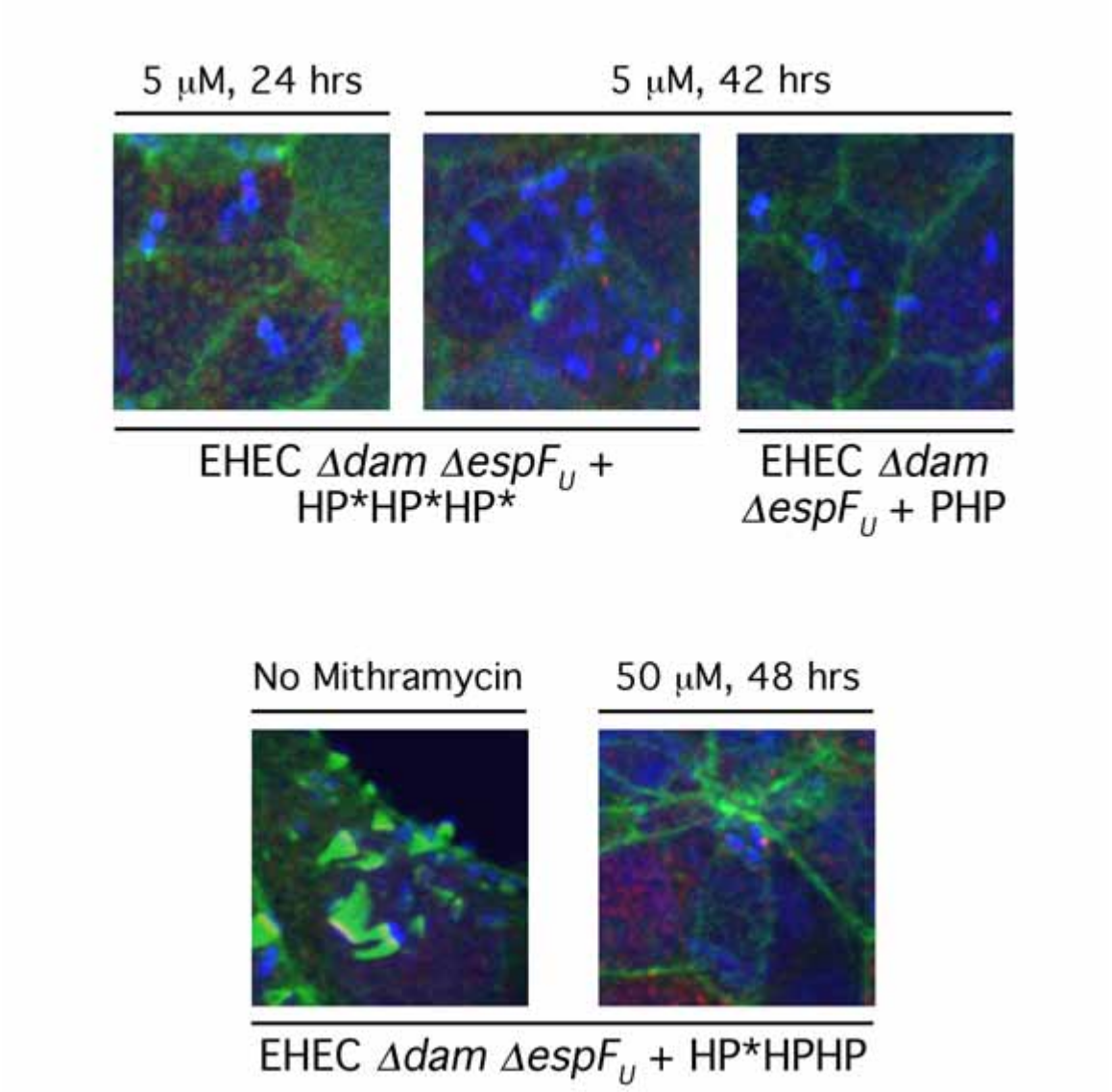

Figure 4.11: Mithramycin treatment of polarized HCT8 cells did not permit pedestal formation by pedestal incompetent $EspF_U$ mutants with W33A mutation.

4.4.6 shRNA knock down of Eps8 in HCT8 cells does not permit pedestal formation by a pedestal incompetent $\mathbf{EspF_U}$ construct

During selection under 10 μg/mL puromycin treatment, 4 out of 5 HCT8 lines transduced with shRNA against Eps8 showed significantly delayed growth and changes in cellular morphology compared to untransduced HCT8 cells or HCT8 cells transduced with scramble shRNA. These four lines recovered to nearly widetype growth levels after two weeks, but did not recover wildtype morphology (figure 4.12).

Only one knock down line (#4) showed significant reduction on Esp8 levels which was also accompanied by a decrease in IRTKS as detected in unfractionated whole cell lysate (figure 4.13). When seeded at subconflence, no lines tested permitted pedestal formation even at subconfluence when infected with EHEC Δdam $\Delta espF_U$ complemented with H*PH*PH*P. In contrast, subconfluent wildtype HCT8 cells infected with EHEC Δdam $\Delta espF_U$ complemented with HPHPHP or full length $EspF_U$ result in robust actin pedestals that are easily apparent (figure 4.14).

Figure 4.12: shRNA knock of Eps8 in HCT8 cells results in altered morphology.

Untransduced HCT8 cells and HCT8 cells transduced with scramble shRNA or shRNAs targetting Eps8 (lines #3 through 7) were imaged under widefield with phase contrast.

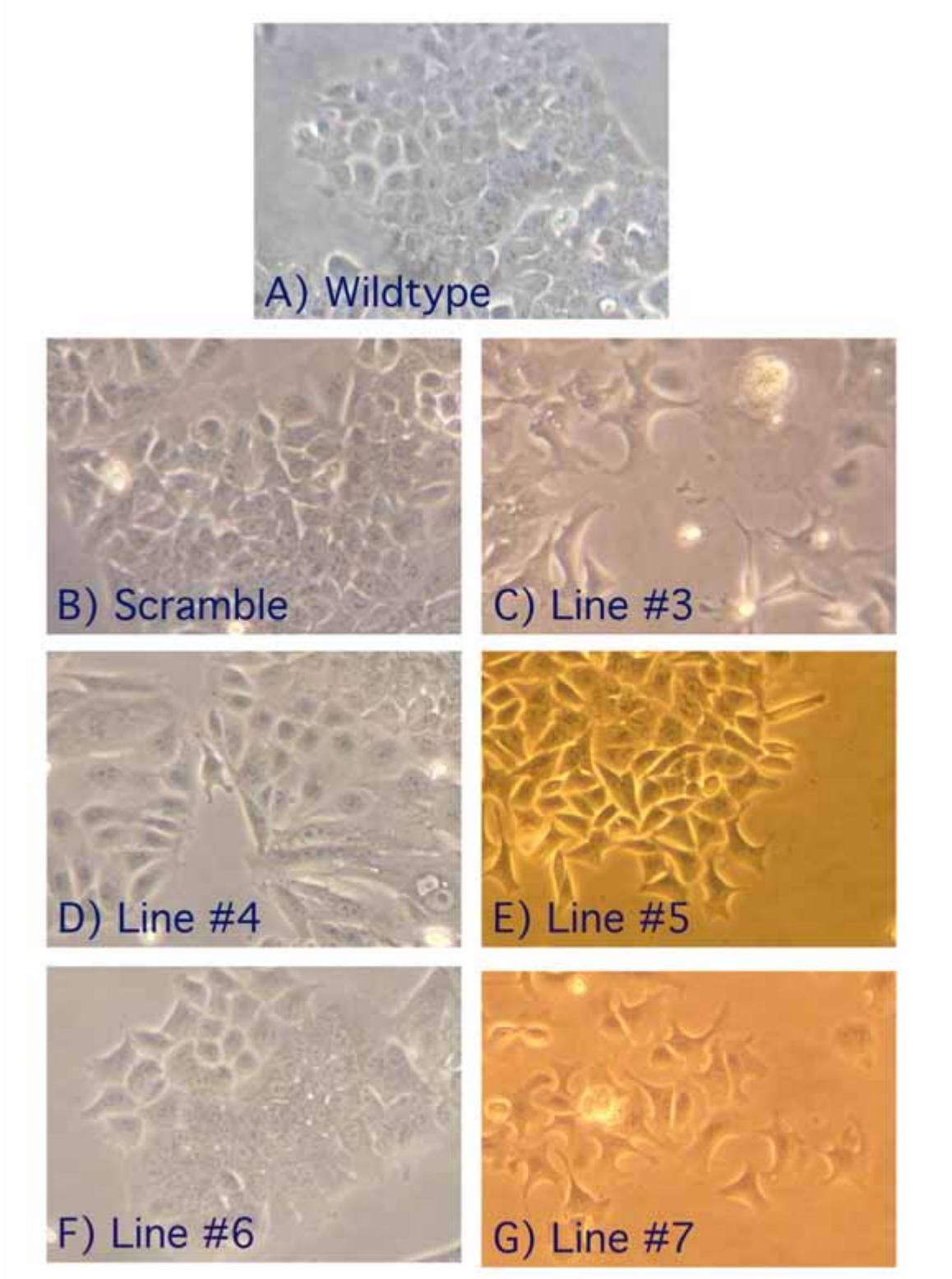

Figure 4.12: shRNA knock of Eps8 in HCT8 cells results in altered morphology.

Figure 4.13: shRNA knock of Eps8 in HCT8 cells

Whole cells lysates of untransduced HCT8 or HCT8 lines transduced with scramble or shRNAs targeting Eps8 were probed for Esp8 and IRTKS.

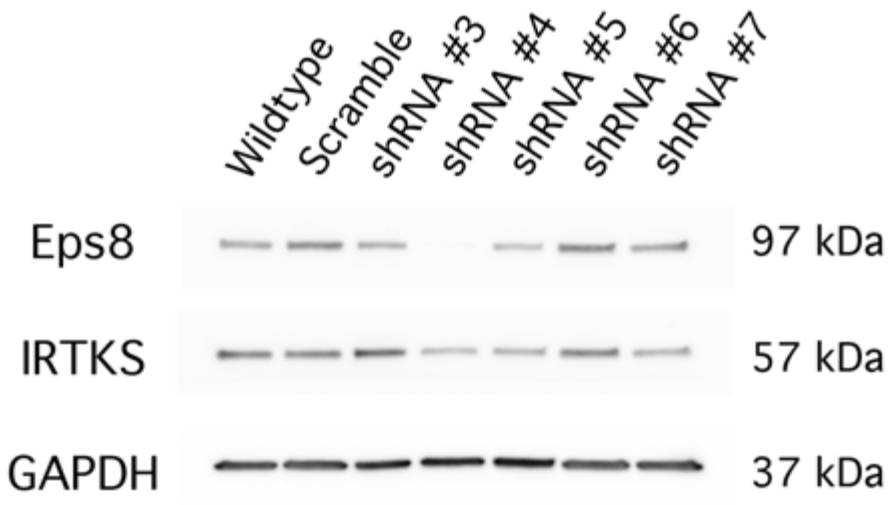

Figure 4.13: shRNA knock of Eps8 in HCT8 cells

Figure 4.14: HCT8 cell lines knocked down for Eps8 did not permit pedestal formation by the pedestal incompetent mutant HP*HP*HP*.

Subconfluent wildtype HCT8 cells infected with EHEC Δdam $\Delta espF_U$ complemented with HPHPHP or full length $EspF_U$ and subconfluent HCT8 lines transduced with shRNA's targeting Eps8 (#3 through 7) infected with EHEC Δdam $\Delta espF_U$ complemented with HP*HP*HP* were stained for bacteria (blue), myc-tagged $EspF_U$ construct (red), and phalloidin (green).

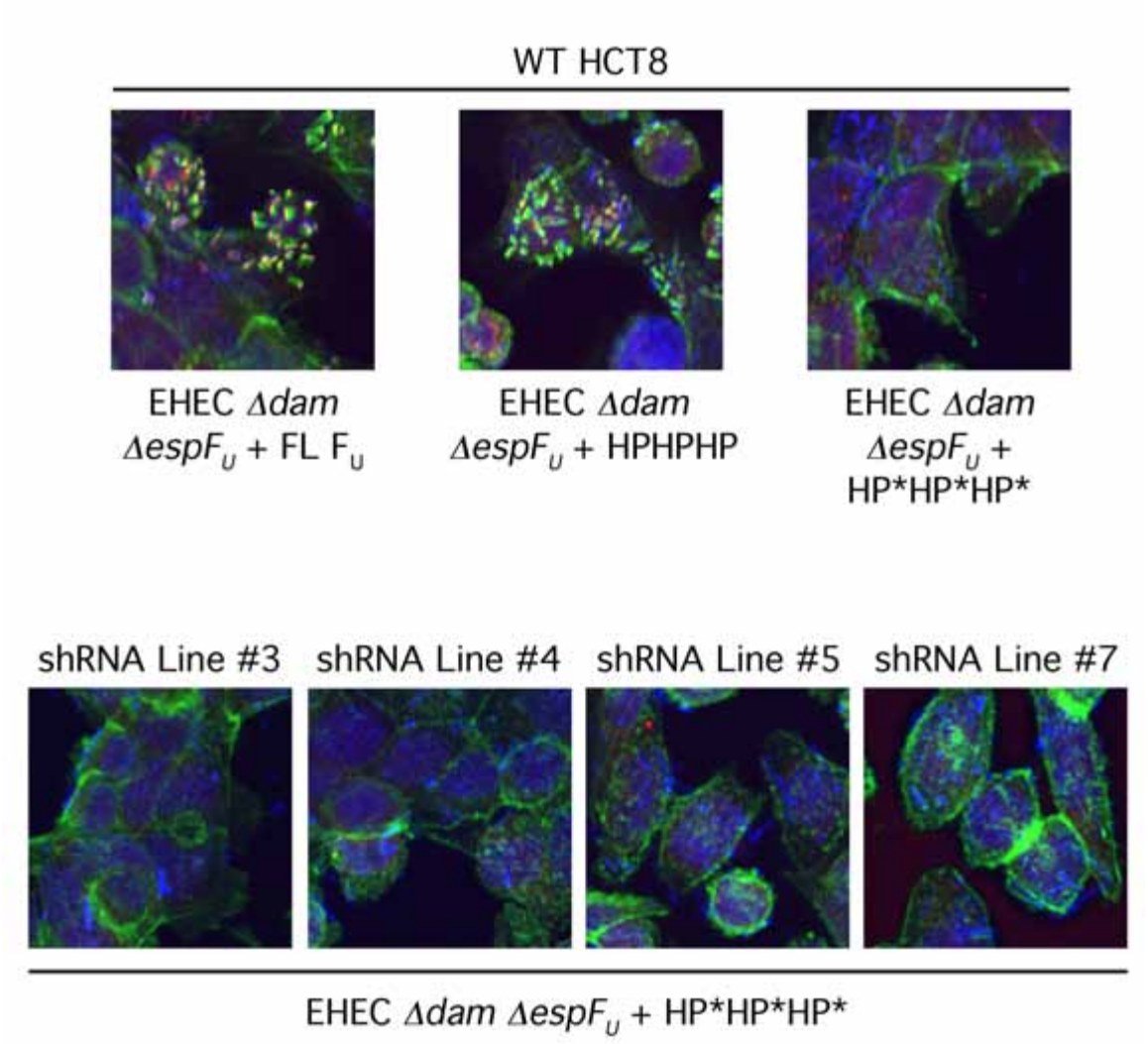

Figure 4.14: HCT8 cell lines knocked down for Eps8 did not permit pedestal formation by the pedestal incompetent mutant HP*HP*HP*.

4.5 Conclusion

Although the tryptophan substitution in between the double PxxP motifs of $EspF_U$'s P domain should give $EspF_U$ an advantage over Eps8 in binding IRTKS [2], multiple P domains are nonetheless required for proper recruitment of $EspF_U$ to sites of bacterial attachment. Polarization additionally increases the minimum number of P domains required. This suggests that despite the advantage afforded by the tryptophan switch, $EspF_U$ needs additional strategies to hijack IRTKS and achieves this perhaps by avidity.

When Eps8 is completely absent from cells, pedestal incompetent mutants with W33A mutations in a three repeat construct are able to form pedestals as robustly as HPHPHP or full length $EspF_U$. Despite lack of competition from Eps8 however, constructs with less than the minimum number of P's required for pedestal formation (two P's for MEFS) still struggle to initiate actin assembly beneath attached bacteria. Clustering and recruitment of the constructs HP and HPH underneath bacteria are much less apparent and actin pedestals appear smaller and less robust. This suggest the presence of other intracellular pressures on $EspF_U$ that make multiple functional repeats advantageous, an observation also seen *in vitro* [104].

Differences in the amount of IRTKS coimmunoprecipitated with Eps8 after infection supports a competition model between Eps8 and $EspF_U$ for binding to IRTKS. In preliminary experiments, pedestal incompetent mutants of $EspF_U$ were not as able to displace IRTKS from Eps8, while pedestal competent mutants clearly decreased IRTKS captured with Eps8. Although not all intracellular IRTKS appears to be associated with Eps8, IRTKS complexed to Eps8 at the apical membrane could provide an accessible pool of IRTKS from which both Tir and $EspF_U$ can recruit to meet at sites of bacterial attachment. The apical localization of Eps8 in polarized

HCT8 may also provide local concentrations of IRTKS in close proximity to sites of bacterial attachment.

Eps8 appears to be just as abundant in subconfluent HCT8 cells as it is in confluent and polarized HCT8 cells. The increased requirement requirement for the number of $EspF_U$ domains needed for actin pedestal formation in confluent and polarized HCT8 may reflect changes in the cellular architecture, subcellular protein organization, or regulatory mechanisms upon polarization that pose challenges to unsurpers of actin signaling pathways. A simple hypothesis is that the relative abundance of Eps8 compared to $EspF_U$ at the apical membrane may be increased polarized cells.

Attempts to reduce Eps8 levels in HCT8 cells did not allow for actin pedestal formation by any $EspF_U$ constructs bearing W33A mutations. Mithramycin treatment of already polarized monolayers reduced Eps8 levels, but perhaps not enough to see an effect. These experiments are preliminary and conducted with at limited set mutants. A more through analysis through treatment and infection of non-polarized HCT8 cells with mutants that display partial activity may provide more conclusive data. Since mithramycin treatment only partially reduces Eps8 levels, its effects on actin pedestal formation by the various $EspF_U$ mutants might be more pronounced under conditions and with mutants that show partial pedestal activity.

shRNA knockdown of Eps8 resulted in severe growth defects and obvious changes in cellular morphology (except in shRNA line #6) that highlight the important role of Eps8 for normal cellular architecture and growth. The only shRNA line (line #4) that showed a significant knockdown of Eps8 by western blot also did not permit pedestal formation by $EspF_U$ with W33A mutations in the P domains. It may be that even minuscule amounts of Eps8 can prevent these weaker mutants from successfully binding IRTKS. We suspect that the amount of $EspF_U$ injected into host cells may be minute compared to host proteins, especially considering the number of bacteria that

can be found on per cell on infected polarized monolayers, (usually less than ten if present). And both injected Tir as well as $EspF_U$ are beyond Western blot detection limits in infected cell lysates (data not shown). Thus, perhaps even a significant knock down in Eps8 protein levels is not permissible for actin pedestal formation by W33A mutants, as it is in Eps8 knock out MEFs.

The infection results for Eps8 knock down line #4 could also indicate that Eps8 may not in fact be a direct competitor for $EspF_U$ or that there may be other redundant host proteins in HCT8 cells not present in MEF. Yet another possible explanation is that the Eps8 in line #4 mutated under selective pressure during puromycin treatment and the mutation affected recognition by the monoclonal antibody used to detect the protein. The growth pattern of this line supports this theory somewhat. Except for line #6, which showed no reduction in Eps8 levels on western blot, all of the other shRNA lines were very slow to grow initially and displayed severe morphological disturbances. for about two weeks after the start of selection under puromycin. Growth rate was minimal, but suddenly increased to near wildtype levels overnight from less than 10 % confluence, suggesting that the cells had adapted to the selective pressure. As with the CO-IP and mithramycin experiments, the shRNA studies are preliminary. The Eps8 knock down cells lines should be further characterized and experiments should be repeated for more conclusive interpretations.

CHAPTER 5

DISCUSSION

5.1 Challenges to establishing infection

EHEC faces many challenges in establishing an infective niche in human hosts. In the course of evolving towards its natural life cycle of inhabiting the gastrointestinal tract of ruminants, shedding into the environment (perhaps on grassy pastures?) and re-ingestion, EHEC may have evolved many traits that also enable it to cause human outbreaks in developed countries today. For example, EHEC must survive refrigeration, sometimes freezing, and conventional processed meat and produce sanitation protocols. Traits that help it survive in the open environment after shedding from animals likely help with survival in food processing facitlies and grocery store environments as well. More recently, specific factors that allow EHEC to bind leafy greens have even been found [7] for example.

Once ingested by unsuspecting humans, EHEC must overcome multiple challenges in the gut environment (For a detailed review, see [46]). EHEC survives the highly acidic environment of the stomach with such success that the infectious dose in humans is thought to be as low as 50-100 bacteria. A number of acid tolerance mechanisms are thought to aid EHEC survival [46]. In the colon, EHEC is able to establish a presence in spite of resident microbiota and a protective mucus layer. In addition, AE lesions made by EHEC and EPEC provide these pathogens with a unique and effective strategy of intimate attachment.

To make AE lesions, EHEC must induce a dramatic reorganization of cytoskeletal structures, beginning with the effacement of microvilli. Highly organized, yet dynamic [12, 43], microvillar structure must be under constant regulation. Pathogen induced calpain activation has now been shown to be involved in microvilli effacement by three gut pathogens, EPEC, EHEC, and *H. pylori* [69, 127]. Through the cleavage of Ezrin, a calpain substrate responsible for anchoring cytoskeletal components to the plasma membrane, these pathogens are able to disrupt a key cellular interaction that leads so instability of the microvillus structure. In the case of *H. pylori*, the effector VacA was identified to initiate these effects [127]. While bacterial components responsible for calpain activation are not currently known for EHEC and EPEC, unpublished evidence from our lab and the Herman lab (Tufts Univesity) point to evidence for T3SS effectors. In manipulating calpain activity, these pathogens have succeeded in disrupting a central regulator of cytoskeletal dynamics, which may also have wider impacts on cellular physiology during infection.

5.2 EspF$_U$ repeats increase functional affinity

The second piece to AE lesion formation is the formation of actin pedestals. While pathogen induced actin assembly is not uncommon, the rebuilding of actin structures by an extracellular pathogen in a directed and organized manner is quite remarkable in the midst of tight cellular regulation. Tir is a rather clever invention in this respect. By being both an extracellular anchoring site for bacterial attachment, and an intracellular signaling molecule, Tir is able to direct location specific actin assembly [132, 70] underneath sites of bacterial attachment. And through recruitment of key adaptor molecules, Tir is able to usurp control of by N-WASP, which is normally kept inactive and under tight regulation [111, 79].

EPEC and EHEC both hijack N-WASP by Tir initiated signaling cascades, but EHEC has evolved to include another T3SS effector in concert with Tir. It is unclear what advantages EHEC may have in using $EspF_U$ in its pedestal formation pathway. $EspF_U$ takes control of key host proteins by molecular mimicry and multivalency through repeating functional units, strategies that are also commonly seem with other T3SS effectors [50], including plant T3SS effectors [134, 8]. Most of the bulk of $EspF_U$ functions in actin pedestal formation and consists of repeating H and P domains, which can be truly be considered as two separate functional entities. The H domains are ultimately responsible for hijacking the actin assembly pathway through activation of N-WASP and the P domains direct localization of $EspF_U$ to sites of bacterial attachment via binding to Tir. These modular entities can even be exchanged. The related effector, EspF, which also consists of repeating H and P domains, can be made to behave like $EspF_U$ by exchanging its native P domain that directs it to SNX9, with that of $EspF_U$ (unpublished data by Didier Vingadassalom). Though both the H and P domains can bind their respective targets with higher affinity than native host binding partners [1, 26], the presence of multiple repeats in nature points to additional challenges in the cell that enhanced affinity alone cannot overcome.

Sallee and coworkers have investigated the degree of actin assembly activity gained by additional $EspF_U$ repeats *in vitro* [104] and observed kinetics that also match well with the number of $EspF_U$ repeats surveyed in nature [54]. In their system, one $EspF_U$ repeat showed miminal N-WASP activation. Adding an additional repeat more than doubled N-WASP activity and a third repeat nearly tripled activity. The degree of gains with the fourth, fifth and sixth repeats were much less with maximal activity peaking at six repeats [104]. In Garmendia's 2005 survey, 99% of $EspF_U$ alleles encoded three or more repeats, with a vast majority (79%) encoding

six repeats. Alleles with more than six repeats were found in less than 1% of strains surveyed[54].

While Sallee's study was *in vitro*, the results also correlate interestingly with observations in our infection model. Upon HCT8 cell polarization, the minimal number of Esp_U repeats need for actin pedestals increases to three repeats, with a particular need for three P domains. This need for additional functional P domains suggests that additional structural challenges may be hindering $EspF_U$ localization after cells undergo polarization. In addition to considering the presence of additional host proteins that may interfere with $EspF_U$ localization, relative concentrations and locations of host and bacterial components are also factors to consider.

$EspF_U$ may have evolved to overcome challenges to hijacking host proteins in polarized cells by increasing its overall functional effectiveness through repetition of its functional units. The need specifically for additional P domains over H domains in actin pedestal formation in polarized HCT8 cells indicate that the challenges lie more against the targeting module of $EspF_U$. Repeating P domains may help "supercharge" this homing/targeting module through increasing avidity, resulting increasing overall functional activity of the P domains in a single $EspF_U$ molecule.

In a more crowded subcellular environment or in an intracellular environment where $EspF_U$ becomes less likely to bind IRTKS for example, increasing the functional activity of this targeting module via multiple repeats may increase the chances that $EspF_U$ actually encounters and binds IRTKS. As well, "supercharging" the targeting module may also increase its functional activity (in binding to IRTKS) in an environment that may be hostile to perturbations of native host protein-protein interactions. As protein-protein interactions are dynamic, concentrating functional domains via repeats may increase the likelihood of dislodging and displacing native

host protein-protein interactions by increasing the local concentration of the "competing" interaction.

Increased functional activity may also help stabilize $EspF_U$ to critical protein complexes underneath sites of bacterial attachment. Immunofluorescence staining shows that Tir and IRTKS can localize underneath sites of bacterial independently of $EspF_U$ and both of these EHEC pedestal components are observed at early time points of infection when no actin assemble occurs yet (data not shown). Both Tir and IRTKS form homo-dimers, as well as intimin on the outer surface of EHEC. It is reasonable to imagine that intimin, Tir, and IRTKS, through association of homo-dimers at multiple levels, form macromolecular complexes concentrated underneath intimately bound EHEC.

A single $EspF_U$ molecular that is "supercharged" for the targeting module may more stably interact with and bind the Tir/IRTKS complex. In a repeating structural arrangement, the binding of a single P domain may bring the next P domain within optimal close proximity to lead to cooperative binding of the next P domain and so forth. Thus, the overall affinity of $EspF_U$ to the Tir/IRTKS complex is enhanced by increasing avidity of the targeting module. And three or more P domains, in particular, may add more to the degree of macromolecular complexing, compared to just two P domains. While an $EspF_U$ with two P's has the potential to bind two SH3's of IRTKS, the SH3's could be from the same IRTKS dimer. In this case, multimerization at this level is not enhanced. With three or more P domains, one $EspF_U$ molecule must bind two or more IRTKS dimers, thus enhancing macromolecular complexing of actin pedestal initiating factors underneath sites of bacterial attachment.

For actin pedestal formation, recruitment of $EspF_U$ to the IRTKS/Tir complex via P domains may be thought of as a critical juncture in recruiting host actin as-

sembly machinery to sites of bacterial attachment. And increased functional activity achieved by increasing the avidity of P domain and IRTKS interactions may help overcome intracellular challenges that require more P domains for actin pedestal formation in polarized intestinal cell.

5.3 Eps8 and $EspF_U$ competition for IRTKS

Considering the abundance and ubiquity of SH3 domains and SH3 ligands in mammalian cells, it is not unreasonable to speculate that $EspF_U$'s P domains may need to outcompete natural host ligands for accessing the SH3 domains of IRTKS dimers. The host protein Eps8 has emerged as likely competitor against which $EspF_U$'s P domains have evolved to outcompete. While the total relative amount of Eps8 does not change, Eps8 may be more concentrated and organized at the apical surface in a polarized intestinal monolayer. Indeed, Eps8 can be found apically, but its position there in relation to its role in EHEC pedestal formation requires further study.

It is tempting to think that Eps8 might provide a readily accessible concentration of IRTKS at the apical membrane that could be used both by Tir and $EspF_U$. Since Tir binds IRTKS in the IMD region, there is no need to dislodge Eps8 from IRTKS. $EspF_U$ may then subsequently bind to the Tir/IRTKS complex by dislodging Eps8. This hypothesis is not well supported by our preliminary imaging data. IRTKS can be easily seen at sites of bacterial attachment by immunoflourescence, while Esp8 is rarely found concentrated underneath bacteria. Eps8 is sometimes seen in pedestals, but not always and never in cells infected with pedestal incompetent constructs of $EspF_U$. This implies that IRTKS bound to Tir do not carry Eps8, against which $EspF_U$ can exchange positions. However, a separate population of IRTKS concentrated at the apical membrane by Eps8 may still aid in directing $EspF_U$

closer to Tir. Separate local concentrations of Eps8-IRTKS-$EspF_U$ complexes at the apical membrane may exist alongside Tir-IRTKS complexes at the apical membrane. Subsequent recruitment of $EspF_U$ to the Tir/IRTKS complex could pontentially be achieved by dimer exchange of IRTKS molecules in close proximity.

5.4 Final thoughts

Additional questions remain about the activities of $EspF_U$ after injection into host cells. How $EspF_U$ finds its way to the Tir/IRTKS complex and its path after injection through the T3SS is still unclear. When ectopically expressed in cultured cells, $EspF_U$ can be found localized very clearly to mitochondria without noticeably perturbing intracellular actin organization (unpublished data by Alenka Lovy, Tufts University) or mitochondrial dynamics. Is actin assembly activity of the H domains dependent on clustering $EspF_U$ at the membrane or perhaps the presence of other bacterial factors? $EspF_U$ has also been shown to complement EspF activity in EPEC, where it is not needed for actin pedestal formation [126]. Could $EspF_U$ have other functions that are redundant with EspF, which differs from $EspF_U$ in the P domains, thereby targeting it to a different cellular target?

Disruption of the host cell architecture not only alters the physical structure of the cell, but most certainly upsets normal cell physiology in a manner that contributes to diarrhea. Apical surface of intestinal cells is adapted for nutrient absorption and effacement of microvilli alone should cause displacement of aquaporins and other apical nutrient transporters. In addition to the activation of calpain and the dramatic rearrangement of the cytoskeleton associated with AE lesion formation, the coordinated activities of other T3SS effectors all together disrupt intestinal cell function and not doubt contribute to EHEC's hallmark symptom of bloody diarrhea.

APPENDIX A

A POTENTIAL STRATEGY FOR STUDYING T3SS EFFECTOR FUNCTION USING APEX FUSION PROTEINS

A.1 Acknowledegments

Plasmids encoding optimized APEX enzymes were generated by the lab of Alice Ting (MIT) and biotin-phenol substrate made by Aditya Bandekar (Sassetti Lab, UMMS).

A.2 Introduction

Knowing the exact intracellular locations and binding partners of bacterial effectors would be a huge advantage in studying effector function. Effector mechanisms are often deduced indirectly. In vitro studies are limited to the components of the in vitro system. And while effector deletions and complementation with effector mutants can provide useful information about critical functional components of the effector itself, such techniques with mammalian cell factors can cause gross defects in the cell (as demonstrated in figure 4.12) or yield phenotypes driven by off target effects.

Recently, a strategy to specifically label proteins by TEM or label proteins in close proximity was developed by the Ting lab [78, 97]. The method involves fusing an optimized plant peroxidase to a protein of interest. In TEM, samples containing the fusion peroxidase can be highlighted and specifically stained for with an EM

compatible substrate for the peroxidase. This staining method offers better labeling than conventional techniques. In live cells, treatment with another peroxidase substrate, biotin-phenol, allows the fusion construct to tag nearby proteins with biotin. Proteomic mass spec analysis of cell lysates with fusion-APEX would yield information about potential binding partners, proteins in complexes, transient interactions, and intracellular localization.

In this study, APEX was cloned as a fusion protein with $EspF_U$ to determine its utility in studying T3SS effectors in infection models.

A.3 Materials and Methods

A.3.1 Cloning $EspF_U$-APEX fusion and bacterial strains

Bacterial complementation plasmids expressing $EspF_U$ and HPHPHP fused to soy or pea APEX were generated by overlap extension PCR according to [13]. Primers used are listed in table C.2. Constructed plasmids encoding $EspF_U$ or HPHPHP fused to soy or pea APEX enzymes were used to complement EHEC Δdam $\Delta espF_U$ (Table C.1).

A.3.2 Cell culture and infection

HCT8 cells were cultured and polarized as described in section 3.3.1. Infection was carried out as described in section 3.3.4.

A.3.3 Intracellular biotin labeling

Cells were supplemented with 7μM HEME in regular cell culture for 24 hours prior to infection. Heme was not included in media during infection. After infection, cells were treated for 30 minutes with biotin-phenol labeling substrate (a generous gift from Aditya Bandekar and Chris Sassetti). Labeling reaction was catalyzed by addition of hydrogen peroxide (final concentration of 1mM)for one minute. The reaction

was stopped by adding "quencher solution" (10 mM sodium azide, 10 mM sodium ascorbate, 5 mM Trolox final concentrations) in cell media. Cells were washed in PBS with quencher solution prior to immunofluorescent staining or lysate collection.

A.3.4 Imaging

Cells were processed for immunofluorescent imaging as described in section 3.3.6 and imaged on a Leica SP5 confocal microscope.

A.3.5 Western blot

Whole cell lysates from infected polarized HCT8 treated for APEX biotin labeling were collected as described in section 4.3.9. Lysates were prepared for western blotting as described in section 4.3.9. and probed with streptavidin-HRP.

A.4 Results

A.4.1 $EspF_U$-APEX fusions retain normal T3SS effector function

$EspF_U$ and HPHPHP-APEX fusions were able to be translocated through the T3SS and function normally in actin pedestal formation. Actin pedestals were clearly discernable by immunofluorescence in polarized HCT8 cells infected with EHEC Δdam $\Delta espF_U$ complemented with $EspF_U$ or HPHPHP fusion APEX constructs (Figure A.1).

Figure A.1: APEX fusions are translocated and do not intefere with effector function

Polarized HCT8 cells infected with EHEC Δdam $\Delta espF_U$ complemented with $EspF_U$ or HPHPHP -APEX fusions were stained for bacteria (blue), Tir (red) and actin (green).

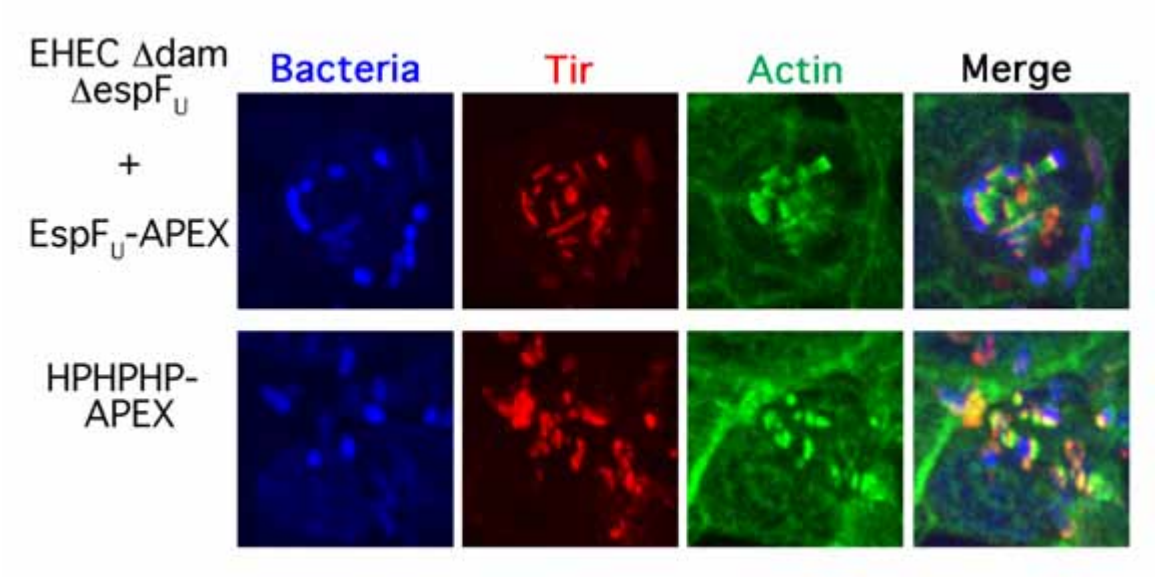

Figure A.1: APEX fusions are translocated and do not intefere with effector function

A.4.2 APEX biotin labeling

Biotin-phenol treatment of HCT8 cells resulted in a general increase in biotinylated proteins, even in HCT8 cells infected with EHEC not delivering APEX. This maybe due to endogenous enzyme activity by either cellular or bacterial T3SS delivered enzymes. However, lysates from HCT8 cells infected with EHEC Δdam $\Delta espF_U$ strains compemented with $EspF_U$-soy or pea APEX showed slightly more biotinylation overall and additional biotinylated bands in soluble fractions.

Figure A.2: APEX Biotin labeling

Lysates of polarized HCT8 cells infected with EHEC Δdam $\Delta espF_U$ complemented with $EspF_U$ or HPHPHP -APEX fusions were probed for biotinylated proteins.

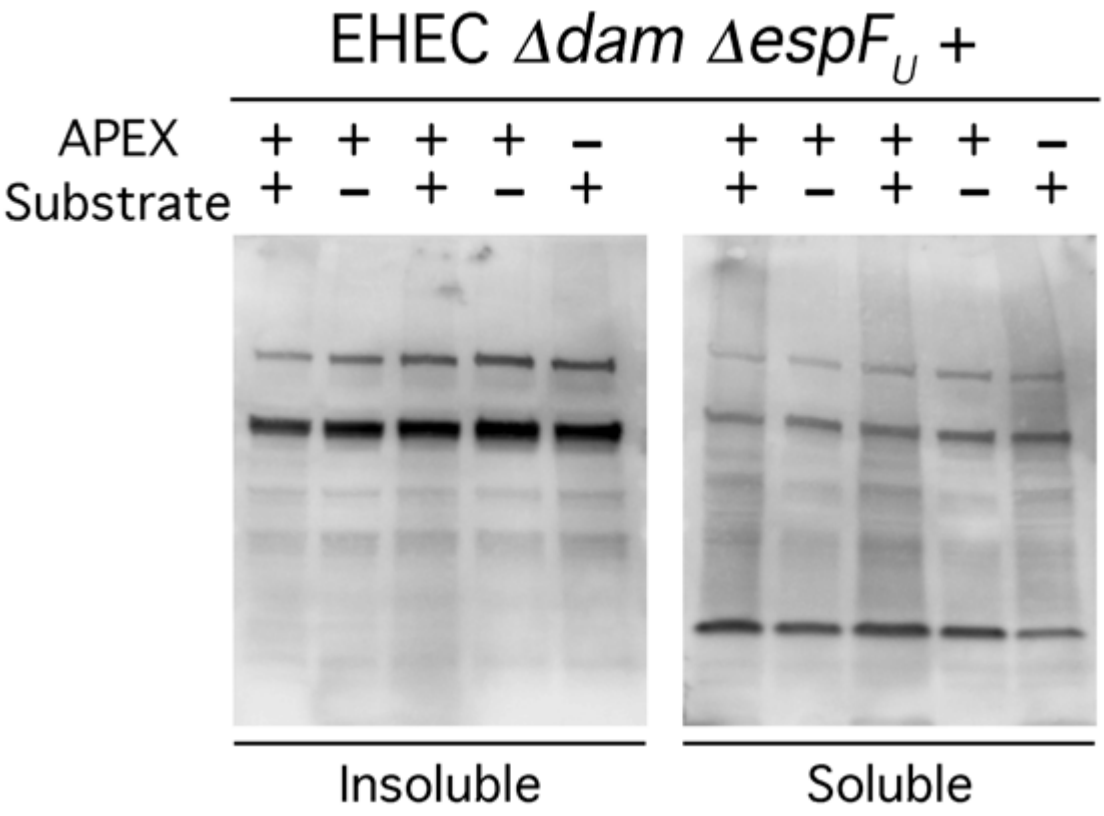

Figure A.2: APEX Biotin labeling

A.5 Conclusions

APEX fusions of bacterial effector proteins could be used as an effective tool in studying the function of known and unknown T3SS effectors. Because APEX can be translocated by the T3SS, effector-APEX fusions could be used in infection models and studied at physiologically relevant concentrations and in correct intracellular compartments.

TEM studies using effector-APEX fusions would provide specific data on effector localization and eliminates the need for TEM compatible antibodies. While data from mass spec will be potentially noisy, APEX labeling could help identify previously unknown protein-protein interactions between bacterial effectors and host proteins as well as between effectors.

A.6 Project Proposal

The utility of using APEX fusions in the study of T3SS effectors could be shown by studying APEX fused to effectors for which effector and host protein interactions have been well characterized. This proposal outlines such experiments using $EspF_U$-APEX fusions as a proof of principle.

A.6.1 Aim 1: Demonstrate that APEX can be used to study T3SS effectors

A.6.1.1 $EspF_U$-APEX fusions function after secretion through the T3SS.

Figure A.1 shows that $EspF_U$-APEX fusions can be secreted through the T3SS into infected host cells without affecting the function of $EspF_U$. APEX activity should also be assessed after T3SS secretion. EHEC strains complemented with $EspF_U$-APEX can be treated with congo red as described in section 3.3.5 to induce secretion of the fusion protein into the media. Supernatants can then be tested for

APEX activity by assaying for reduction of nitroblue tetrazolium in native gel as described in [81].

A.6.1.2 $EspF_U$-APEX labels known binding partners.

Proteomic mass spec analysis of cell lysates infected with EHEC strains delivering $EspF_U$-APEX under conditions that produce actin pedestals should show that N-WASP and IRTKS are biotinylated by APEX. Tir and Arp2/3 may also be labeled if they are within close enough proximity. Labeling of other host proteins that have also been reported to localized to actin pedestals, but not involved in pedestal formation process, may result in noise in the proteomic analysis, but nonetheless would also help confirm the proximity labeling activity of APEX.

A.6.2 Aim 2: Demonstrate that APEX can provide new information on known interactions

Interactions of $EspF_U$ with its host binding partners (N-WASP and IRTKS) have been well characterized *in vitro* and in infected cells. However, specific questions about these interactions during the time course of infection remain unanswered.

A.6.2.1 Which comes first, N-WASP or IRTKS?

Proteomic mass spec analysis of cell lysates infected with EHEC strains delivering $EspF_U$-APEX at different time points of infection may show differences in the degree of N-WASP and IRTKS labeling by APEX. If one protein is preferentially labeled over the other at earlier time points, then this would indicate that $EspF_U$ associates with that protein first.

A.6.2.2 IRTKS versus IRSp53?

Both IRTKS and IRSp53 have been reported to link $EspF_U$ to Tir [125, 128] in actin pedestal formation. The disparate results of different labs may simply be due to

differences in cell type or lines used in their respective studies. Proteomic mass spec analysis of $EspF_U$-APEX labeled cell lysates may confirm the relative roles of IRTKS and IRSp53 in $EspF_U$ recruitment during actin pedestal formation in different cell types.

A.6.3 Aim 3: Demonstrate that APEX can provide new information on unknown functions of effectors

APEX can be used in TEM for single molecule intracellular localization as well as in mass spec for proteomic analysis by promiscuous biotinylation. Both of these techniques performed at various timepoints in a variety of biological samples may give valuable information about other unknown functions and behaviors of $EspF_U$.

A.6.3.1 Other binding partners?

Proteomic mass spec analysis of cell lysates infected with EHEC strains delivering $EspF_U$-APEX has the potential to be noisy given that the fusion protein may encounter and label non-specific interactions or non-binding proteins within close proximity. However, the frequency of labeling individual proteins may be used as a threshold for true interactions. Labeling frequency of known binding partners (namely N-WASP and IRTKS) may be useful in determining a fair threshold level. Heavy isotope or radiolabeling of bacterial cultures in prior to infection may allow for distinguishing new protein-protein interactions between $EspF_U$ and other bacterial effectors.

A.6.3.2 Mitochondrial association?

$EspF_U$ can localize to the mitochondria via targeting sequences in its N-terminal domain (unpublished data by Alenka Lovy, Tufts University, and other groups). TEM labeling of APEX may shed light on the degree, timing and frequency of

this localization compared to localization at actin pedestals. Both TEM and mass spec analysis would also provide information on whether $EspF_U$ enters the inner mitochondrial compartment.

A.6.3.3 Tight junction disruption?

$EspF_U$ has also been reported to complement EPEC in [126]. Direct targeting to tight junctional structures and proteins may also be seen by TEM and mass spec proteomic analysis.

A.6.3.4 What's the difference between non-polarized and polarized cells?

We speculate that structural differences in the cellular architecture between non-polarized and polarized intestinal cell cultures contribute to the increase in number of P domains required for successful $EspF_U$ recruitment to the IRTKS/Tir complex. Proteomic mass spec analysis of $EspF_U$-APEX labeled cell lysates from non-polarized and polarized cells may show differences in the presence and abundance of host proteins underneath sites of bacterial attachment that may be contributing to this phenotype.

APPENDIX B

N-WASP INDEPENDENT PEDESTAL FORMATION BY EHEC

B.1 Introduction

A minor pathway for EHEC pedestal formation was observed when the KC12 strain was used to infect MEFs deficient for N-WASP [124]. For less than 5% percent for attached bacteria, pedestals were apparent on N-WASP-/- MEFs infected with KC12 complemented with $EspF_U$; none were observed without $EspF_U$ complementation. Pedestal activity depended on the number of $EspF_U$ repeats. However, the repeat sequence used in the Vingadassalom et al. study do not match the $EspF_U$ repeat sequence used in the current study. Whether this minor pathway contributes to actin pedestal formation in polarized intestinal cells is unclear.

B.2 Materials and Methods

B.2.1 Cell culture

MEFs were cultured like HeLa cells as described in section 3.3.1.

B.2.2 Stable shRNA knockdown of N-WASP in HCT8 cells

Plasmids expressing shRNA sequences targeted against N-WASP (code #'s 258, 163, 86, 84, and 83) in the pSMC2 vector were ordered from OpenBioSystems (a prior incarnation of the current UMMS RNAi core) and transfected into subconfluent HCT8 cells using Arrest-In transfection reagent and Opti-MEM according to

manufacturers' instructions. Transfected HCT8 cells were subjected to selection under 1 μg/mL of puromycin 24 hours after transfection. Cells surviving 4 days of selection were seeded at low confluence into 96-well tissue culture plates in an attempt to isolate clonal populations and cells were kept under puromycin selection during culture.

B.2.3 Bacterial strains and infection

KC12 strains complemented with various mutations of $EspF_U$ were cultured for infection as described in section 3.3.4. Infection was carried out for 3 to 3.5 hours infection.

B.2.4 Immunofluorescent staining and imaging

Infect cells were processed for immunofluorescence imaging as described in section 3.3.6. Images with acquired using a DeltaVision microscope system with deconvolution.

B.3 Results

B.3.1 shRNA knock down of N-WASP in HCT8

Creation of stable N-WASP knock down lines of HCT8 were attempted to address the role of the N-WASP independent pathway in actin pedestal formation in polarized intestinal cells. Combinations of 3, 4, and 5 shRNA sequences were used to generate knockdown lines. Lines that survived puromycin selection were expanded and screened for N-WASP activity. Since EPEC relies on N-WASP in all of its known pedestal formation pathways, actin pedestal formation after EPEC infection was used as a functional screening assay for the degree of functional N-WASP knockdown. Unfortunately, no lines prevented EPEC actin pedestal formation upon infection (data not shown).

B.3.2 Actin pedestal formation by $EspF_U$ truncation and three repeat mutants in N-WASP -/- MEFs

Given the lack of a good functional knockdown in HCT8 cells, N-WASP-/- MEFs were used to investigate the possible involvement of the N-WASP independent pathway in polarized HCT8 cells. The requirement for more $EspF_U$ repeats for actin pedestal formation in N-WASP deficient cells may parallel the conditions in polarized HCT8 cells that lead to an increase in the number of P domains needed for actin pedestal formation. Table B.1 summarizes the results of infection of wildtype and N-WASP -/- MEFs by KC12 strains complemented with every $EspF_U$ construct studied in the previous chapters.

Table B.1: N-WASP Independent Actin Pedestal Pathway

Strain	**$EspF_U$ Foci in WT MEF**	**Pedestals in WT MEF**	**$EspF_U$ Foci in NW-/- MEF**	**Pedestals in NW-/- MEF**
KC12 + p$EspF_U$	Yes	Yes	Yes	Yes
KC12 + HP	No	No	No	No
KC12 + HPH	No	No	No	No
KC12 + PHP	Yes	Yes	No	No
KC12 + HPHP	Yes	Yes	No	No
KC12 + HPHPH	Yes	Yes	No	No
KC12 + HPHPHP	Yes	Yes	V. weak	No/Yes
KC12 + H*PH*PH*P	Yes	No	Yes	No
KC12 + HP*HP*HP*	No	No	No	No

Continued on the next page

Strain	**$EspF_U$ Foci in WT MEF**	**Pedestals in WT MEF**	**$EspF_U$ Foci in NW-/- MEF**	**Pedestals in NW-/- MEF**
KC12 + H*PHPHP	Yes	Yes	V. weak	V. weak
KC12 + HPH*PHP	Yes	Yes	V. weak	V. weak
KC12 + HPHPH*P	Yes	Yes	V. weak	V. weak
KC12 + HPH*PH*P	Yes	Yes	Yes	No
KC12 + H*PHPH*P	Yes	Yes	Yes	No
KC12 + H*PH*PHP	Yes	Yes	No/Yes	No/Yes
KC12 + HP*HPHP	Yes	Yes	No	No
KC12 + HPHP*HP	Yes	Yes	No	No
KC12 + HPHPHP*	Yes	Yes	No	No
KC12 + HPHP*HP*	Weak	Weak	No	No
KC12 + HP*HPHP*	Weak	Weak	No	No
KC12 + HP*HP*HP	No	No	No	No

B.4 Conclusions

The pattern of minor actin pedestal activity observed in N-WASP-/- cells infected with strains delivering the various $EspF_U$ mutants studied in Chapter 3 does not correlate well with the $EspF_U$ domain requirement phenotype observed in polarized cells.

The construct HPHPHP was only weakly recruited to sites of bacterial attachment in N-WASP -/- cells and actin pedestal formation was unclear and consistently reproducible between experiments. This contrasts to infection in polarized

cells where recruitment of HPHPHP is strong and actin pedestals are usually as robust as that made by full length $EspF_U$.

The control $EspF_U$ mutants H*PH*PH*P and HP*HP*HP* showed the expected patterns of recruitment and pedestal formation in both wildtype and N-WASP -/- MEFs. Neither construct could generate actin pedestals in either cell type, but H*PH*PH*P was readily recruited to sites of bacterial attachment.

However, mutant sets with L12A mutations in one or two H domains resulted in unexpected $EspF_U$ recruitment and actin pedestal phenotypes in N-WASP deficient cells. Mutants with one L12A mutation in one H domain displayed an attenuated recruitment phenotype, despite having three wildtype P domains (in contrast to H*PH*PH*P). And two out of three mutants with two L12A mutations in two H domains displayed no attenuation in recruitment but did not produce actin pedestals.

While mutant sets with W33A mutations in one or two P domains resulted in a recruitment and actin pedestal phenotype in N-WASP -/- cells that similar to the phenotype seen in polarized HCT8 cells, it is clear how the absence of N-WASP should affect recruitment of these constructs to IRTKS via P domains. The results from this set of mutants might suggest that N-WASP actually contributes to proper localization of $EspF_U$ to IRTKS. However, the construct H*PH*PH*P was recruited to sites of bacterial attachment clearly without the ability to bind and activate N-WASP. An alternative hypothesis is that N-WASP somehow makes the intracellular environment more permissible to $EspF_U$ IRTKS binding.

The identity of factors involved in the N-WASP independent pathway are also as yet unknown, which limits interpretation of these results. Based on known studies (only one [124]) and our observations, it is unclear what role (if any) the N-WASP independent pathway plays in polarized intestinal cells during actin pedestal formation.

APPENDIX C

TABLES

Table C.1: Bacterial Strains used in this study

Strain ID	**Description**	**Source**
CYL1	EHEC strain TUV-93.0	Lab stock [18]
CYL2	EPEC strain JPN15	Lab stock
CYL85	EHECΔ*dam* Δ*espF*$_U$	This study
CYL96	EHECΔ*dam*Δ*espF*$_U$ + pCL15(HPHPHP)	This study
CYL154	EHECΔ*dam* Δ*espF*$_U$ + pCL1 (HP)	This study
CYL157	EHECΔ*dam* Δ*espF*$_U$ + pCL2 (HPH)	This study
CYL160	EHECΔ*dam* Δ*espF*$_U$ + pCL12 (PHP)	This study
CYL163	EHECΔ*dam* Δ*espF*$_U$ + pCL14 (HPHP)	This study
CYL166	EHECΔ*dam* Δ*espF*$_U$ + pCL20 (HPHPH)	This study
CYL172	EHECΔ*dam* Δ*espF*$_U$ + pKC471 (EspF$_U$)	This study
CYL175	EHECΔ*dam* Δ*espF*$_U$ + pCL39 (H*PHPHP)	This study
CYL178	EHECΔ*dam* Δ*espF*$_U$ + pCL42 (HPH*PHP)	This study
CYL181	EHECΔ*dam* Δ*espF*$_U$ + pCL44 (HPHPH*P)	This study
CYL184	EHECΔ*dam* Δ*espF*$_U$ + pCL25 (HP*HPHP)	This study
CYL187	EHECΔ*dam* Δ*espF*$_U$ + pCL31 (HPHP*HP)	This study

Continued on the next page

Strain ID	**Description**	**Source**
CYL190	EHECΔ*dam* Δ*espF*$_U$ + pCL35 (HPHPHP*)	This study
CYL219	EHECΔ*dam* Δ*espF*$_U$ + pCL55 (HPH*PH*P)	This study
CYL222	EHECΔ*dam* Δ*espF*$_U$ + pCL52 (H*PHPH*P)	This study
CYL225	EHECΔ*dam* Δ*espF*$_U$ + pCL49 (H*PH*PHP)	This study
CYL228	EHECΔ*dam* Δ*espF*$_U$ + pCL64 (HPHP*HP*)	This study
CYL231	EHECΔ*dam* Δ*espF*$_U$ + pCL61 (HP*HPHP*)	This study
CYL234	EHECΔ*dam* Δ*espF*$_U$ + pCL58 (HP*HP*HP)	This study
CYL255	EHECΔ*dam* Δ*espF*$_U$ + pCL73 (HP*H*P*H*P)	This study
CYL258	EHECΔ*dam* Δ*espF*$_U$ + pCL76 (HP*HP*HP*)	This study
CYL261	EHECΔ*dam* Δ*espF*$_U$ + pCL79 (H*PH*PH*P)	This study
CYL411	EHECΔ*dam* Δ*espF*$_U$ + pCL84 (PHPHP)	This study
CYL414	EHECΔ*dam* Δ*espF*$_U$ + pCL87 (PH*PHP)	This study
CYL417	EHECΔ*dam* Δ*espF*$_U$ + pCL90 (PHPH*P)	This study
KC12	EPEC ΔTir-eae::EHEC Tir-eae	[21]
KC12 + pEspF$_U$	EPEC ΔTir-eae::EHEC Tir-eae + pEspF$_U$	[21]
CYL266	KC12 + pCL1 (HP)	This study
CYL269	KC12 + pCL2 (HPH)	This study
CYL272	KC12 + pCL12 (PHP)	This study
CYL275	KC12 + pCL14 (HPHP)	This study
CYL278	KC12 + pCL20 (HPHPH)	This study
CYL281	KC12 + pCL15 (HPHPHP)	This study

Continued on the next page

Strain ID	**Description**	**Source**
CYL290	KC12 + pCL73 (HP*H*P*H*P)	This study
CYL293	KC12 + pCL76 (HP*HP*HP*)	This study
CYL296	KC12 + pCL79 (H*PH*PH*P)	This study
CYL299	KC12 + pCL39 (H*PHPHP)	This study
CYL302	KC12 + pCL42 (HPH*PHP)	This study
CYL305	KC12 + pCL44 (HPHPH*P)	This study
CYL308	KC12 + pCL25 (HP*HPHP)	This study
CYL311	KC12 + pCL31 (HPHP*HP)	This study
CYL314	KC12 + pCL35 (HPHPHP*)	This study
CYL317	KC12 + pCL55 (HPH*PH*P)	This study
CYL320	KC12 + pCL52 (H*PHPH*P)	This study
CYL323	KC12 + pCL49 (H*PH*PHP)	This study
CYL326	KC12 + pCL64 (HPHP*HP*)	This study
CYL329	KC12 + pCL61 (HP*HPHP*)	This study
CYL332	KC12 + pCL58 (HP*HP*HP)	This study
CYL464	EHECΔ*dam* Δ*espF*$_U$ + pCL93 (HPHPHP-Soy APEX)	This study
CYL467	EHECΔ*dam* Δ*espF*$_U$ + pCL98 (HPHPHP-Pea APEX)	This study
CYL470	EHECΔ*dam* Δ*espF*$_U$ + pCL105 (EspF$_U$-Soy APEX)	This study
CYL472	EHECΔ*dam* Δ*espF*$_U$ + pCL105 (EspF$_U$-Soy APEX)	This study
CYL476	EHECΔ*dam* Δ*espF*$_U$ + pCL110 (EspF$_U$-Pea APEX)	This study

Table C.2: Primer Table

Primer Name	**Sequence**	**Use**
DAMZeoF	5'-CTGAA GCGCT GGATG CTGTC GGAGC TTTCT CCACA GCCGG AGAAG GTGTA ATTAG TTAGT CAGC GGTCA TGATC AGCAC GTGTT GACAA TTAAT CATCG G-3	forward primer for replacement of *dam* gene from EHEC with zeocin cassette by λ reb recombineering
DAMZeoR	5'-GCAAA ATCAGC CGACA GAATT GAGGG GGCAA TCAAA TACTG TTTCA TCCGC TTCTC CTTGA GAATC AGTCC TGCTC CTCGG CCACG AAGTG CACGC AGTT-3	reverse primer for replacement of *dam* gene from EHEC with zeocin cassette by λ reb recombineering
damF	5'-TCG GTG TTT CTC AAC ACC-3	screening primer for EHEC Δ*dam*
damR	5'-CGC TTG TTG TTC AAG CGT-3	screening primer for EHEC Δ*dam*
damU	5'-CTG GTC GTT CTC GTC AAT CTT CTG-3	screening primer for EHEC Δ*dam*
damD	5'-AAT CAC CAC GCT GAA GTA TTT GGC-3	screening primer for EHEC Δ*dam*
CLdamF	5'-GTC GGT GTT TCT CAA CAC CGA C-3	screening primer for EHEC Δ*dam*

Continued on the next page

Primer Name	**Sequence**	**Use**
CLdamR	5'-CGA TCT CCG CCA GAT GCG CTT-3	screening primer for EHEC Δ*dam*
CLdamU	5'-GAA CCA CGT CTG CGG AAA ATA CT-3	screening primer for EHEC Δ*dam*
CLdamD	5'-CAC TGC GCA TTT CAT CAA TGA C-3	screening primer for EHEC Δ*dam*
NEW SLIM1	5- CCC CCA GCG CCG AAC GCG CCT GCC CCT ACT CCG CCT GTT CAA AAT GAA CAG AGC CGC -3	SLIM long forward primer for HP*HPHP (*=W33A) mutation
NEW SLIM2	5- CCT GTT CAA AAT GAA CAG AGC CGC -3	SLIM short forward primer for HP*HPHP (*=W33A) mutation
NEW SLIM3	5- AAT GTG CTC GGC CAT GTT ACG TGC -3	SLIM short reverse primer for HP*HPHP (*=W33A) mutation
NEW SLIM4	5- CGG AGT AGG GGC AGG CGC GTT CGG CGC TGG GGG AAT GTG CTC GGC CAT GTT ACG TGC -3	SLIM long reverse primer for HP*HPHP (*=W33A) mutation

Continued on the next page

Primer Name	Sequence	Use
P2 SLIM1	5-CCG CCG GCG CCT AAT GCG CCT GCA CCA ACC CCC CCG GTT CAG AAT GAA CAG TCA CGC-3	SLIM long forward primer for HPHP*HP (*=W33A) mutation
P2 SLIM2	5-CCG GTT CAG AAT GAA CAG TCA CGC-3	SLIM short forward primer for HPHP*HP (*=W33A) mutation
P2 SLIM3	5-AAT ATG TTC AGC CAT GTT ACG AGC-3	SLIM short reverse primer for HPHP*HP (*=W33A) mutation
P2 SLIM4	5-GGG GGT TGG TGC AGG CGC ATT AGG CGC CGG CGG AAT ATG TTC AGC CAT GTT ACG AGC-3	SLIM long reverse primer for HPHP*HP (*=W33A) mutation
P2 SLIM1	5-CCA CCT GCA CCA AAC GCG CCA GCT CCG ACA CCT CCA GTG CAG AAT GAG CAA TCT AGA-3	SLIM long forward primer for HPHPHP* (*=W33A) mutation
P2 SLIM2	5-CCA GTG CAG AAT GAG CAA TCT AGA-3	SLIM short forward primer for HPHPHP* (*=W33A) mutation

Continued on the next page

Primer Name	Sequence	Use
P2 SLIM3	5-TAT ATG CTC TGC CAT ATT TCT CGC-3	SLIM short reverse primer for HPH-PHP* (*=W33A) mutation
P2 SLIM4	5-AGG TGT CGG AGC TGG CGC GTT TGG TGC AGG TGG TAT ATG CTC TGC CAT ATT TCT CGC-3	SLIM long reverse primer for HPH-PHP* (*=W33A) mutation
H1 SLIM1	5-GGT ACC TTA CCA GAT GTA GCA CAA CGT CTT ATG CAA CAT GCT GCT GAA CAC GGC ATT-3	SLIM long forward primer for H*PHPHP (*=L12A) mutation
H1 SLIM2	5-GGT ACC TTA CCA GAT GTA GCA CAA-3	SLIM short forward primer for H*PHPHP (*=L12A) mutation
H1 SLIM3	5-CTC GGC CAT GTT ACG TGC CGG CTG-3	SLIM short reverse primer for H*PHPHP (*=L12A) mutation
H1 SLIM4	5-CTC GGC CAT GTT ACG TGC CGG CTG AAT GCC GTG TTC AGC AGC ATG TTG CAT AAG ACG-3	SLIM long reverse primer for H*PHPHP (*=L12A) mutation

Continued on the next page

Primer Name	Sequence	Use
H2 SLIM1	5-CGC CCG CTT CCG GAC GTT GCG CAG CGT TTA ATG CAG CAC GCT GCT GAA CAT GGG ATT-3	SLIM long forward primer for HPH*PHP (*=L12A) mutation
H2 SLIM2	5-CGC CCG CTT CCG GAC GTT GCG CAG-3	SLIM short forward primer for HPH*PHP (*=L12A)
H2 SLIM3	5-TTC AGC CAT GTT ACG AGC TGG TTG-3	SLIM short reverse primer for HPH*PHP (*=L12A) mutation
H2 SLIM4	5-TTC AGC CAT GTT ACG AGC TGG TTG AAT CCC ATG TTC AGC AGC GTG CTG CAT TAA ACG-3	SLIM long reverse primer for HPH*PHP (*=L12A) mutation
H3 SLIM1	5-CGC CCA CTA CCT GAT GTC GCT CAG AGA CTC ATG CAG CAT GCG GCA GAG CAT GGT ATC-3	SLIM long forward primer for HPHPH*P (*=L12A) mutation
H3 SLIM2	5-CGC CCA CTA CCT GAT GTC GCT CAG-3	SLIM short forward primer for HPHPH*P (*=L12A) mutation

Continued on the next page

Primer Name	Sequence	Use
H3 SLIM3	5-CTC TGC CAT ATT TCT CGC AGG CTG-3	SLIM short reverse primer for HPHPH*P (*=L12A) mutation
H3 SLIM4	5-CTC TGC CAT ATT TCT CGC AGG CTG GAT ACC ATG CTC TGC CGC ATG CTG CAT GAG TCT-3	SLIM long reverse primer for HPHPH*P (*=L12A) mutation
PHPHP SLIM1	5-CGA CAG TCT ACT GCT GAA AGT TCG TTA CAT CAA CAA GGT ACC CCG GCA CGT AAC ATG GCC GAG CAC ATT CCC CCA GCG CCG AAC TGG-3	SLIM long forward primer for deletion for 1st H from HPHPHP
PHPHP SLIM2	5-CCG GCA CGT AAC ATG GCC GAG CAC ATT CCC CCA GCG CCG AAC TGG-3	SLIM short forward primer for deletion for 1st H from HPHPHP
PHPHP SLIM3	5-ATG AAA TGA TGC CGA ATG GGC GTT TGG GGC TCG AAA GAG AGT TGT TGC-3	SLIM short reverse primer for deletion for 1st H from HPHPHP
PHPHP SLIM4	5-GGT ACC TTG TTG ATG TAA CGA ACT TTC AGC AGT AGA CTG TCG ATG AAA TGA TGC CGA ATG GGC GTT TGG GGC TCG AAA GAG AGT TGT TGC-3	SLIM long reverse primer for deletion for 1st H from HPHPHP

Continued on the next page

Primer Name	Sequence	Use
Soy-pCL15	5 GAC ACC TCC AGT GCA GAA TGA GCA ATC TAG ACC TGG ATC CGG AAA GTC TTA CCC AAC TGT GAG TGC TGA TTA CC-3	Forward primer for overlap extension PCR of soy APEX into pCL15
Soy-pKC471	5 TTG CAG AGC ATG GCA TTA ATA CAT CTA AGC GCT CGG GAT CCG GAA AGT CTT ACC CAA CTG TGA GTG CTG ATT ACC-3	Forward primer for overlap extension PCR of soy APEX into pKC471
Soy-Rev	5- CCG GTA ACT GTC AGG TCA GAG CTA ATA TAG GTA ATT ATA TTA TAA TCA CTG CAG TTA GGC ATC AGC AAA CCC AAG CTC GGA AA-3	Reverse primer for overlap extension PCR of soy APEX into pCL15 or pKC471
Pea-pCL15	5 GAC ACC TCC AGT GCA GAA TGA GCA ATC TAG ACC TGG ATC CGG AAA GTC ATA CCC AAC CGT GAG CCC AGA TTA CC-3	Forward primer for overlap extension PCR of pea APEX into pCL15
Pea-pKC471	5 TTG CAG AGC ATG GCA TTA ATA CAT CTA AGC GCT CGG GAT CCG GAA AGT CAT ACC CAA CCG TGA GCC CAG ATT ACC-3	Forward primer for overlap extension PCR of pea APEX into pKC471

Continued on the next page

Primer Name	**Sequence**	**Use**
Pea-Rev	5- CCG GTA ACT GTC AGG TCA GAG CTA ATA TAG GTA ATT ATA TTA TAA TCA CTG CAG TTA TGC CTC GGC GAA TCC CAG TTC AGA CAG-3	Reverse primer for overlap extension PCR of pea APEX into pCL15 or pKC471

Table C.3: Plasmid Table

Plasmid Name	**Description**	**Source**
pRC/CMV-3ΔCSN	mammalian transfection vector for stable expression of Calpastat	[94]
pRC/CMV	empty mammalian transfection vector control	[94]
pKM208	λ red recombinase	Kenan Murphy
pDONRZeo	Zeocin cassette	Lab stock
pDV48	bacterial complementation plasmid expressing $EspF_U$ N-term-5 myc tag	Lab stock
pCL1	bacterial complementation plasmid expressing $EspF_U$ N-term-HP-5 myc tag	This study, created from pDV48
pCL2	bacterial complementation plasmid expressing $EspF_U$ N-term-HPH-5 myc tag	This study, created from pDV48
pCL12	bacterial complementation plasmid expressing $EspF_U$ N-term-PHP-5 myc tag	This study, created from pDV48
HPHPHP	minigene encoding HPHPHP in IDTSmart	IDT
pCL15	bacterial complementation plasmid expressing $EspF_U$ N-term-HPHPHP-5 myc tag	This study, created from pDV48
pCL20	bacterial complementation plasmid expressing $EspF_U$ N-term-HPHPH-5 myc tag	This study, created from pDV48
pCL25	bacterial complementation plasmid expressing $EspF_U$ N-term-HP*HPHP-5 myc tag	This study, created from pCL15
pCL31	bacterial complementation plasmid expressing $EspF_U$ N-term-HPHP*HP-5 myc tag	This study, created from pCL15

Continued on the next page

Plasmid Name	Description	Source
pCL35	bacterial complementation plasmid expressing $EspF_U$ N-term-HPHPHP*-5 myc tag	This study, created from pCL15
pCL39	bacterial complementation plasmid expressing $EspF_U$ N-term-H*PHPHP-5 myc tag	This study, created from pCL15
pCL42	bacterial complementation plasmid expressing $EspF_U$ N-term-HPH*PHP-5 myc tag	This study, created from pCL15
pCL44	bacterial complementation plasmid expressing $EspF_U$ N-term-HPHPH*P-5 myc tag	This study, created from pCL15
pCL49	bacterial complementation plasmid expressing $EspF_U$ N-term-H*PH*PHP-5 myc tag	This study, created from pCL39
pCL52	bacterial complementation plasmid expressing $EspF_U$ N-term-H*PHPH*P-5 myc tag	This study, created from pCL39
pCL55	bacterial complementation plasmid expressing $EspF_U$ N-term-HPH*PH*P-5 myc tag	This study, created from pCL44
pCL58	bacterial complementation plasmid expressing $EspF_U$ N-term-HP*HP*HP-5 myc tag	This study, created from pCL25
pCL61	bacterial complementation plasmid expressing $EspF_U$ N-term-HP*HPHP*-5 myc tag	This study, created from pCL25
pCL64	bacterial complementation plasmid expressing $EspF_U$ N-term-HPHP*HP*-5 myc tag	This study, created from pCL35
pCL73	bacterial complementation plasmid expressing $EspF_U$ N-term-HP*H*P*H*P-5 myc tag	This study, created from pCL67

Continued on the next page

Plasmid Name	Description	Source
pCL76	bacterial complementation plasmid expressing $EspF_U$ N-term-HP*HP*HP*-5 myc tag	This study, created from pCL58
pCL79	bacterial complementation plasmid expressing $EspF_U$ N-term-H*PH*PH*P-5 myc tag	This study, created from pCL49
pCL84	bacterial complementation plasmid expressing $EspF_U$ N-term-PHPHP-5 myc tag	This study, created from pCL15
pCL87	bacterial complementation plasmid expressing $EspF_U$ N-term-PH*PHP-5 myc tag	This study, created from pCL42
pCL90	bacterial complementation plasmid expressing $EspF_U$ N-term-PHPH*P-5 myc tag	This study, created from pCL44
soy-mito-APEX	Mitochondria targeted Soy-APEX for promiscuous biotinylation	Addgene #42607
pea APEX	Cassette for pea APEX for promiscuous biotinylation	Addgene #40306
pKC471	bacterial complementation plasmid expressing full length $EspF_U$-5 myc tag	Lab strain
pCL93	bacterial complementation plasmid expressing $EspF_U$-N-term-HPHPHP-Soy APEX	This study, created from pCL15
pCL98	bacterial complementation plasmid expressing HPHPHP-Pea APEX	This study, created from pCL15
pCL105	bacterial complementation plasmid expressing full length $EspF_U$-Soy APEX	This study, created from pKC471

Continued on the next page

Plasmid Name	Description	Source
pCL108	bacterial complementation plasmid expressing full length $EspF_U$-Pea APEX	This study, created from pKC471
pCL110	bacterial complementation plasmid expressing full length $EspF_U$-Pea APEX	This study, created from pKC471
pGFP-Eps8	mammalian expression plasmid producing GFP-mEps8 on	Giorgio Scita
psPAX2	Lentiviral packaging plasmid producing gag-pol	Abe Brass (UMMS)
pMD.2G	Lentiviral packaging plasmid producing VSV-G envelope protein	Abe Brass (UMMS)
TRCN0000061543	shRNA against human Eps8 in pLKO.1	UMass shRNA core
TRCN0000061544	shRNA against human Eps8 in pLKO.1	UMass shRNA core
TRCN0000061545	shRNA against human Eps8 in pLKO.1	UMass shRNA core
TRCN0000061546	shRNA against human Eps8 in pLKO.1	UMass shRNA core
TRCN0000061547	shRNA against human Eps8 in pLKO.1	UMass shRNA core
#258	shRNA against human N-WASP in pSMC2	OpenBioSystems
#163	shRNA against human N-WASP in pSMC2	OpenBioSystems
#86	shRNA against human N-WASP in pSMC2	OpenBioSystems
#84	shRNA against human N-WASP in pSMC2	OpenBioSystems
#83	shRNA against human N-WASP in pSMC2	OpenBioSystems

Table C.4: Antibodies Used

Antibody	**Vendor**	**Catalog**	**IMF**	**WB**
Anti-ezrin	Zymed	357300	1:100	1:1000
Anti-O157	Gibco	Discontinued		
Anti-O157	Fitzgerald Industries	70-XG13		
Anti-Myc (9E10)	Santa Cruz	sc-40	1:100	1:500
Anti-Tir	Lab generated sera		1:1000	1:5000
Anti-Eps8	BD	610143	1:100 to 1:1000	1:1000
Anti-IRTKS	Novus	H00055971-M01	1:1000	1:1000 to 1:5000
Anti-IRSp53	Novus	H00010458-M01	1:1000	1:1000 to 1:5000
Anti-Tubulin	various vendors			1:5000
Anti-GAPDH	various vendors			1:5000
Anti-mouse-Alexa 568	Invitrogen	A-11004	1:400	
Anti-mouse-Alexa 488	Invitrogen	A10667	1:400	
Anti-mouse-Alexa 647	Invitrogen	A31571	1:400	
Anti-rabbit-Alexa 488 or 568	Invitrogen		1:100	
Anti-goat-Alexa 488 or 568	Invitrogen		1:100	
Anti-GFP-Alexa 647	Invitrogen	A31852	1:400	
Anti-mouse-HRP	various vendors			1:10,000

BIBLIOGRAPHY

[1] Aitio, Olli, Hellman, Maarit, Kazlauskas, Arunas, Vingadassalom, Didier F., Leong, John M., Saksela, Kalle, and Permi, Perttu. Recognition of tandem pxxp motifs as a unique src homology 3-binding mode triggers pathogen-driven actin assembly. *Proc Natl Acad Sci U S A 107*, 50 (December 2010), 21743–8.

[2] Aitio, Olli, Hellman, Maarit, Skehan, Brian, Kesti, Tapio, Leong, John M., Saksela, Kalle, and Permi, Perttu. Enterohaemorrhagic escherichia coli exploits a tryptophan switch to hijack host f-actin assembly. *Structure 20* (October 2012), 1692–1703.

[3] Antón, Inés, Anton, M., Lu, Wange, Mayer, Bruce J., Ramesh, Narayanaswamy, and Geha, Raif S. The wiskott-aldrich syndrome protein-interacting protein (wip) binds to the adaptor protein nck. *J Biol Chem 273*, 33 (August 1998), 20992–20995.

[4] Baldwin, Tom J., Ward, William, Aitken, Alastair, Knutton, Stuart, and Williams, Peter H. Elevation of intracellular free calcium levels in hep-2 cells infectedwithenteropathogenicescherichiacoli. *Infect Immun 59*, 5 (May 1991), 1599–1604.

[5] Berger, Cedric N., Crepin, Valerie F., Jepson, Mark A., Arbeloa, Ana, and Frankel, Gad. The mechanisms used by enteropathogenic escherichia coli to control filopodia dynamics. *Cell Microbiol 11*, 2 (Feb 2009), 309–22.

[6] Berger, Cedric N., Shaw, Robert K., Ruiz-Perez, Fernando, Nataro, James P., Henderson, Ian R., Pallen, Mark J., and Frankel, Gad. Interaction of enteroaggregative escherichia coli with salad leaves. *Environ Microbiol Rep. 1*, 4 (August 2009), 234–239.

[7] Berger, Cedric N., Sodha, Samir V., Shaw, Robert K., Griffin, Patricia M., Pink, David, Hand, Paul, and Frankel, Gad. Fresh fruit and vegetables as vehicles for the transmission of human pathogens. *Environ Microbiol 12*, 9 (Sep 2010), 2385–97.

[8] Boutemy, Laurence S., King, Stuart R. F., Win, Joe, Hughes, Richard K., Clarke, Thomas A., Blumenschein, Tharin M. A., Kamoun, Sophien, and Banfield, Mark J. Structures of phytophthora rxlr effector proteins: a conserved but adaptable fold underpins functional diversity. *J Biol Chem 286*, 41 (Oct 2011), 35834–42.

[9] Brady, Michael J., Campellone, Kenneth G., Ghildiyal, Megha, and Leong, John M. Enterohaemorrhagic and enteropathogenic escherichia coli tir proteins trigger a common nck-independent actin assembly pathway. *Cell Microbiol 9*, 9 (Sep 2007), 2242–53.

[10] Bretscher, Anthony. Microfilament structure and function in the cortical cytoskeleton. *Annu. Rev. Cell Biol. 7*, 337 (1991), 74.

[11] Bretscher, Anthony, Edwards, Kevin, and Fehon, Richard G. Erm proteins and merlin: integrators at the cell cortex. *Nat Rev Mol Cell Biol 3*, 8 (Aug 2002), 586–99.

[12] Brown, Jeffrey W., and McKnight, C. James. Molecular model of the microvillar cytoskeleton and organization of the brush border. *PLoS One 5*, 2 (2010), e9406.

[13] Bryksin, A, and Matsumura, I. Overlap extension pcr cloning. *Methods Mol Biol 1073* (2013), 31–42.

[14] Buday, László, Wunderlich, Livius, and Tamás, Peter. The nck family of adapter proteins: regulators of actin cytoskeleton. *Cell Signal 14*, 9 (Sep 2002), 723–31.

[15] Bulgin, Richard, Raymond, Benoit, Garnett, James A., Frankel, Gad, Crepin, Valerie F, Berger, Cedric N., and Arbeloa, Ana. Bacterial guanine nucleotide exchange factors sope-like and wxxxe effectors. *Infect Immun 78*, 4 (Apr 2010), 1417–25.

[16] Campellone, Kenneth G., Brady, Michael J., Alamares, Judith G., Rowe, Daniel C., Skehan, Brian M., Tipper, Donald J., and Leong, John M. Enterohaemorrhagic escherichia coli tir requires a c-terminal 12-residue peptide to initiate espf-mediated actin assembly and harbours n-terminal sequences that influence pedestal length. *Cell Microbiol 8*, 9 (Sep 2006), 1488–503.

[17] Campellone, Kenneth G., Cheng, Hui-Chun, Robbins, Douglas, Siripala, Anosha D., McGhie, Emma J., Hayward, Richard D., Welch, Matthew D., Rosen, Michael K., Koronakis, Vassilis, and Leong, John M. Repetitive n-wasp-binding elements of the enterohemorrhagic escherichia coli effector espf(u) synergistically activate actin assembly. *PLoS Pathog 4*, 10 (Oct 2008), e1000191.

[18] Campellone, Kenneth G., Giese, Andrew, Tipper, Donald J., and Leong, John M. A tyrosine-phosphorylated 12-amino-acid sequence of enteropathogenic escherichia coli tir binds the host adaptor protein nck and is required for nck localization to actin pedestals. *Mol Microbiol 43*, 5 (2002), 1227–1241.

[19] Campellone, Kenneth G., and Leong, John M. Nck-independent actin assembly is mediated by two phosphorylated tyrosines within enteropathogenic escherichia coli tir. *Mol Microbiol 56*, 2 (2005), 416–432.

[20] Campellone, Kenneth G., Rankin, Susannah, Pawson, Tony, Kirschner, Marc W., Tipper, Donald J., and Leong, John M. Clustering of nck by a 12-residue tir phosphopeptide is sufficient to trigger localized actin assembly. *J Cell Biol 164*, 3 (Feb 2004), 407–16.

[21] Campellone, Kenneth G., Robbins, Douglas, and Leong, John M. Espfu is a translocated ehec effector that interacts with tir and n-wasp and promotes nck-independent actin assembly. *Dev Cell 7*, 2 (Aug 2004), 217–28.

[22] Caron, Emmanuelle, Crepin, Valerie F., Simpson, Nandi, Knutton, Stuart, Garmendia, Junkal, and Frankel, Gad. Subversion of actin dynamics by epec and ehec. *Curr Opin Microbiol 9*, 1 (Feb 2006), 40–5.

[23] Carragher, Neil O. Calpain inhibition: a therapeutic strategy targeting multiple disease states. *Curr Pharm Des 12*, 5 (2006), 615–638.

[24] CDC. E. coli (escherichia coli). *http://www.cdc.gov/ecoli/* (March 2014).

[25] Chan, Keefe T., Bennin, David A., and Huttenlocher, Anna. Regulation of adhesion dynamics by calpain-mediated proteolysis of focal adhesion kinase (fak). *J Biol Chem 285*, 15 (Apr 2010), 11418–26.

[26] Cheng, Hui-Chun, Skehan, Brian M., Campellone, Kenneth G., Leong, John M., and Rosen, Michael K. Structural mechanism of wasp activation by the enterohaemorrhagic e. coli effector espf(u). *Nature 454*, 7207 (Aug 2008), 1009–13.

[27] Chiu, Joyce, March, Paul E., Lee, Ryan, and Tillett, Daniel. Site-directed, ligase-independent mutagenesis (slim): a single-tube methodology approaching 100% efficiency in 4 h. *Nucleic Acids Res 32*, 21 (2004), e174.

[28] Clements, Abigail, Young, Joanna C., Constantinou, Nicholas, and Frankel, Gad. Infection strategies of enteric pathogenic escherichia coli. *Gut Microbes 3*, 2 (2012), 71–87.

[29] Cory, Giles O. C., and Cullen, Peter J. Membrane curvature: the power of bananas, zeppelins and boomerangs. *Curr Biol 17*, 12 (Jun 2007), R455–7.

[30] Crepin, Valérie F., Girard, Francis, Schüller, Stephanie, Phillips, Alan D., Mousnier, Aurelie, and Frankel, Gad. Dissecting the role of the tir:nck and tir:irtks/irsp53 signalling pathways in vivo. *Mol Microbiol 75*, 2 (Jan 2010), 308–23.

[31] Croall, Dorothy E., and Ersfeld, Klaus. The calpains: modular designs and functional diversity. *Genome Biol 8*, 6 (2007), 218.

[32] Croce, Kevin, Flaumenhaft, Robert, Rivers, Marc, Furie, Bruce, Furie, Barbara C., Herman, Ira M., and Potter, David A. Inhibition of calpain blocks platelet secretion, aggregation, and spreading. *J Biol Chem 274*, 51 (December 1999), 36321–36327.

[33] Croxen, Matthew A., and Finlay, B. Brett. Molecular mechanisms of escherichia coli pathogenicity. *Nat Rev Microbiol 8*, 1 (Jan 2010), 26–38.

[34] de Groot, Jens C., Schlüter, Kai, Carius, Yvonne, Quedenau, Claudia, Vingadassalom, Didier, Faix, Jan, Weiss, Stefanie M., Reichelt, Joachim, Standfuss-Gabisch, Christine, Lesser, Cammie F., Leong, John M., Heinz, Dirk W., Büssow, Konrad, and Stradal, Theresia E. B. Structural basis for complex formation between human irsp53 and the translocated intimin receptor tir of enterohemorrhagic e. coli. *Structure 19*, 9 (Sep 2011), 1294–306.

[35] Dean, Paul, Mühlen, Sabrina, Quitard, Sabine, and Kenny, Brendan. The bacterial effectors espg and espg2 induce a destructive calpain activity that is kept in check by the co-delivered tir effector. *Cell Microbiol 12*, 9 (Sep 2010), 1308–21.

[36] Dean, Paul, Young, Lorna, Quitard, Sabine, and Kenny, Brendan. Insights into the pathogenesis of enteropathogenic e. coli using an improved intestinal enterocyte model. *PLoS One 8*, 1 (2013), e55284.

[37] DeVinney, Rebekah, Puente, Jose Luis, Gauthier, Annick, Goosney, Danika, and Finlay, B. Brett. Enterohaemorrhagic and enteropathogenic escherichia coli use a different tir-based mechanism for pedestal formation. *Mol Microbiol 41*, 6 (2001), 1445–1458.

[38] DeVinney, Rebekah, Stein, Markus, Reinscheid, Dieter, Abe, Akio, Ruschkowski, Sharon, and Finlay, B. Brett. Enterohemorrhagic escherichia coli o157:h7 produces tir, which is translocated to the host cell membrane but is not tyrosine phosphorylated. *Infect Immun 67*, 5 (1999), 2389–2398.

[39] Di Fiore, Pier Paolo, and Scita, Giorgio. Eps8 in the midst of gtpases. *Int J Biochem Cell Biol 34*, 10 (Oct 2002), 1178–83.

[40] Disanza, Andrea, Mantoani, Sara, Hertzog, Maud, Gerboth, Silke, Frittoli, Emanuela, Steffen, Anika, Berhoerster, Kerstin, Kreienkamp, Hans-Juergen, Milanesi, Francesca, Di Fiore, Pier Paolo, Ciliberto, Andrea, Stradal, Theresia E B, and Scita, Giorgio. Regulation of cell shape by cdc42 is mediated by the synergic actin-bundling activity of the eps8-irsp53 complex. *Nat Cell Biol 8*, 12 (December 2006), 1337–47.

[41] Dong, Na, Liu, Liping, and Shao, Feng. A bacterial effector targets host dh-ph domain rhogefs and antagonizes macrophage phagocytosis. *EMBO J 29*, 8 (Apr 2010), 1363–76.

[42] Donnenberg, Michael S., Tzipori, Saul, McKee, Manan L., O'Brien, Alison D., Alroy, Joseph, and Kaper, James B. The role of the eae gene of enterohemorrhagic escherichia coli in intimate attachment in vitro and in a porcine model. *J Clin Invest 92* (September 1993), 1418–1424.

[43] Drenckhahn, Detlev, and Dermietzel, Rolf. Organization of the actin filament cytoskeleton in the intestinal brush border: A quantitative and qualitative immunoelectron microscope study. *J Cell Biol 107* (September 1988), 1038–1048.

[44] Fehon, Richard G., McClatchey, Andrea I., and Bretscher, Anthony. Organizing the cell cortex: the role of erm proteins. *Nature 11* (April 2010), 276–287.

[45] Fettucciari, Katia, Fetriconi, Ilaria, Mannucci, Roberta, Nicoletti, Ildo, Bartoli, Andrea, Coaccioli, Stefano, and Marconi, Pierfrancesco. Group b streptococcus induces macrophage apoptosis by calpain activation. *J Immunol 176* (2006), 7542–7556.

[46] Foster, Debora Barnett. Modulation of the enterohemorrhagic e. coli virulence program through the human gastrointestinal tract. *Virulence 4*, 4 (May 2013), 1–9.

[47] Frame, Margaret C., Fincham, Valerie J., Carragher, Neil O., and Wyke, John A. v-src's hold over actin and cell adhesions. *Nat Rev Mol Cell Biol 3*, 4 (Apr 2002), 233–45.

[48] Franco, Santos J., and Huttenlocher, Anna. Regulating cell migration: calpains make the cut. *J Cell Sci 118*, Pt 17 (Sep 2005), 3829–38.

[49] Funato, Yosuke, Terabayashi, Takeshi, Suenaga, Naoko, Seiki, Motoharu, Takenawa, Tadaomi, and Miki, Hiroaki. Irsp53/eps8 complex is important for positive regulation of rac and cancer cell motility/invasiveness. *Cancer Research 64*, 5237-5244 (August 2004).

[50] Galán, Jorge E. Common themes in the design and function of bacterial effectors. *Cell Host Microbe 5*, 6 (Jun 2009), 571–9.

[51] Garber, John J., Takeshima, Fuminao, Antón, Inés M., Oyoshi, Michiko K., Lyubimova, Anna, Kapoor, Archana, Shibata, Tomoyuki, Chen, Feng, Alt, Frederick W., Geha, Raif S., Leong, John M., and Snapper, Scott B. Enteropathogenic escherichia coli and vaccinia virus do not require the family of wasp-interacting proteins for pathogen-induced actin assembly. *Infect Immun 80*, 12 (Dec 2012), 4071–7.

[52] Garmendia, Junkal, Carlier, Marie-France, Egile, Coumaran, Didry, Dominique, and Frankel, Gad. Characterization of tccp-mediated n-wasp activation during enterohaemorrhagic escherichia coli infection. *Cell Microbiol 8*, 9 (Sep 2006), 1444–55.

[53] Garmendia, Junkal, Phillips, Alan D., Carlier, Marie-France, Chong, Yuwen, Schüller, Stephanie, Marches, Olivier, Dahan, Sivan, Oswald, Eric, Shaw, Robert K., Knutton, Stuart, and Frankel, Gad. Tccp is an enterohaemorrhagic escherichia coli o157:h7 type iii effector protein that couples tir to the actin-cytoskeleton. *Cell Microbiol 6*, 12 (Dec 2004), 1167–83.

[54] Garmendia, Junkal, Ren, Zhihong, Tennant, Sharon, Midolli Viera, Monica Aparecida, Chong, Yuwen, Whale, Andrew, Azzopardi, Kristy, Dahan, Sivan, Sircili, Marcelo Palma, Franzolin, Marcia Regina, Trabulsi, Luiz R., Phillips, Alan, Gomes, Tânia A. T., Xu, Jianguo, Robins-Browne, Roy, and Frankel, Gad. Distribution of tccp in clinical enterohemorrhagic and enteropathogenic escherichia coli isolates. *J Clin Microbiol 43*, 11 (Nov 2005), 5715–20.

[55] Goldmann, Oliver, Sastalla, Inka, Wos-Oxley, Melissa, Rohde, Manfred, and Medina, Eva. Streptococcus pyogenes induces oncosis in macrophages through the activation of an inflammatory programmed cell death pathway. *Cell Microbiol 11*, 1 (Jan 2009), 138–55.

[56] Goosney, Danika L., Gruenheid, Samantha, and Finlay, B. Brett. Gut feelings: Enteropathogenic e. coli (epec) interactions with the host. *Annu Rev Cell Dev Biol 16* (2000), 173–189.

[57] Gorsic, Lidija K., Stark, Amy L., Wheeler, Heather E., Wong, Shan S., Im, Hae K., and Dolan, M. Eileen. Eps8 inhibition increases cisplatin sensitivity in lung cancer cells. *PLoS One 8*, 12 (2013), e82220.

[58] Gruenheid, Samantha, DeVinney, Rebekah, Bladt, Friedhelm, Goosney, Danika, Gelkop, Sigal, Gish, Gerald D., Pawson, Tony, and Finlay, B. Brett. Enteropathogenic e. coli tir binds nck to initiate actin pedestal formation in host cells. *Nat Cell Biol 3* (September 2001), 856–859.

[59] Guttman, Julian A., Li, Yuling, Wickham, Mark E., Deng, Wanyin, Vogl, A. Wayne, and Finlay, B. Brett. Attaching and effacing pathogen-induced tight junction disruption in vivo. *Cell Microbiol 8*, 4 (Apr 2006), 634–45.

[60] Guttman, Julian A., Samji, Fereshte N., Li, Yuling, Deng, Wanyin, Lin, Ann, and Finlay, B. Brett. Aquaporins contribute to diarrhoea caused by attaching and effacing bacterial pathogens. *Cell Microbiol 9*, 1 (Jan 2007), 131–41.

[61] Hardwidge, Philip R., Rodriguez-Escudero, Isabel, Goode, David, Donohoe, Sam, Eng, Jimmy, Goodlett, David R., Aebersold, Reudi, and Finlay, B. Brett. Proteomic analysis of the intestinal epithelial cell response to enteropathogenic escherichia coli. *J Biol Chem 279*, 19 (May 2004), 20127–36.

[62] Hayward, Richard D., Hume, Peter J., Humphreys, Daniel, Phillips, Neil, Smith, Katherine, and Koronakis, Vassilis. Clustering transfers the translocated escherichia coli receptor into lipid rafts to stimulate reversible activation of c-fyn. *Cell Microbiol 11*, 3 (Mar 2009), 433–41.

[63] Hayward, Richard D., Leong, John M., Koronakis, Vassilis, and Campellone, Kenneth G. Exploiting pathogenic escherichia coli to model transmembrane receptor signalling. *Nat Rev Microbiol 4*, 5 (May 2006), 358–70.

[64] Huett, Alan, Leong, John M., Podolsky, Daniel K., and Xavier, Ramnik J. The cytoskeletal scaffold shank3 is recruited to pathogen-induced actin rearrangements. *Exp Cell Res 315*, 12 (Jul 2009), 2001–11.

[65] Kenny, Brendan. Phosphorylation of tyrosine 474 of the enteropathogenic escherichia coli (epec) tir receptor molecule is essential for actin nucleating activity and is preceded by additional host modifications. *Mol Microbiol 31*, 4 (1999), 1229–1241.

[66] Kenny, Brendan. The enterohaemorrhagic escherichia coli (serotype o157:h7) tir molecule is not functionally interchangeable for its enteropathogenic e. coli (serotype o127:h6) homologue. *Cell Microbiol 3*, 8 (2001), 499–510.

[67] Kenny, Brendan, DeVinney, Rebekah, Stein, Markus, Reinscheid, Dieter J., Frey, Elizabeth A., and Finlay, B. Brett. Enteropathogenic e. coli (epec) transfers its receptor for intimate adherence into mammalian cells. *Cell 91* (November 1997), 511–520.

[68] Kotecki, Maciej, Zeiger, Adam S., Van Vliet, Krystyn J., and Herman, Ira M. Calpain- and talin-dependent control of microvascular pericyte contractility and cellular stiffness. *Microvasc Res 80*, 3 (Dec 2010), 339–48.

[69] Lai, Yushuan, Riley, Kathleen, Cai, Andrew, Leong, John M., and Herman, Ira M. Calpain mediates epithelial cell microvillar effacement by enterohemorrhagic escherichia coli. *Front Microbiol 2* (2011), 222.

[70] Lai, Yushuan, Rosenshine, Ilan, Leong, John M., and Frankel, Gad. Intimate host attachment: enteropathogenic and enterohaemorrhagic escherichia coli. *Cell Microbiol 15*, 11 (Nov 2013), 1796–808.

[71] Lange, Klaus. Fundamental role of microvilli in the main functions of differentiated cells: Outline of an universal regulating and signaling system at the cell periphery. *J Cell Physiol 226*, 4 (Apr 2011), 896–927.

[72] Lebart, Marie-Christine, and Benyamin, Yves. Calpain involvement in the remodeling of cytoskeletal anchorage complexes. *FEBS J 273*, 15 (Aug 2006), 3415–26.

[73] Luo, Zhao-Qing, and Isberg, Ralph R. Multiple substrates of the legionella pneumophila doticm system identified by interbacterial protein transfer. *Proc Natl Acad Sci U S A 101*, 3 (January 2004), 841–846.

[74] Mallick, Emily M., Brady, Michael J., Luperchio, Steven A., Vanguri, Vijay K., Magoun, Loranne, Liu, Hui, Sheppard, Barbara J., Mukherjee, Jean, Donohue-Rolfe, Art, Tzipori, Saul, Leong, John M., and Schauer, David B. Allele- and tir-independent functions of intimin in diverse animal infection models. *Front Microbiol 3* (2012), 11.

[75] Mallick, Emily M., McBee, Megan E., Vanguri, Vijay K., Melton-Celsa, Angela R., Schlieper, Katherine, Karalius, Brad J., O'Brien, Alison D., Butterton, Joan R., Leong, John M., and Schauer, David B. A novel murine infection model for shiga toxin-producing escherichia coli. *J Clin Invest 122*, 11 (Nov 2012), 4012–24.

[76] Manor, Uri, Disanza, Andrea, Grati, M'Hamed, Andrade, Leonardo, Lin, Harrison, Di Fiore, Pier Paolo, Scita, Giorgio, and Kachar, Bechara. Regulation of stereocilia length by myosin xva and whirlin depends on the actin-regulatory protein eps8. *Curr Biol 21*, 2 (Jan 2011), 167–72.

[77] Marches, Olivier, Nougayrede, Jean-Philippe, Boullier, Severine, Manil, Jacques, Charlier, Gerard, Raymond, Isabelle, Pohl, Pierre, Boury, Michele, Rycke, Jean De, Milon, Alain, and Oswald, Eric. Role of tir and intimin in the virulence of rabbit enteropathogenic escherichia coli serotype o103:h2. *Infect Immun 68*, 4 (April 2000), 2171–2182.

[78] Martell, Jeffrey D., Deerinck, Thomas J., Sancak, Yasemin, Poulos, Thomas L., Mootha, Vamsi K., Sosinsky, Gina E., Ellisman, Mark H., and Ting, Alice Y. Engineered ascorbate peroxidase as a genetically encoded reporter for electron microscopy. *Nat Biotechnol 30*, 11 (Nov 2012), 1143–8.

[79] Miki, Hiroaki, and Takenawa, Tadaomi. Regulation of actin dynamics by wasp family proteins. *J Biochem 134* (2003), 309–313.

[80] Millard, Thomas H., Dawson, John, and Machesky, Laura M. Characterisation of irtks, a novel irsp53/mim family actin regulator with distinct filament bundling properties. *J Cell Sci 120*, Pt 9 (May 2007), 1663–72.

[81] Mittler, Ron, and Zilinskas, Barbara A. Detection of ascorbate peroxidase activity in native gels by inhibition of the ascorbate-dependent reduction of nitroblue tetrazolium. *Analytical Biochemistry 212* (1993), 540–546.

[82] Moreau, Violaine, Frischknecht, Friedrich, Reckmann, Inge, Vincentelli, Renaud, Rabut, Gwénaël, Stewart, Donn, and Way, Michael. A complex of n-wasp and wip integrates signalling cascades that lead to actin polymerization. *Nat Cell Biol 2* (2000), 441–448.

[83] Murphy, Kenan, and Campellone, Kenneth G. Lambda red-mediated recombinogenic engineering of enterohemorrhagic and enteropathogenic e. coli. *BMC Molecular Biology 4*, 1 (2003), 11.

[84] Muza-Moons, Michelle M., Koutsouris, Athanasia, and Hecht, Gail. Disruption of cell polarity by enteropathogenic escherichia coli enables basolateral membrane proteins to migrate apically and to potentiate physiological consequences. *Infect Immun 71*, 2 (December 2003), 7069–7078.

[85] Muza-Moons, Michelle M., Schneeberger, Eveline E., and Hecht, Gail A. Enteropathogenic escherichia coli infection leads to appearance of aberrant tight junctions strands in the lateral membrane of intestinal epithelial cells. *Cell Microbiol 6*, 8 (Aug 2004), 783–93.

[86] Neil, Karen P., Biggerstaff, Gwen, MacDonald, J. Kathryn, Trees, Eija, Medus, Carlota, Musser, Kimberlee A., Stroika, Steven G., Zink, Don, and Sotir, Mark J. A novel vehicle for transmission of escherichia coli o157:h7 to humans: multistate outbreak of e. coli o157:h7 infections associated with consumption of ready-to-bake commercial prepackaged cookie dough–united states, 2009. *Clin Infect Dis 54*, 4 (Feb 2012), 511–8.

[87] Nelson, W. James. Epithelial cell polarity from the outside looking in. *News Physiol Sci 18* (2003), 143–146.

[88] Offenhauser, Nina, Borgonovo, Alessandro, Disanza, Andrea, Romano, Pascale, Ponzanelli, Isabella, Iannolo, Gioacchin, Fiore, Pier Paolo Di, and Scita, Giorgio. The eps8 family of proteins links growth factor stimulation to actin reorganization generating functional redundancy in the ras/rac pathway. *Molecular Biology of the Cell 15* (2004), 91–98.

[89] Ogura, Yoshitoshi, Ooka, Tadasuke, Whale, Andrew, Garmendia, Junkal, Beutin, Lothar, Tennant, Sharon, Krause, Gladys, Morabito, Stefano, Chinen, Isabel, Tobe, Toru, Abe, Hiroyuki, Tozzoli, Rosangela, Caprioli, Alfredo, Rivas, Marta, Robins-Browne, Roy, Hayashi, Tetsuya, and Frankel, Gad. Tccp2 of o157:h7 and non-o157 enterohemorrhagic escherichia coli (ehec): challenging the dogma of ehec-induced actin polymerization. *Infect Immun 75*, 2 (Feb 2007), 604–12.

[90] Ooka, Tadasuke, Vieira, Mônica A. M., Ogura, Yoshitoshi, Beutin, Lothar, La Ragione, Roberto, van Diemen, Pauline M., Stevens, Mark P., Aktan, Ilknur, Cawthraw, Shaun, Best, Angus, Hernandes, Rodrigo T., Krause, Gladys, Gomes, Tania A. T., Hayashi, Tetsuya, and Frankel, Gad. Characterization of tccp2 carried by atypical enteropathogenic escherichia coli. *FEMS Microbiol Lett 271*, 1 (Jun 2007), 126–35.

[91] Padrick, Shae B., Cheng, Hui-Chun, Ismail, Ayman M., Panchal, Sanjay C., Doolittle, Lynda K., Kim, Soyeon, Skehan, Brian M., Umetani, Junko, Brautigam, Chad A., Leong, John M., and Rosen, Michael K. Hierarchical regulation of wasp/wave proteins. *Mol Cell 32*, 3 (Nov 2008), 426–38.

[92] Peralta-Ramírez, Janneth, Hernandez, J Manuel, Manning-Cela, Rebeca, Luna-Muñoz, José, Garcia-Tovar, Carlos, Nougayréde, Jean-Philippe, Oswald, Eric, and Navarro-Garcia, Fernando. Espf interacts with nucleation-promoting factors to recruit junctional proteins into pedestals for pedestal maturation and disruption of paracellular permeability. *Infect Immun 76*, 9 (Sep 2008), 3854–68.

[93] Perry, Seth W., Barbieri, Justin, Tong, Ning, Polesskaya, Oksana, Pudasaini, Santosh, Stout, Angela, Lu, Rebecca, Kiebala, Michelle, Maggirwar, Sanjay B., and Gelbard, Harris A. Human immunodeficiency virus-1 tat activates calpain proteases via the ryanodine receptor to enhance surface dopamine transporter levels and increase transporter-specific uptake and vmax. *J Neurosci 30*, 42 (Oct 2010), 14153–64.

[94] Potter, David A., Srirangam, Anjaiah, Fiacco, Kerry A., Brocks, Daniel, Hawes, John, Herndon, Carter, Maki, Masatoshi, Acheson, David, and Herman, Ira M. Calpain regulates enterocyte brush border actin assembly and pathogenic escherichia coli-mediated effacement. *J Biol Chem 278*, 32 (Aug 2003), 30403–12.

[95] Potter, David A., Tirnauer, Jennifer S., Janssen, Richard, Croall, Dorothy E., Hughes, Christina N., Fiacco, Kerry A., Mier, James W., Maki, Masatoshi, and Herman, Ira M. Calpain regulates actin remodeling during cell spreading. *J Cell Biol 141*, 3 (May 1998), 647–662.

[96] Pujuguet, Philippe, Maestro, Laurence Del, Gautreau, Alexis, Louvard, Daniel, and Arpin, Monique. Ezrin regulates e-cadherin-dependent adherens junction assembly through rac1 activation. *Molecular Biology of the Cell 14* (May 2003), 2181–2191.

[97] Rhee, Hyun-Woo, Zou, Peng, Udeshi, Namrata D., Martell, Jeffrey D., Mootha, Vamsi K., Carr, Steven A., and Ting, Alice Y. Proteomic mapping of mitochondria in living cells via spatially restricted enzymatic tagging. *Science 339*, 6125 (Mar 2013), 1328–31.

[98] Riley, Lee W., Remis, Robert S., Helgerson, Steven D., McGee, Harry B., Wells, Joy G., Davis, Betty R., Hebert, Richard J., Olcott, Ellen S., Johnson, Linda M., Hargrett, Nancy T., Blake, Paul A., and Cohen, Mitchell L. Hemorrhagic colitis associated with a rare escherichia coli serotype. *New England Journal of Medicine 308*, 12 (1983), 681–685. PMID: 6338386.

[99] Ritchie, Jennifer M., Brady, Michael J., Riley, Kathleen N., Ho, Theresa Deland, Campellone, Kenneth G., Herman, Ira M., Donohue-Rolfe, Arthur, Tzipori, Saul, Waldor, Matthew K., and Leong, John M. Espfu, a type iii-translocated effector of actin assembly, fosters epithelial association and late-stage intestinal colonization by e. coli o157:h7. *Cell Microbiol 10*, 4 (Apr 2008), 836–47.

[100] Ritchie, Jennifer M., Thorpe, Cheleste M., Rogers, Arlin B., and Waldor, Matthew K. Critical roles for stx2, eae, and tir in enterohemorrhagic escherichia coli-induced diarrhea and intestinal inflammation in infant rabbits. *Infect Immun 17*, 12 (December 2003), 7129–7139.

[101] Ross, Nathan T., Mace, Charles R., and Miller, Benjamin L. Biophysical analysis of the epec translocated intimin receptor-binding domain. *Biochem Biophys Res Commun 362*, 4 (Nov 2007), 1073–8.

[102] Saarikangas, Juha, Zhao, Hongxia, Pykäläinen, Anette, Laurinmäki, Pasi, Mattila, Pieta K, Kinnunen, Paavo K. J., Butcher, Sarah J., and Lappalainen, Pekka. Molecular mechanisms of membrane deformation by i-bar domain proteins. *Curr Biol 19*, 2 (Jan 2009), 95–107.

[103] Saksela, Kalle, and Permi, Perttu. Sh3 domain ligand binding: What's the consensus and where's the specificity? *FEBS Letters 586* (2012), 2609–2614.

[104] Sallee, Nathan A., Rivera, Gonzalo M., Dueber, John E., Vasilescu, Dan, Mullins, R. Dyche, Mayer, Bruce J., and Lim, Wendell A. The pathogen protein espf(u) hijacks actin polymerization using mimicry and multivalency. *Nature 454*, 7207 (Aug 2008), 1005–8.

[105] Saotome, Ichiko, Curto, Marcello, and McClatchey, Andrea I. Ezrin is essential for epithelial organization and villus morphogenesis in the developing intestine. *Dev Cell 6*, 6 (Jun 2004), 855–64.

[106] Scita, Giorgio, Confalonieri, Stefano, Lappalainen, Pekka, and Suetsugu, Shiro. Irsp53: crossing the road of membrane and actin dynamics in the formation of membrane protrusions. *Trends Cell Biol 18*, 2 (Feb 2008), 52–60.

[107] Shuster, Charles B., and Herman, Ira M. Indirect association of ezrin with f-actin: Isoform specificity and calcium sensitivity. *J Cell Biol 128* (March 1995), 837–848.

[108] Shuster, Charles B., Lin, Alice Y., Nayak, Ramesh, and Herman, Ira M. betacap73: A novel beta actin-specific binding protein. *Cell Motility and the Cytoskeleton 35* (1996), 175–187.

[109] Simonovic, Ivana, Arpin, Monique, Koutsouris, Athanasia, Falk-Krzesinski, Holly J., and Hecht, Gail A. Enteropathogenic escherichia coli activates ezrin, which participates in disruption of tight junction barrier function. *Infect Immun 69*, 9 (September 2001), 5679–5688.

[110] Skehan, Brian. *Functional Elements of EspFU, an Enterohemorrhagic E. coli effector that stimulates actin assembly.* Doctor of philosophy, University of Massachusetts Medical School, 55 Lake Ave North, Worcester MA 01655, June 2009.

[111] Snapper, Scott B., and Rosen, Fred S. The wiskott-aldrich syndrome protein (wasp): Roles in signaling and cytoskeletal organization. *Annu Rev Immunol 17* (1999), 905–29.

[112] Sorimachi, Hiroyuki, Hata, Shoji, and Ono, Yasuko. Expanding members and roles of the calpain superfamily and their genetically modified animals. *Exp Anim 59*, 5 (2010), 549–566.

[113] Spears, Kevin J., Roe, Andrew J., and Gally, David L. A comparison of enteropathogenic and enterohaemorrhagic escherichia coli pathogenesis. *FEMS Microbiol Lett 255*, 2 (Feb 2006), 187–202.

[114] Sumitomo, Tomoko, Nakata, Masanobu, Higashino, Miharu, Jin, Yingji, Terao, Yutaka, Fujinaga, Yukako, and Kawabata, Shigetada. Streptolysin s contributes to group a streptococcal translocation across an epithelial barrier. *J Biol Chem 286*, 4 (Jan 2011), 2750–61.

[115] Swimm, Alyson, Bommarius, Bettina, Li, Yue, Cheng, David, Reeves, Patrick, Sherman, Melanie, Veach, Darren, Bornmann, William, and Kalman, Daniel. Enteropathogenic escherichia coli use redundant tyrosine kinases to form actin pedestalsd. *Molecular Biology of the Cell 15* (August 2004), 3520–3529.

[116] Tacket, Carol O., Sztein, Marcelo B., Losonsky, Genevieve, Abe, Akio, Finlay, B. Brett, McNamara, Barry P., Fantry, George T., James, Stephen P., Nataro, James P., Levine, Myron M., and Donnenberg, Michael S. Role of espb in experimental human enteropathogenic escherichia coli infection. *Infect Immun 68*, 6 (June 2000), 3689–3695.

[117] Tarr, Phillip I., Gordon, Carrie A., and Chandler, Wayne L. Shiga-toxin-producing escherichia coli and haemolytic uraemic syndrome. *Lancet 365*, 9464 (2005), 1073–86.

[118] Tobe, Toru, Beatson, Scott A., Taniguchi, Hisaaki, Abe, Hiroyuki, Bailey, Christopher M., Fivian, Amanda, Younis, Rasha, Matthews, Sophie, Marches, Olivier, Frankel, Gad, Hayashi, Tetsuya, and Pallen, Mark J. An extensive repertoire of type iii secretion effectors in escherichia coli o157 and the role of lambdoid phages in their dissemination. *Proc Natl Acad Sci U S A 103*, 40 (October 2006), 14941–14946.

[119] Tocchetti, Arianna, Soppo, Charlotte Blanche Ekalle, Zani, Fabio, Bianchi, Fabrizio, Gagliani, Maria Cristina, Pozzi, Benedetta, Rozman, Jan, Elvert, Ralf, Ehrhardt, Nicole, Rathkolb, Birgit, Moerth, Corinna, Horsch, Marion, Fuchs, Helmut, Gailus-Durner, Valérie, Beckers, Johannes, Klingenspor, Martin, Wolf, Eckhard, Hrabé de Angelis, Martin, Scanziani, Eugenio, Tacchetti, Carlo, Scita, Giorgio, Di Fiore, Pier Paolo, and Offenhäuser, Nina. Loss of the actin remodeler eps8 causes intestinal defects and improved metabolic status in mice. *PLoS One 5*, 3 (2010), e9468.

[120] Touzé, Thierry, Hayward, Richard D., Eswaran, Jeyanthy, Leong, John M., and Koronakis, Vassilis. Self-association of epec intimin mediated by the b-barrel-containing anchor domain: a role in clustering of the tir receptor. *Mol Microbiol 51*, 1 (2004), 73–87.

[121] Tyska, M. J., and Mooseker, M. S. Myo1a (brush border myosin i) dynamics in the brush border of llc-pk1-cl4 cells. *Biophys J 82* (April 2002), 1869–1883.

[122] Tzipori, Saul, Gunzer, Florian, Donnenberg, Michael S., Montigny, Lina De, Kaper, James B., and Donohue-Rolfe, Arthur. The role of the eaea gene in diarrhea and neurological complications in a gnotobiotic piglet model of enterohemorrhagic escherichia coli infection. *Infect Immun 63*, 9 (September 1995), 3621–3627.

[123] Vaggi, Federico, Disanza, Andrea, Milanesi, Francesca, Di Fiore, Pier Paolo, Menna, Elisabetta, Matteoli, Michela, Gov, Nir S., Scita, Giorgio, and Ciliberto, Andrea. The eps8/irsp53/vasp network differentially controls actin capping and bundling in filopodia formation. *PLoS Comput Biol 7*, 7 (Jul 2011), e1002088.

[124] Vingadassalom, Didier, Campellone, Kenneth G., Brady, Michael J., Skehan, Brian, Battle, Scott E., Robbins, Douglas, Kapoor, Archana, Hecht, Gail, Snapper, Scott B., and Leong, John M. Enterohemorrhagic e. coli requires n-wasp for efficient type iii translocation but not for espfu-mediated actin pedestal formation. *PLoS Pathog 6*, 8 (2010), e1001056.

[125] Vingadassalom, Didier, Kazlauskas, Arunas, Skehan, Brian, Cheng, Hui-Chun, Magoun, Loranne, Robbins, Douglas, Rosen, Michael K., Saksela, Kalle, and Leong, John M. Insulin receptor tyrosine kinase substrate links the e. coli o157:h7 actin assembly effectors tir and espfu during pedestal formation. *Proc Natl Acad Sci U S A 106*, 16 (2009), 6754–6759.

[126] Viswanathan, V. K., Koutsouris, Athanasia, Lukic, Sandra, Pilkinton, Mark, Simonovic, Ivana, Simonovic, Miljan, and Hecht, Gail. Comparative analysis of espf from enteropathogenic and enterohemorrhagic escherichia coli in alteration of epithelial barrier function. *Infect Immun 72*, 6 (Jun 2004), 3218–27.

[127] Wang, Fengsong, Xia, Peng, Wu, Fang, Wang, Dongmei, Wang, Wei, Ward, Tarsha, Liu, Ya, Aikhionbare, Felix, Guo, Zhen, Powell, Michael, Liu, Bingya, Bi, Feng, Shaw, Andrew, Zhu, Zhenggang, Elmoselhi, Adel, Fan, Daiming, Cover, Timothy L., Ding, Xia, and Yao, Xuebiao. Helicobacter pylori vaca disrupts apical membrane-cytoskeletal interactions in gastric parietal cells. *J Biol Chem 283*, 39 (Sep 2008), 26714–25.

[128] Weiss, Stefanie M., Ladwein, Markus, Schmidt, Dorothea, Ehinger, Julia, Lommel, Silvia, Städing, Kai, Beutling, Ulrike, Disanza, Andrea, Frank, Ronald, Jänsch, Lothar, Scita, Giorgio, Gunzer, Florian, Rottner, Klemens, and Stradal, Theresia E. B. Irsp53 links the enterohemorrhagic e. coli effectors tir and espfu for actin pedestal formation. *Cell Host Microbe 5*, 3 (Mar 2009), 244–58.

[129] Whale, Andrew D., Garmendia, Junkal, Gomes, Tania A., and Frankel, Gad. A novel category of enteropathogenic escherichia coli simultaneously utilizes the nck and tccp pathways to induce actin remodelling. *Cell Microbiol 8*, 6 (Jun 2006), 999–1008.

[130] Whale, Andrew D., Hernandes, Rodrigo T., Ooka, Tadasuke, Beutin, Lothar, Schüller, Stephanie, Garmendia, Junkal, Crowther, Lynette, Vieira, Mônica A. M., Ogura, Yoshitoshi, Krause, Gladys, Phillips, Alan D., Gomes, Tania A. T., Hayashi, Tetsuya, and Frankel, Gad. Tccp2-mediated subversion of actin dynamics by epec 2 - a distinct evolutionary lineage of enteropathogenic escherichia coli. *Microbiology 153*, Pt 6 (Jun 2007), 1743–55.

[131] Wong, Alexander R. C., Clements, Abigail, Raymond, Benoit, Crepin, Valerie F., and Frankel, Gad. The interplay between the escherichia coli rho guanine nucleotide exchange factor effectors and the mammalian rhogef inhibitor esph. *MBio 3*, 1 (2012).

[132] Wong, Alexander R. C., Pearson, Jaclyn S., Bright, Michael D., Munera, Diana, Robinson, Keith S., Lee, Sau Fung, Frankel, Gad, and Hartland, Elizabeth L. Enteropathogenic and enterohaemorrhagic escherichia coli: even more subversive elements. *Mol Microbiol 80*, 6 (Jun 2011), 1420–38.

[133] Wong, Alexander R. C., Raymond, Benoit, Collins, James W., Crepin, Valerie F., and Frankel, Gad. The enteropathogenic e. coli effector esph promotes actin pedestal formation and elongation via wasp-interacting protein (wip). *Cell Microbiol 14*, 7 (Jul 2012), 1051–70.

[134] Xu, Rong-Qi, Blanvillain, Servane, Feng, Jia-Xun, Jiang, Bo-Le, Li, Xian-Zhen, Wei, Hong-Yu, Kroj, Thomas, Lauber, Emmanuelle, Roby, Dominique, Chen, Baoshan, He, Yong-Qiang, Lu, Guang-Tao, Tang, Dong-Jie, Vasse, Jacques, Arlat, Matthieu, and Tang, Ji-Liang. Avrac(xcc8004), a type iii effector with a leucine-rich repeat domain from xanthomonas campestris pathovar campestris confers avirulence in vascular tissues of arabidopsis thaliana ecotype col-0. *J Bacteriol 190*, 1 (Jan 2008), 343–55.

[135] Yang, Tzi-Peng, Chiou, Hui-Ling, Maa, Ming-Chei, and Wang, Chau-Jong. Mithramycin inhibits human epithelial carcinoma cell proliferation and migration involving downregulation of eps8 expression. *Chem Biol Interact 183*, 1 (Jan 2010), 181–6.

[136] Zhang, Feng, Wang, Qi, Ye, Lihong, Feng, Yingming, and Zhang, Xiaodong. Hepatitis b virus x protein upregulates expression of calpain small subunit 1 via nuclear factor-kappab/p65 in hepatoma cells. *J Med Virol 82*, 6 (May 2010), 920–8.

[137] Zhao, Hongxia, Pykäläinen, Anette, and Lappalainen, Pekka. I-bar domain proteins: linking actin and plasma membrane dynamics. *Curr Opin Cell Biol 23*, 1 (Feb 2011), 14–21.